Development and Characterisation of Solid-State Ion-Selective Electrodes, and their Application to Sweat Analysis for Cystic Fibrosis Diagnosis

Aogán Lynch

MSc.

2010

Thesis Title: **Development and Characterisation of Solid-State Ion-Selective Electrodes, and their Application to Sweat Analysis for Cystic Fibrosis Diagnosis.**

Candidate: **Aogán Lynch.**

School of Chemical Sciences, Dublin City University.

Supervisor: **Prof. Dermot Diamond**

Date: **September 2010**

I hereby certify that this material which I now submit for assessment on the programme of study leading to the award of Master of Science is entirely my own work, that I have exercised reasonable care to ensure that the work is original, and does not to the best of my knowledge breach any law of copyright, and has not been taken from the work of others save and to the extent that such work has been cited and acknowledged within the text of my work.

Signed: _____

ID: _____

Date: _____

I would like to acknowledge the help and support of my supervisor Prof. Dermot Diamond throughout my time in DCU. Many thanks also to my friends, colleagues, fellow students, and the staff and technicians of the BEST Centre, the NCSR and the DCU chemistry department.

Abstract

Title: **Development and Characterisation of Solid-State Ion-Selective Electrodes, and their Application to Sweat Analysis for Cystic Fibrosis Diagnosis.**

Author: **Aogán Lynch**

Cystic Fibrosis (CF) is one of the most common genetic diseases affecting Caucasians that leads to early death[i]. It is Ireland's most common life-threatening inherited disease. Early diagnosis facilitates early implementation of therapy, which can significantly improve the prognosis and life quality of the affected patient. The gold standard diagnostic test for CF is the Quantitative Pilocarpine Iontophoresis Test (QPIT) for the sweat electrolytes sodium and chloride[ii]. In the QPIT, the sweat glands are artificially stimulated, a sweat sample is collected, and the concentrations of sodium and chloride ions determined separately using standard benchtop analytical instrumentation. In this thesis, the use of miniature solid-state Ion-Selective Electrodes (ISE's) to monitor both target ions simultaneously, for the purpose of CF diagnosis, is investigated. A commercially available sensor array in a flow-cell was initially used in both simulated and live clinical trials, involving the analysis of real sweat samples from confirmed CF and non CF populations[iii]. Solid-state ISE's were then designed, constructed, tested and incorporated into a bespoke flow-cell device compatible with modern sweat sampling equipment. Finally a working prototype of a wearable, watch-type device for the rapid on-line diagnosis of (CF) was designed, constructed and employed in a live clinical trial to assess its usefulness as a possible real-world diagnostic / screening device.

---

i Committee for a Study for Evaluation of Testing for Cystic Fibrosis; Journal of Pediatrics, 1976, 88, 4, Part 2, 711-750

ii L.E. Gibson, R.E. Cooke; Pediatrics, 1959, 23, 545-549.

iii Lynch, D Diamond and M Leader; Analyst, 2000, 125, 2264-2267.

Chapter 1

1 Cystic Fibrosis

1.1 Introduction

Cystic Fibrosis (CF) is one of the most common genetic diseases affecting Caucasians that leads to early death[1]. It occurs in approximately 1 in every 2500 live births and has a carrier incidence of ca 4-5 %. The symptoms of CF vary greatly in their severity, but include pulmonary and respiratory disease, malnutrition, pancreatic and hepatic insufficiency, and sterility, leading ultimately to premature death. Affected patients may die in the neonatal period or in early childhood, but only in rare cases do patients survive to middle age. The diagnosis of CF is an important issue, as with any disease, because the early implementation of therapy can significantly improve the prognosis and life quality of the affected patient. The gold standard diagnostic test for CF, introduced by Gibson and Cooke[2] in 1959, is the Quantitative Pilocarpine Iontophoresis Test (QPIT) for the sweat electrolytes sodium and chloride. In the QPIT, the sweat glands are artificially stimulated, a sweat sample is collected, and the concentrations of sodium and chloride ions determined using standard bench-top analytical instrumentation. This study investigated the simultaneous determination of both target ions, using a commercially available sensor array in a flow-cell, manufactured by SendX® Inc. The suitability of the device for the analysis of sweat samples was assessed by first applying it to the analysis of simulated samples in the expected normal, borderline and CF diagnostic concentrations ranges. A clinical trial

was then carried out involving the analysis of real sweat samples from both a normal and a CF-positive population.

1.2 Cause of CF

CF is caused by a mutation in the gene which codes for the cystic fibrosis transmembrane conductance regulator (CFTR). The CFTR gene was described by Lap-Chee Tsui et al., in three seminal papers in Science in September of 1989[3,4,5]. The CFTR itself is a protein of 1480 amino acids, which functions as a chloride channel, but mutations in the gene, which codes for this protein, render the resultant protein defective. To what extent it is defective is dependant on the mutations present. Around 70% of the CF positive population exhibit Lap-Chee Tsui et al's demonstrated mutation, a deletion of 3 base pairs coding for phenylalanine at amino acid position 508 in the predicted protein, and this mutation is termed ΔF508. Many other mutations have since been, and continue to be, discovered and the current number of known mutations (as of April 2010) is in excess of 1600[6], although not all are disease causing.

1.3 Effects of CF

CF results in a general increase in the viscosity of bodily secretions. The regulation of ion transport across epithelial cell membranes is affected, resulting in non-functional chloride transport and sodium reabsorption. This leads to increased viscosity of bronchial secretions, which impairs airway clearance and increases the risk of infection[1]. The resultant chronic pulmonary disease characteristic of CF initially gave rise to the term "mucoviscidosis" for the condition, and it is the leading cause of lung damage and death in CF sufferers. Chronic and irreversible colonisation of the lungs by bacteria such as *Staphylococcus Aureus* often occurs initially, followed by *Pseudomonas Aeruginosa*. These recurrent and persistent infections, together with by-products of the organism-neutrophil interactions with the body's immune system, clog the lungs in the already abnormally viscous airway secretions. Other secretions are also affected; indeed another term given to CF was "fibrocystic disease of the pancreas" due to the fact that 85-90% of all patients exhibit some form of exocrine pancreatic insufficiency[7]. The pancreas functions in part as an exocrine gland, secreting enzymes into the gut to aid digestion. CF exocrine secretions are abnormal, leading to obstruction of the pancreatic ducts, preventing the secretion of these digestive enzymes into the stomach thus leading to malabsorption of fats and proteins and poor weight gain. Similar secretory abnormalities lead to sterility in males due to obstruction of the Vas Deferens; but perhaps the most important manifestation, diagnostically at least, of this chloride channel failure is the elevated sodium and chloride levels in the sweat of CF affected individuals identified by Di Sant'Agnese et al. in 1953[8], as a result of a heat wave in New York in 1948. A positive sweat test for CF occurs when sweat sodium and chloride levels are equal to,

or greater than, 50mM and 60 mM respectively. Normal levels should be below these thresholds.

1.4 Diagnosing CF

The gold standard test for CF, introduced in 1959, is the Gibson and Cooke QPIT (Quantitative Pilocarpine Iontophoresis Test) based on the characteristic elevated levels of sodium and chloride in sweat (≥50mM sodium and ≥60mM for chloride)[2], This diagnostic test is still in use today. Suspicion of CF may arise from the knowledge of a family history of the disease, or from one of many available screening tests (where they are in place), or from clinical presentation. Though CF is a well-characterised disorder, diagnosis is not always straightforward[9] for many reasons, some of which are discussed below. In all cases, however, the QPIT remains the definitive and only accepted confirmatory diagnostic procedure for the disease.

The classic presentation of CF is a child with respiratory disease, and malabsorption due to pancreatic insufficiency – "failure to thrive". A standard QPIT for elevated sodium and chloride in sweat usually confirms CF, and the test should be carried out in triplicate for validation. A correctly performed sweat test has ca. 98% accuracy[10]. Where diagnostic difficulty arises is in atypical cases relating to novel and unusual CFTR gene mutations where sweat electrolytes are borderline or normal; or when neonatal diagnosis is required. There are many examples of such atypical cases in the

literature where clinical presentation is suggestive of CF and mutation analysis identifies CFTR mutations but sweat test results are persistently normal[11,12,13]. Such cases are relatively rare, however, and in >98% of cases the sweat test is accurate. A positive sweat test and the identification of 2 CF mutations is a clear diagnosis of CF in most cases. In atypical cases a repeat of the QPIT and thorough evaluation of the respiratory system, pancreatic sufficiency and liver functions, as well as an extended search for rare mutations is required.

Neonatal diagnosis is important because early diagnosis means early implementation of preventative and palliative treatment. Neonatal diagnosis is difficult because the cornerstone QPIT cannot be carried out on newborns, as they do not sweat sufficiently in the first 6 weeks of life to facilitate sample collection. Even after those 6 weeks the QPIT is at any rate considered too laborious and expensive a test for blanket screening of all newborns. Current screening methods include the measurement of Immuno-reactive Trypsin (IRT) in the blood of neonates[14], CFTR mutation analysis, pancreatic sufficiency tests for meconium albumin[15], and sweat conductivity tests[16]. These tests all have their advantages but they are only screening tests, and any positive results indicative of CF must be followed up with a standard QPIT.

As has been said, the current number of identified mutations is in excess of 1600, though the vast majority occur at a frequency of less than 0.1% in the affected population[6]. This hampers the screening for the disease via the genetic route as it is difficult and expensive to screen every individual for every possible mutation. Selectively screening for a small number of the most common or likely mutations can be carried out but the results depend on the mutations screened for, and indeed on the

population being screened. The most common mutation in the UK is the three base pair deletion, ΔF508, which accounts for approximately 75% of carriers. The same mutation appears in approximately 90% of the CF cases in the United States[17]. Commercial multiple-mutation assays are available that can detect about 86% of carriers in Scotland, Wales and the North of England, or 80% elsewhere. Different proportions apply to other populations such as Asians (35%), Ashkenazi Jews (95%) and African Americans (41%)[18]. Clearly, the detection rate of DNA mutation testing is highly dependent on racial and ethnic background. No consensus exists as to the best multi-mutation screening panel to use because the frequency distribution of CFTR mutations varies across racial and ethnic groups[19]. Ethnic variation is not an issue with the standard QPIT test for sodium and chloride in sweat.

1.5 The Sweat Test

The QPIT is widely regarded as one of the best diagnostic tests in clinical medicine[20]. It consists of three separate stages:

(i) stimulation of sweating by pilocarpine iontophoresis

(ii) sample collection e.g. onto gauze or filter paper or the Wescor Macroduct® (see Figure 1.1b & c), and

(iii) analysis for sodium or chloride or both.

Stimulation of sweat is carried out by pilocarpine, a cholinergic drug, introduced to the skin by iontophoresis to induce sweating in a localised area. The pilocarpine is purchasable in convenient "use once and throw away" gel disks compatible with the iontophoresis unit available from the same company – ACCU Science, Ireland – a division of Wescor Inc. (Logan, Utah 84321 USA). Pilocarpine, activated by a low voltage electrical current, is drawn into the dermal layer of the skin where it stimulates the sweat glands, activating their secretion [Figure 1.1a]. Sample collection is carried out using filter paper or gauze, or another Wescor device called the Macroduct® [Figure 1.1b & c].

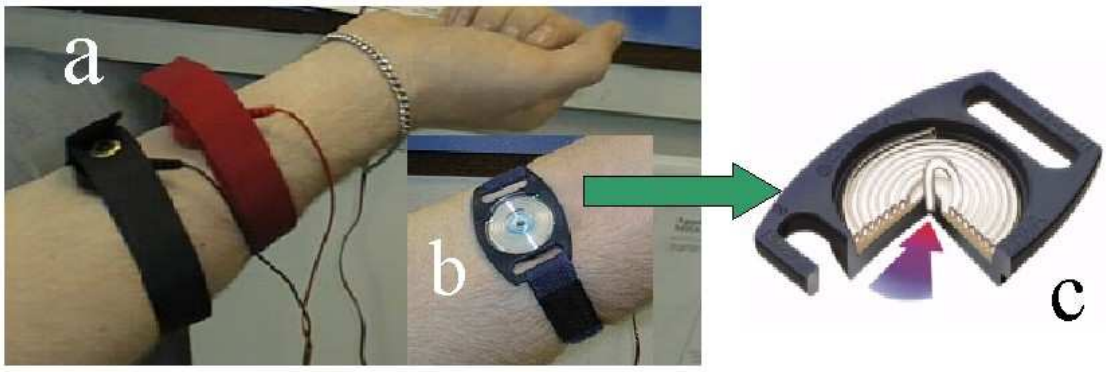

Figure 1.1 Following iontophoresis with pilocarpine to stimulate sweating (a), the sweat is collected using the Macroduct® unit which is strapped over the stimulated region like a wristwatch (b). The neat sweat collects in a coiled tube through a hole in the back of the unit. (c) A blue marker dye is used to indicate the progress of the sweat collecting in the tubing (image taken from www.wescor.com).

It is equally accepted, however, that the QPIT is difficult to perform, laborious, and notoriously prone to errors if not executed correctly with strict adherence to

procedure[21], leading to higher incidences of false positive and negative results. For this reason, many efforts have been made to simplify and speed up the standard procedure while cutting the cost of it, in order to make it more suitable to both mass screening and less frequent use, in hospitals as well as centralised CF centres.

On-skin ion selective electrodes (ISE's) have been used[22,23,24] for on-skin sweat analysis after stimulation to eliminate the sample collection and weighing stages and their associated problems, but in general these devices have performed rather poorly due to problems with evaporation of the sweat during sampling, poor reproducibility, contamination of sample by leakage from the liquid junction of the reference electrode, difficulty in achieving good contact with the skin surface and mV-signal artefacts arising from pressure changes or patient movement etc.

The Scandipharm Cystic Fibrosis Indicator System (CFIS) chloride patch[25,26] is another diagnostic device consisting of a filter paper patch placed over the site of iontophoresis. The sweat is absorbed and meets a "chloride-complexing chemical" to form a precipitate and the circumference of the precipitate ring is related to the concentration of chloride. A number of devices based on conductivity measurements also exist and are in use, most notably the Wescor Sweat Chek® conductivity meter, which is the only screening test approved by the United States Cystic Fibrosis Foundation. Again, however, as with all of the above tests, it remains a screening test only, and is not accepted as a valid diagnosis without a confirmatory QPIT.

One of the most significant sources of error in the QPIT sweat test is the sample collection stage which involves the use of pre-weighed filter paper or gauze to be

placed over the site of iontophoresis for a period of 30 minutes to absorb the sweat being produced. This procedure is fraught with the problem of evaporation and resultant concentration of the sample during collection and also during transfer of the filter paper to a stoppered flask for re-weighing. These problems were significantly improved by the development of the Wescor Macroduct® system[27,28]. As shown in Figure 1.1, the Macroduct® is strapped to the site of iontophoresis (usually the patient's arm), the sweat collects in the shallow concave region underneath of the plastic disk and through the hydraulic pressure of the sweat glands (stimulated by the action of pilocarpine) the sweat is forced into the coiled capillary tubing via a small hole in the centre of the disk connected to a collection coil of plastic tubing. A spot of blue dye at the entrance to the coil is taken up by the sweat and aids visualisation of the collection process. Wescor Inc. encourages the coupling of the Macroduct® with its own commercially available Sweat Chek® conductivity meter, but as a sweat sample collection system it can of course be coupled with any subsequent analytical technique. The advantage of the Macroduct is it facilitates easy collection of up to 75 μg of liquid sweat while eliminating traditional sweat test difficulties with evaporation. After collection the device can be dismantled and the sample extracted using a syringe and transferred to an appropriate vial for storage or analysis.

ISE analysis of samples collected via the Macroduct has been successfully carried out and found to be a valid alternative[29]. In this study, the use of a miniature ion-selective electrode array to analyse sweat samples and therefore diagnose CF, is proposed. The device, manufactured by SendX® Inc, a commercially available blood gas and blood electrolyte analyser was investigated as an analytical system for liquid sweat samples collected via the Macroduct. As the device is basically a series of miniature sensors

in a flow-cell, it is capable of analysing small volumes of any compatible liquid sample that can be pumped through the device, for a variety of analytes. The ability to simultaneously analyse sodium and chloride is also a big advantage. Many current sweat analysis techniques such as flame photometry and anion exchange chromatography have several major disadvantages for occasional users in physician's offices or hospital outpatient departments[30]. They require relatively sophisticated and expensive analytical instrumentation and a high degree of technical competence to operate them. This is especially true when undertaking the determination of both the sodium and chloride levels in sweat samples, as is recommended for optimum reliability[31]. This would most likely necessitate the splitting of sweat samples into two portions for the different methods of analysis for the two ions and, almost certainly, dilution of samples to ensure sufficient volumes for replicate analyses. This makes the analytical procedure lengthy and tedious. Using a microelectrode array allows, in principle, the simultaneous analysis of sodium and chloride (as well as potassium if required). No bulky or expensive instrumentation is required, and it is quite simple to use. Multi-component analysis using micro-sensor arrays is attractive as it reduces both analysis time and expense. It also presents a more convincing assay, as contributions from other components in the same sample matrix can be investigated simultaneously. Furthermore there is a rapidly growing demand for devices which allow 'point of need measurements' rather than sending samples to centralised analytical laboratories. The use of sensor arrays such as the SendX® array used in this study offers a convenient route to achieving this goal. By simply passing samples through the array, delays associated with collection and storage and eventual analysis are minimised. In preliminary studies, it was identified that CF diagnosis could in principle be performed with an array of this type, as the marker ions (Na^+ and

Cl^-) present in sweat can be easily and accurately measured by reconfiguring sensor arrays produced for blood analysis[32, 33].

This chapter describes the assessment of the suitability of the array for the analysis of sweat samples by applying it to the analysis of simulated samples in the expected normal, borderline and CF diagnostic concentrations ranges. A clinical trial was subsequently carried out involving the analysis of real sweat samples from both a normal and a CF population, and this is described in the following chapter.

1.6 Experimental

2 litres of a mixed 0.1 mol l^{-1} (100 mM) stock solution of potassium, sodium and chloride was made up (14.912g KCl and 16.998g of $NaNO_3$) and diluted to give 0.02, 0.04, 0.06, 0.08 and 0.1 mol l^{-1} standard solutions. Four simulated samples were also made up containing all three ions of interest at equal concentrations of 0.035, 0.050, 0.075 and 0.085 mol l^{-1} and numbered 1 to 4, respectively. Analytical grade potassium chloride and sodium nitrate were obtained from Fluka Chemie AG and used to make up the simulated samples and standards. Ultrapure water (Barnstead EASYpure RF Ultrapure water system, 18.2MΩ-cm resistivity) was used throughout this study.

1.7 Instrumentation

The sensor array was received from SendX Inc as pictured in Figure 1.2. A Gilson Minipuls 3 peristaltic pump connected to the array with microbore capillary tubing was used to pump standard and sample solutions through the flow-cell. Signals from the sensors were transferred after impedance conversion to a portable PC, *via* a National Instruments DAQ-Card AI-16XE-50 I/O data acquisition card. The multichannel data was captured and displayed using LabView software written in-house.

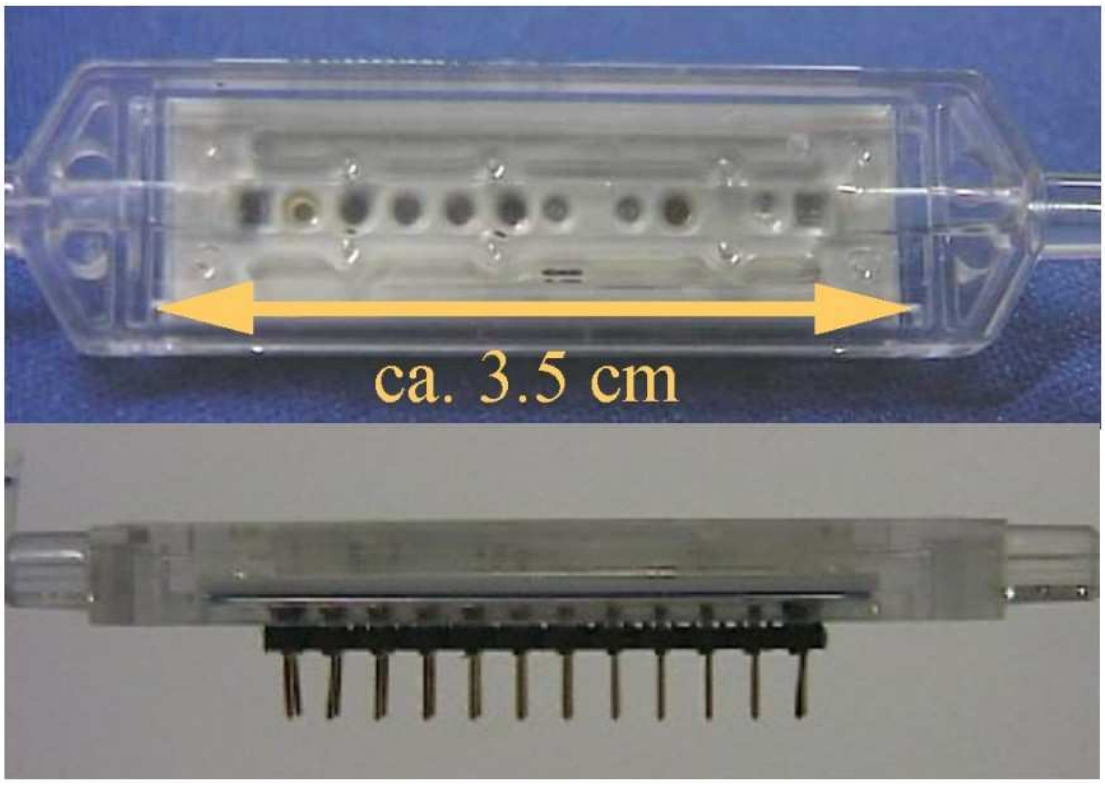

Figure 1.2 SendX Array. The top image shows the sensor array and the transparent plastic flow-cell in which it is encased. Below it is the same array pictured side-on showing the 24-pin-out arrangement underneath the array.

The digital data acquired from each sensor were displayed simultaneously as real time millivolt readings on the PC screen, and saved as ASCII text files. Microsoft Excel was used for post-acquisition data analysis and for graphical representation of the data obtained.

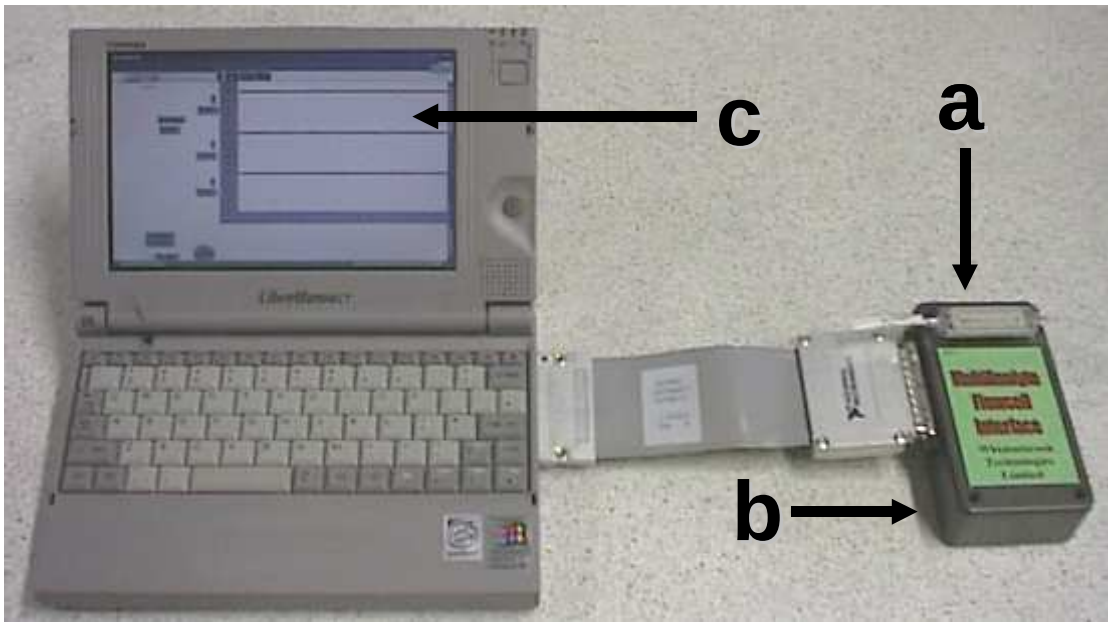

Figure 1.3 CF analytical system: The signals taken from the array (a) are routed through a shielded box containing an impedance conversion circuit (b). This is connected to a mini-PC running a LabVIEW program which captures the signals and plots voltage response against time (c).

1.8 Procedures

A Gilson Minipuls 3 peristaltic pump connected to the array with microbore capillary tubing (0.1 mm internal diameter) was used to pump standard and sample solutions through the flow-cell. The sensor array was obtained from SendX® and connected to

a portable PC via an impedance conversion circuit housed in an rf-shielded box. Signals from the sensors were transferred after impedance conversion to a portable PC, *via* a National Instruments Lab-PC 1200 data acquisition card. The multichannel data was captured and displayed using LabView software written in-house. The digital data acquired from each sensor were displayed simultaneously as real time millivolt readings on the PC screen, and saved as ASCII text files. Microsoft Excel '98 was used for post-acquisition data analysis and for graphical representation of the data obtained.

1.9 Results and discussion

Figure 1.4 shows one of the LabView user interfaces employed in the study. This relatively simple interface displays three sensor signals (Na^+, K^+ and Cl^-). In each case, the baseline is shown to be stable, exhibiting minimal drift and hysteresis, particularly for the Na^+ and K^+ sensors. The baseline represents the 0.01 mol l^{-1} standard while the responses from left to right are the 0.02, 0.04, 0.06, 0.08 and 0.1 mol l^{-1} standard solutions. Figure 1.5 shows the same calibration sequence followed by analysis of the simulated samples (0.035, 0.050, 0.075 and 0.085 mol l^{-1} mixtures of Na^+, K^+ and Cl^-, numbered 1 to 4 respectively) analysed in a random order (#2, 4, 3, 1, 3, 2, 2, 3, 4, 1, 4, and 1.)

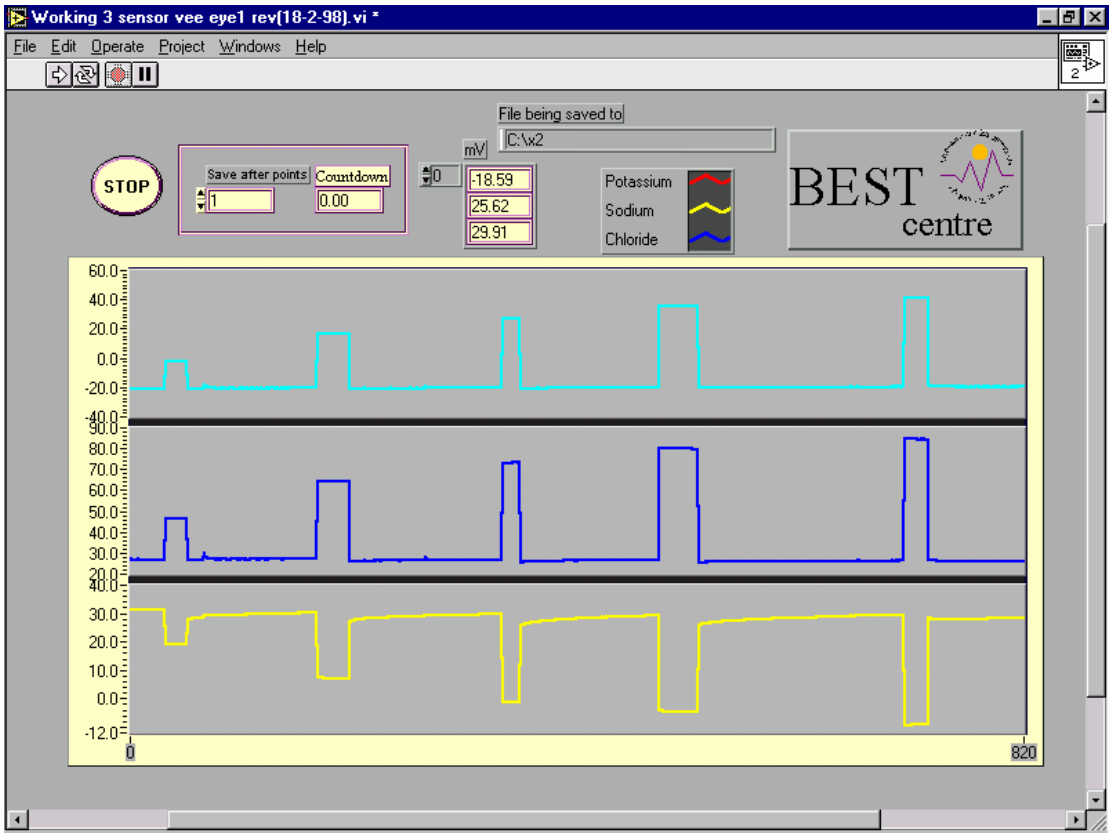

Figure 1.4 LabView Virtual Instrument Interface showing real-time responses to standards containing 20, 40, 60, 80 and 100 mM sodium, potassium and chloride. Baseline is a solution, which is 10 mM in all three ions. Sodium is the topmost trace, potassium the middle and chloride the bottom.

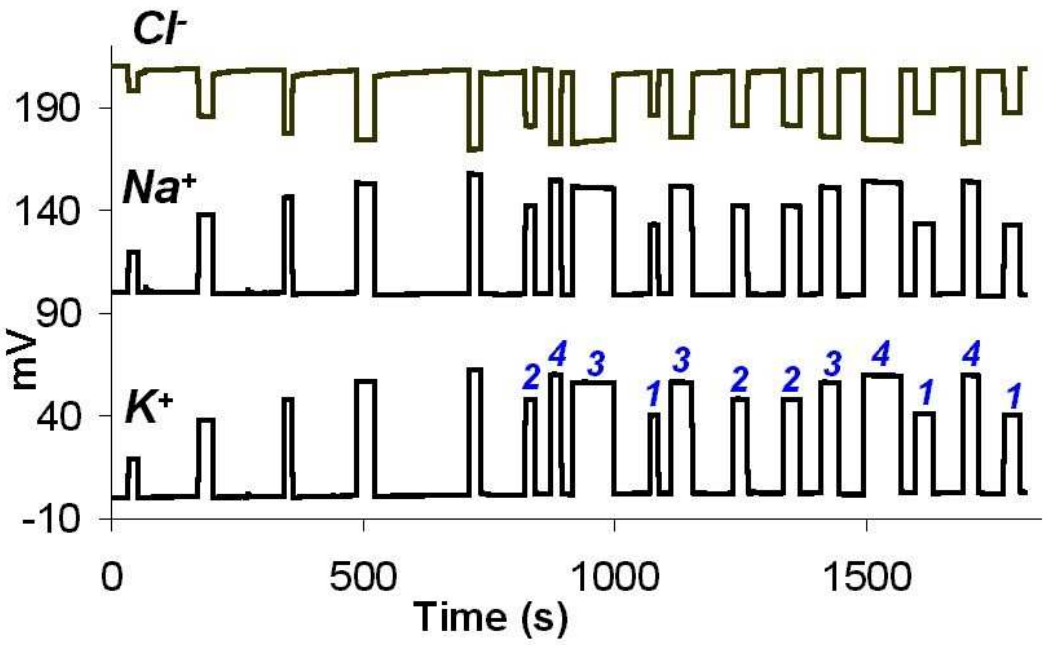

Figure 1.5 Extended data display of three data channels after importation in to EXCEL. The first 5 response peaks represent the 5 standards (0.02, 0.04, 0.06, 0.08 and 0.1 mol l^{-1} in all three ions) against the base line (0.1 mol l^{-1}) in each case, random unknowns (1 to 4, see text for details) follow.

The response was seen to be very rapid, and a steady-state signal was obtained almost immediately. The return to the 10 mM baseline is equally fast, with minimal tailing, drift or hysteresis (Figure 1.5). It must be noted that the above trace is not representative of continuous, flow-injection analysis. The data collection software was paused during each solution changeover. Sample turn-around, including flushing and filling of the array with the solutions, was approximately 1 minute. However, this could be further shortened if the array was used in flow-injection mode, and considerably shorter flushing times could also be used as the dead volume of the array is only ca 40 µl. The calibration curves (Figure 1.6) generated from the data in Figure 1.5 show good linearity for each of the electrodes.

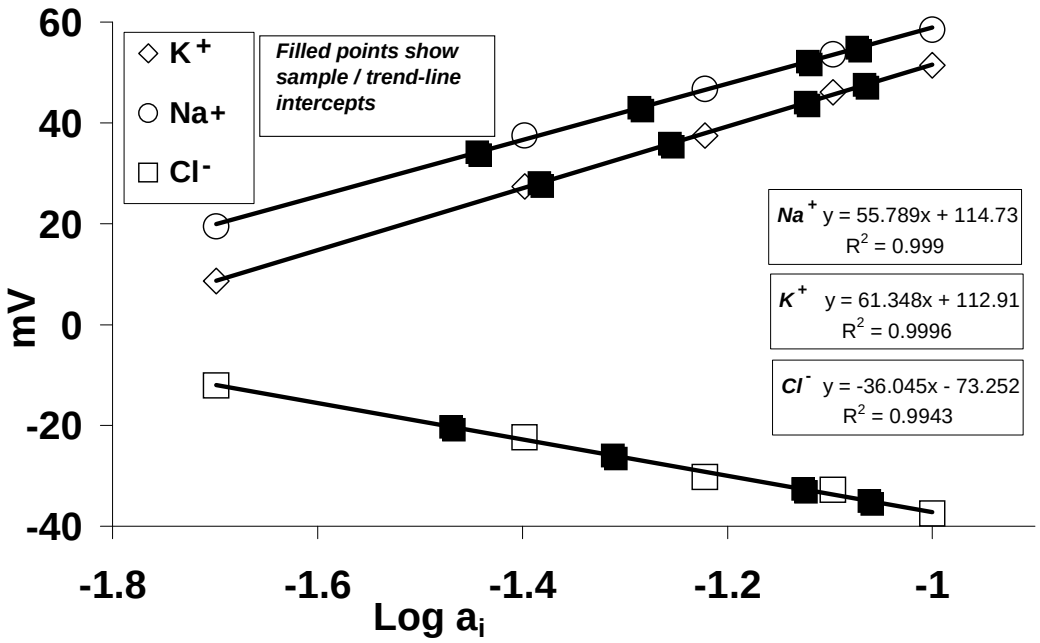

Figure 1.6. Calibration curves for Sodium, Potassium and Chloride. The unfilled symbols are standards, the filled symbols are unknowns. Y error bars were calculated for standards and samples but were sufficiently small as to be invisible in this graph at this scale (see Table 1.1).

The unfilled symbols signify the five standards and the filled points represent the unknowns. An excellent correlation was obtained in each case, but the slope of the AG/AgCl electrode was sub-Nernstian to Cl^- at ca. –36.1 mV/decade. Later work seems to show that this was peculiar to the chloride electrode in this array only. Devices received and used in later work subsequently yielded Nernstian slopes for chloride.

Electrode	Standard				
	20mM	40mM	60mM	80mM	100mM
K^+	8.63 (0.08)	27.38 (0.08)	37.51 (0.06)	46.05 (0.08)	51.39 (0.07)
Na^+	19.48 (0.04)	37.47 (0.05)	46.70 (0.04)	53.57 (0.14)	58.50 (0.01)
Cl^-	-12.09 (0.05)	-22.38 (0.01)	-30.25 (0.02)	-32.78 (0.10)	-37.51 (0.19)

Table 1.1 Steady state values in mV used to generate the calibration plots. The calibration regime was only carried out once, but for each standard the steady state reading was monitored for 30 seconds, with the system automatically recording a reading every second. The deviation of the response for each electrode over those 30 seconds was calculated and is included here (in brackets after the average mV reading for each electrode and standard) to demonstrate the stability of the signals. All show a deviation of less than 0.2 mV and all but 2 are less than 0.1 mV.

sample	**K^+**				**Na^+**				**Cl^-**			
	1	**2**	**3**	**$\sigma_{n=3}$**	**1**	**2**	**3**	**$\sigma_{n=3}$**	**1**	**2**	**3**	**$\sigma_{n=3}$**
35mM	27.88	28.27	27.99	*0.20*	34.05	34.50	33.98	*0.28*	-20.30	-20.94	-19.61	*0.67*
50mM	36.28	35.65	35.62	*0.37*	42.87	43.18	42.95	*0.16*	-26.03	-25.95	-25.92	*0.06*
75mM	44.24	44.02	43.71	*0.27*	52.29	52.31	51.91	*0.23*	-33.55	-32.38	-32.07	*0.78*
85mM	47.71	47.72	47.10	*0.36*	54.83	55.12	54.60	*0.26*	-35.84	-35.70	-35.42	*0.21*

Table 1.2 Triplicate millivolt responses of each of the three electrodes to the four simulated sample solutions, along with calculated n=3 standard deviations. These data were used to estimate the sample ion concentrations from the calibration curves, presented in Table 1.3.

True sample concentration	Electrode K^+		Na^+		Cl^-	
35mM	**41.37**	(18.2%)	**35.99**	(2.8%)	**33.95**	(-3.0%)
50mM	**55.45**	(10.9%)	**51.79**	(3.6%)	**48.77**	(-2.5%)
75mM	**75.27**	(0.4%)	**75.62**	(0.8%)	**74.88**	(-0.2%)
85mM	**85.90**	(1.1%)	**84.46**	(-0.6%)	**86.94**	(2.3%)

Table 1.3 A comparison of the true sample values with those estimated from the calibration curves. Relative percentage errors between the true and estimated sample concentrations are also shown.

From the data in Table 1.2 and the results obtained from the calibration curves in Table 1.3 it can be seen that the best results were obtained for sodium with a very good level of accuracy as reflected in the relative percentage error values, and good precision also with low mV standard deviations (≤ 0.28 mV); i.e. results obtained using the array correlated very well with the known concentrations of sodium in the samples. The results for chloride were also encouraging, though less consistent. The results for potassium show slight inaccuracies in the lower concentration samples. The slope exhibited by the potassium electrode was higher than the expected slope (61.35 mV/decade) and the potassium results also show a larger than expected value for the lowest unknown (0.0409 mol l^{-1} instead of 0.035 mol l^{-1}). This may be an outlier, as the other unknowns are all determined to an accuracy of less than 1.0 $x10^{-3}$ mol l^{-1}, and the triplicate mV data for that "35 mM" solution are very consistent; therefore the

error could simply be a dilution or similar practical error in the making up of the solution.

The concentrations of sodium and chloride used in this study are typical of those found in sweat and used to diagnose cystic fibrosis[34]. The most appropriate thresholds are a matter of some debate. Generally ≥50mM sodium and ≥60mM for chloride is considered diagnostic for CF as originally suggested by Gibson and Cook in 1959[2], but other investigators have suggested revision of these thresholds. For example, one study of 233 children[35] found that all CF positive children had chloride >80 mM and sodium >50 mM, while normal children all had chloride <40 mM and sodium <50 mM. Whatever the thresholds, these results suggested that the array could be adapted for this diagnosis. If the performance of the array is assessed on the basis of, for example, the Gibson and Cooke levels, the 35 mM simulated sample would be representative of a sample taken from a normal population, the 50 mM would a normal borderline, and the 75 mM and 85 mM would be considered (as part of a full clinical assessment) to be diagnostic of CF. From Table 1.3, which compares the known concentrations of the samples with those estimated from the array data, the close agreement of between the 2 sets of data, with an average %error of < 2% for the sodium and chloride electrodes indicates that the array might well be used to analyse real sweat samples with sufficient accuracy to differentiate between normal samples and CF samples, based on the expected marker ion concentrations and their accepted diagnostic thresholds.

1.10 Conclusions

Commercially available sensor arrays primarily aimed at the blood gas market can be easily adapted for other applications. Portable instruments capable of rapid multicomponent analysis can be produced by coupling the blood analyser arrays to portable PCs fitted with data acquisition cards. The Labview software development environment enables sophisticated graphical user interfaces to be rapidly produced and customised for particular applications. The analytical results demonstrate that the array can easily be calibrated and used for assays outside the normal range employed in blood analysis. They also show that the cell can be used as a component in a portable instrument suitable for simultaneous multi-sensing of ion mixtures. The success of this study in the accurate determination of the CF marker ions in simulated positive and negative sweat samples in the expected concentration ranges for real-life samples was very encouraging.

1.11 References

[1] Committee for a Study for Evaluation of Testing for Cystic Fibrosis; Journal of Pediatrics, 1976, 88, 711-750

[2] L.E. Gibson, R.E. Cooke; Pediatrics, 1959, 23, 545-549.

[3] J.R. Riordan, J.M. Rommens, B.S. Kerem, L.C. Tsui; Science, 1989, 245, 1066-1073

[4] B.S. Kerem, J.M. Rommens, J.A. Buchanan, L.C. Tsui; Science, 1989, 245,

1073-1080.

5 J.M. Rommens, M.C. Iannuzzi, B.S. Kerem, L.C. Tsui; Science, 1989, 245, 1059-1065.

6 Cystic Fibrosis Mutation Database, Cystic Fibrosis Consortium Web site. Available at http://www.genet.sickkids.on.ca/cftr/. Accessed April 2010.

7 M.R. Bye, J.M. Ewig, L.M. Quitell; Lung, 1994, 172, 251-270

8 P.A. Di Sant' Agnese, R.C. Darling, G.A. Perera, E. Shea; Pediatrics, 1953, 12, 549-563

9 B.J. Rosenstein; Clin. Chest. Med., 1998, 19, 423-441

10 V.A. LeGrys, R.W. Burnett; Arch. Pathol. Lab. Med., 1994, 118, 865-867

11 T.T. Kingdom, K.C. Lee, G.J. Cropp; American J. of Rhinology, 1995, 9, 225-228

12 P. van Biezen, S.E. Overbeek, C. Hilvering; Thorax, 1992, 47, 202-203

13 W.E. Highsmith, L.H. Burgh, Z. Zhou, J.G. Olsen, T.E. Boat, A. Spock, J.D. Gorvoy, L. Quittell, K.J. Friedman, L.M. Silverman, R.C. Boucher, M.R. Knowles; New Engl. J. Med., 1994, 331, 974-980

14 J.R. Crossley, R.B. Elliot, P.A. Smith; The Lancet, 1979, March, 3, 472-474

15 U. Stephan, E.W. Busch, H. Kollberg, K. Hellsing; Pediatrics, 1975, 55, 1

16 K.B. Hammond, N.L. Turcios, L.E. Gibson; Journal of Pediatrics, 1994, 124, 255-260

17 B.L. Therrell, M.A. Lloyd-Puryear, M.Y. Mann; Journal of Pediatrics, 2005, 147, S6-S10.

18 J. Murray, H. Cuckle, G.Taylor, J. Littlewood, J. Hewison; Health Technology Assessment, 1999, 3, 1-104

[19] Connecticut Department of Health, Office of Genomics, Issue Brief . "Universal Newborn Screening for Cystic Fibrosis in Connecticut", July 2006

[20] C.R. Denning, N.N. Huang, L.R. Cuasay, H. Shwachman, P. Tocci, W.J. Warwick, L.E. Gibson; Pediatrics, 1980, 66, 752-757

[21] L.E. Gibson; Clinical Pediatrics, 1973, 12, 7

[22] H. Northall, G.A. York; British Journal of Biomedical Science., 1995, 52, 68-70

[23] P.T. Bray, G.C.F. Clark, G.J. Moody, J.D.R. Thomas; Clinica Chimica Acta, 1977, 77, 69-76

[24] C.R. Denning, N.N. Huang, L.R. Cuasay, H. Shwachman, P. Tocci, W.J. Warwick, L.E. Gibson; Pediatrics, 1980, 66, 5, 752-757

[25] W.J. Warwick, L.G. Hansen, I. Brown; Clinical Chemistry, 1993, 39, 1748

[26] W.J. Warwick, L.G. Hansen, M.E. Werness; Clinical Chemistry, 1990, 36, 96-98

[27] M. Constantinescu, B.C. Hilman; Laboratory Medicine, 1996, 27, 472-477

[28] K.B. Hammond, N.L. Turcios, L.E. Gibson; Journal of Pediatrics, 1994, 124, 255-260

[29] H. Northall, G.A. York; British Journal of Biomedical Science, 1995, 52, 68-70

[30] NAS / NRC Report, Journal of Pediatrics, 1976**,** 88, 711.

[31] H. J. Veeze, Netherlands Journal of Medicine, 1995, 46, 271-274

[32] S. Walsh, D. Diamond, J. McLaughlin, E. McAdams, D. Woolfson, D. Jones, M. Bonner; Electroanalysis, 1997, 9, 1318-1324.

[33] A. Lynch, D. Diamond, P. Lemoine, J. McLaughlin, M.Leader,

Electroanalysis, 1998, 10, 1096-1100

[34] L.E. Gibson, R.E. Cooke; Pediatrics, 1959, 23, 545-549.

[35] M. Gleeson and R.L. Henry, Clin. Chem., 37 (1991) 112b.

Chapter 2

2.1 Introduction

The work described in chapter 1 demonstrated the successful employment of the Sendx® array in the detection and monitoring of the electrolytes indicative of, and over the concentrations relevant to, a cystic fibrosis (CF) diagnosis. This indicated that the array might be applicable to the analysis of real sweat samples for diagnosing CF. This chapter describes the use of that same analytical set-up in a CF clinical trial involving real sweat samples collected from both CF positive and normal populations. The analytical performance of the array was referenced against standard bench-top Ion Chromatographic and Atomic Absorption Spectroscopic methods.

2.2 Experimental

2.2.1 Reagents and Instrumentation

Analytical-reagent grade potassium chloride and sodium nitrate were obtained from Fluka Chemie AG and used to prepare sample and standard solutions. Ultrapure water (Barnstead EASYpure RF Ultrapure water system) was used throughout.

All sweat samples were collected by pilocarpine iontophoresis using a Macroduct 3700-SYS Sweat Collection system obtained from Wescor. Ion chromatography was carried out using a Dionex DX-120 ion chromatograph. AAS for potassium and sodium was carried out on a Perkin Elmer Model 3100 atomic absorption

spectrometer. The same analytical system was employed as in the previous chapter (Chapter 1)

2.2.2 Procedures

Sample Collection:

The normal and CF positive sweat samples were collected on-site in Dublin City University and in the CF Clinic in Our Lady's Hospital in Crumlin, respectively. Ethical approval was sought from and granted by the hospital ethics committee prior to the trial. This facilitated attendance of the morning outpatients' CF clinic in the hospital, which takes place on an almost weekly basis. Patients regularly attend such clinics for routine tests such as respiratory function and nutrition to assess their general progress as well as any specific issues, which might arise. In the waiting room of the clinic, patients and their parents were approached, and their participation in the trial requested. The aims of the trial and the nature of the sweat test were explained and any other questions or concerns answered. Given the parents' and or patients' consent, a sweat sample was collected via the standard QPIT (Quantitative Pilocarpine Iontophoresis Test) method. The equipment and method used are described below.

A Macroduct 3700-SYS Sweat Collection system was used to collect the samples. This is a complete system for sweat sample collection. It consists of the "Webster Sweat Inducer" (see Figure 2.1a). This is basically a sophisticated battery pack with two electrodes and a 5-minute timer. Wescor also manufacture and provide Pilogel®

discs, solid aqueous based gel discs containing 0.5% pilocarpine nitrate which fit into the electrodes as shown in Figure 2.1b .

Figure 2.1 (a) The "Webster Sweat Inducer" available from Wescor and (b) the Pilogel® discs as they fit into the electrodes (images taken from www.wescor.com)

For each patient, the site of iontophoresis (usually the patient's arm) was cleaned with deionised water, and the electrodes, fitted with fresh pilogel® discs, were strapped to the chosen limb, a couple of inches apart, with Velcro straps (provided) as previously described and illustrated in chapter 1, Figure 1.1. The Webster Sweat Inducer was then switched on. The device is designed to carry out automatic iontophoretic stimulation of the local sweat glands by passing a DC current of 1.5 mA between the electrodes for a period of 5 minutes, after which the current is automatically switched off and a brief alarm signal is sounded. During stimulation the electric current polarises the electrodes and the pilocarpine cation is repelled away from the positive (red) electrode and down into the sweat glands, activating their secretion (Figure 2.2).

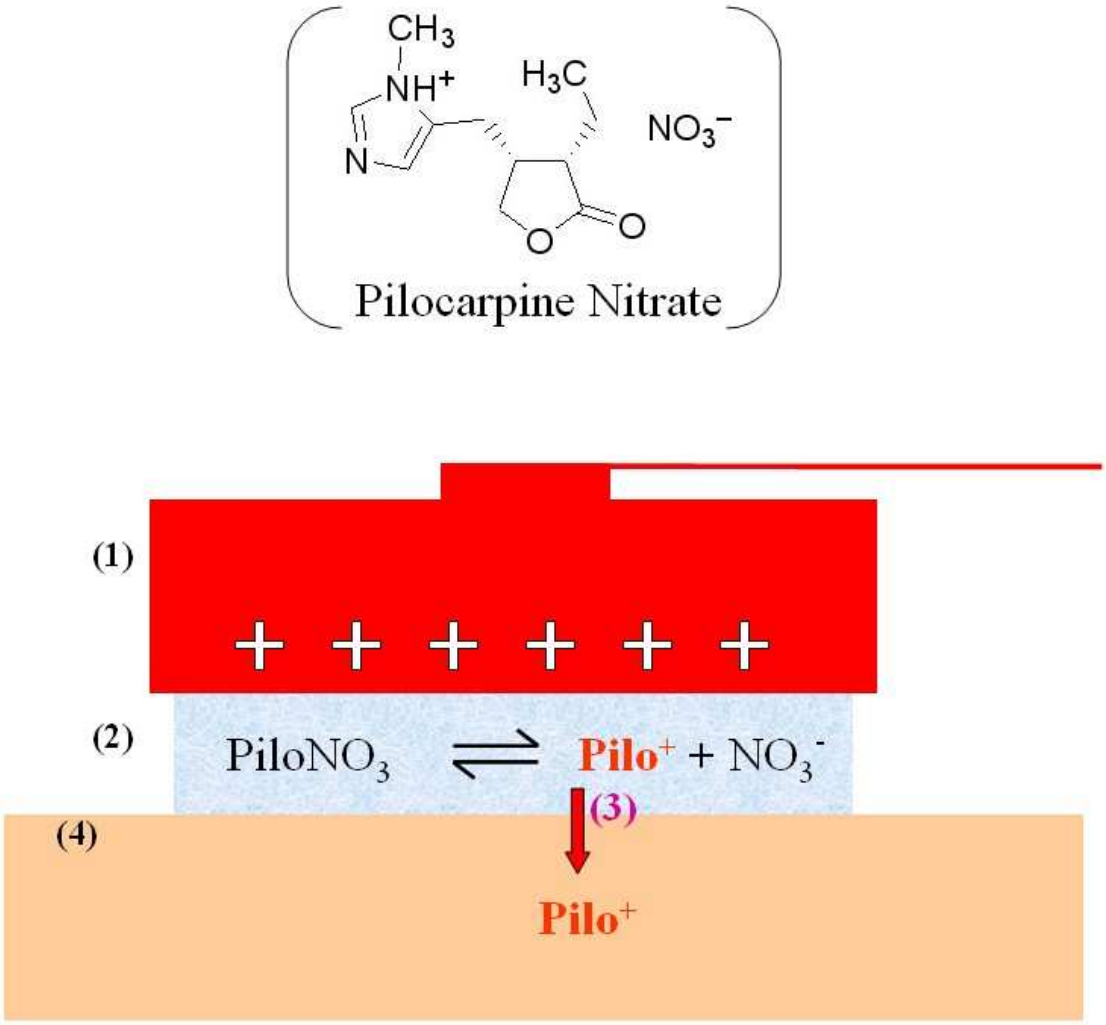

Figure 2.2 The positively polarised red electrode (1) is in contact with the aqueous Pilogel® disk (2) containing pilocarpine nitrate (chemical structure also pictured) which is partially ionised into positive pilocarpine ($Pilo^+$) and negative NO_3^- ions. The pilocarpine ion $Pilo^+$ (3) is repelled into the skin (4) where it activates the sweat glands. The removal of P^+ disturbs the equilibrium leading to further dissociation of free $Pilo^+$ ions and the process continues until a steady state is reached.

After iontophoresis the electrodes were removed, the site of iontophoresis cleaned once more with distilled water, and a Wescor Macroduct strapped to the circle of skin with which the red (+) electrode was in contact, to collect the sweat produced by the pilocarpine stimulated sweat glands.

After a collection period of approximately 30 minutes the Wescor Macroduct was removed, dismantled and the sweat sample expunged into a vial. This was done using a small forceps and a syringe, provided with the sampling kit. The forceps was used to remove the lid of the Macroduct, exposing the coiled tubing. The syringe was filled with air and inserted into the open end of the coiled tubing at the outer circumference of the coil, with which it forms a tight seal. The tubing was then pulled free and uncoiled and could be snipped at its base at the other end where it was attached to the centre of the Macroduct, i.e. the point at which the sweat enters the device during collection. One now has a length of capillary tubing containing a sample of sweat, with an air-filled syringe at one end; therefore by depressing the plunger on the syringe the sweat sample can be forced out of the tubing into an appropriate container. All samples were placed into separate 200 µl, capped vials in this way, and stored at 4 ºC until analysis was carried out. Overall 12 sweat samples were obtained from CF-positive patients in the CF clinic of Our Lady's Hospital for Sick Children, Crumlin, Dublin. A further 13 normal samples were collected from non-CF sufferers in Dublin City University. On average 50 to 75 µl of sweat was collected from subjects ranging from 13 to 27 years of age.

Analytical procedure:

A mixed 1.00 mol l^{-1} stock standard solution of potassium, sodium and chloride was prepared by dissolving 7.456g and 8.499g of KCl and $NaNO_3$, respectively, in water and making up to volume in a 100ml volumetric flask. This was diluted to give 0.02, 0.04, 0.06, 0.08, 0.1, and 0.12 mol l^{-1} standard solutions.

To facilitate analysis of the samples via the array and the two separate reference methods, it was decided necessary to dilute the samples due to the volume constraints imposed by the small (<100µl) sample volumes which may be collected via the Macroduct. Two of the CF positive samples were rejected before analysis, as the volume of sweat collected was insufficient (<10 µl). From the remainder of the samples approximately 75 µl of neat sweat from each sample was accurately transferred to a pre-weighed 2 ml vial and diluted to 500 µl, using 0.1 M magnesium acetate to buffer the ionic strength. The sample volumes were accurately transferred into the 2 ml vials using a 100 µl Transferpette® and the vials were also weighed before and after addition to confirm the sweat sample volume transferred. In preliminary work, lithium acetate was used as a diluent and ionic strength buffer but the lithium ion peak was found to be masking the sodium peak in the cation IC reference method chromatograms. Magnesium acetate was tried and the problem was remedied.

The 6 standards (0.02, 0.04, 0.06, 0.08, 0.1, and 0.12 mol l^{-1} standard solutions) were diluted by the same dilution factor (and with the same ionic strength buffer). A volume of 400 µl of each diluted sample was reserved for analysis *via* the array. Activity coefficients for the ions were calculated according to the Davies equation[1] (Equation 2.1).

$$\log f_i = -0.51 z_i^2 \left[\frac{\sqrt{I}}{1+\sqrt{I}} - 0.15I \right] \qquad \text{Equation 2.1}$$

The array was conditioned overnight in the 0.1 mol l^{-1} standard. Before use, the array was flushed with Milli-Q water for several minutes at a flow rate of 2.1 ml min^{-1}. The array was then flushed with each solution for approximately 15 s before measuring the response. During the measurement period, the analyte solution flow rate was reduced to 0.1 ml min^{-1} and the steady state signal measured for approximately 30 s after stabilisation had occurred (usually within 1-2 seconds). The lowest standard (0.02 mol l^{-1} in sodium, potassium and chloride) was used to set the baseline. Then each of the other standards (0.04, 0.06, 0.08, 0.1, and 0.12 mol l^{-1} in sodium, potassium and chloride) were passed through in the same way, with the 0.02 mol l^{-1} standard being re-analysed between each standard to investigate the possibility of hysteresis or baseline drift. The sample unknowns were then analysed, with the 0.02 mol l^{-1} standard again being re-run between each sample. When all samples had been analysed the calibration regime was repeated, ending as before with the lowest standard.

A Gilson Minipuls 3 peristaltic pump connected to the array with microbore capillary tubing was used to pump standard and sample solutions through the flow-cell. Signals from the sensors were transferred after impedance conversion to a portable PC, *via* a National Instruments Lab-PC 1200 data acquisition card. The digital data acquired from each sensor were displayed simultaneously as real time millivolt readings on the PC screen, as in the previous study and saved as ASCII text files. Microsoft Excel was used for post-acquisition data analysis and for graphical representation of the data obtained, as usual.

The remaining 100 µl of each diluted sample was reserved for analysis by the reference methods. A tenfold dilution with Ultrapure water was carried out to bring the volume up to 1 ml. 0.5 ml of this was set aside for ion chromatographic analysis, and the remaining 0.5 ml was further diluted volume in 25 ml volumetric flasks for AAS analysis.

2.2.3 Reference Methods

Anion analysis

Chloride determination for all samples was carried out on a Dionex DX-120 ion chromatograph with suppressed conductivity detection. The analytical column was a standard Dionex Ionpac® AS-14, 4mm column with mobile phase 4 mM p-hydroxy-benzoic acid with 2.5% methanol, adjusted to pH 8.5 with NaOH, at a flowrate of 1 ml min^{-1}. The method used was obtained from www.dionex.com. The Ionpac® AS-14 is a universal column for the fast separation of inorganic anions[23]. The stationary phase is a surface-functionalized polymer-based ethylvinylbenzene / divinylbenzene (EVB / DVB), and p-HBA is a commonly used mobile phase which facilitates single-column chromatography and direct conductivity detection, as well as suppressed conductivity.

A note on ion suppression in IC

Ion suppression is designed to enhance conductivity detection sensitivity in ion chromatography[4]. Traditional ion chromatography eluants such as NaOH (Anion IC) and HCl (Cation IC) are highly dissociating and present a constant high background conductivity against which it can be difficult to attribute small conductivity changes to eluting analytes. The situation can be improved through the use of weak organic acids, such as hydroxybenzoic acid (HBA), which facilitate single column chromatography and direct conductivity detection as they are weakly dissociating and therefore have a lower background conductivity. Nevertheless, suppressors can still provide sensitivity with such eluants, and presently ion suppression methods are commercially available for most instruments and applications. These suppressor units perform post separation neutralization of mobile phase salts to lower the background conductivity before entry to the detector. The units are also now available with self-regenerating mechanisms, which continuously generate H^+ and OH^- ions through the electrolysis of water (oxidation at the anode to produce H^+ ions and reduction at the cathode to form OH^- ions). In anion chromatography the suppressor unit has a cation exchange membrane, which exchanges eluting mobile phase cations, such as Na^+, for H^+ ions. Similarly in cation IC, an anion exchange membrane exchanges eluting anions for OH^-. The end result is that the analyte ions enter the detector in a water solution eluant with greatly reduced background conductivity, while analyte conductivity remains high (Figure 2.3).

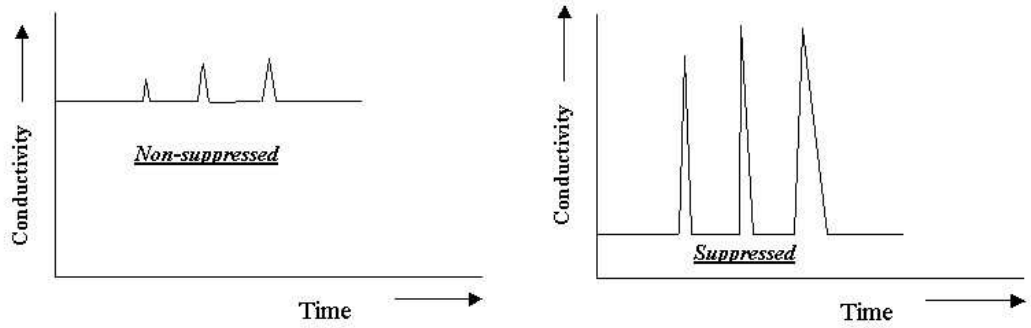

Figure 2.3 Ion chromatography with suppressed conductivity detection.

Cation Analysis

(i) Ion Chromatography

Cation analysis was carried out using two methods due to equipment constraints. Samples 1 to 16 were analysed by AAS (see below) and samples 16 to 23 analysed by cation IC. The IC was again carried out on a Dionex instrument using a CG14 guard column and an Ionpac® CS14 analytical column, with a Dionex cation self-regenerating suppressor (CSRS-II) unit and conductivity detection. The mobile phase was 10mM Methane Sulphonic Acid, at a flowrate of 1 ml min^{-1}.

(ii) AAS

AAS for sodium and potassium determination was carried out on a Perkin Elmer Model 3100 atomic absorption spectrometer under the following conditions:

	Sodium	Potassium
Lamp:	Sodium Hollow Cathode	Potassium Hollow Cathode
Lamp current:	5mA	5mA
Fuel:	Acetylene	Acetylene
Support:	Air	Air
Flame stoichiometry:	Oxidising	Oxidising
Wavelength:	589.0 nm	766.5 nm
Slit width:	0.5 nm	0.5 nm
Working range:	0.002 to 1.0 ppm	0.1 to 2.0 ppm

Calibration curves were constructed for each method and used to estimate sample concentrations.

2.3 Results and discussion

Table 2.1 below shows the mV responses of the electrodes in the array to the calibration regimes. Mean values were calculated and used to construct standard calibration curves, shown in Figure 2.4. These calibrations were carried out at the beginning and end of the trial, approximately 30 minutes apart, so some drift is expected. This drift appears to be more pronounced for the chloride electrode than for

sodium and potassium. The slopes for the three electrodes are, however, quite consistent.

Standard	**Electrode**					
	K^+_{before} (mV)	K^+_{after} (mV)	Na^+_{before} (mV)	Na^+_{after} (mV)	Cl^-_{before} (mV)	Cl^-_{after} (mV)
20	14.0	15.8	-14.0	-16.0	-102.2	-109.0
40	31.0	31.8	1.2	5.2	-119.7	-123.7
60	41.5	42.0	11.4	14.0	-130.5	-134.9
80	48.6	49.0	18.7	19.9	-137.4	-142.4
100	54.8	54.8	24.2	25.0	-142.5	-148.5
120	59.2	59.6	29.1	29.7	-147.0	-153.0
Slope (mV/dec)	60.48	58.39	57.60	59.59	-59.89	-59.45

Table 2.1 mV responses of the electrodes in the array to the standard calibration regimes, carried out before and after sample analysis.

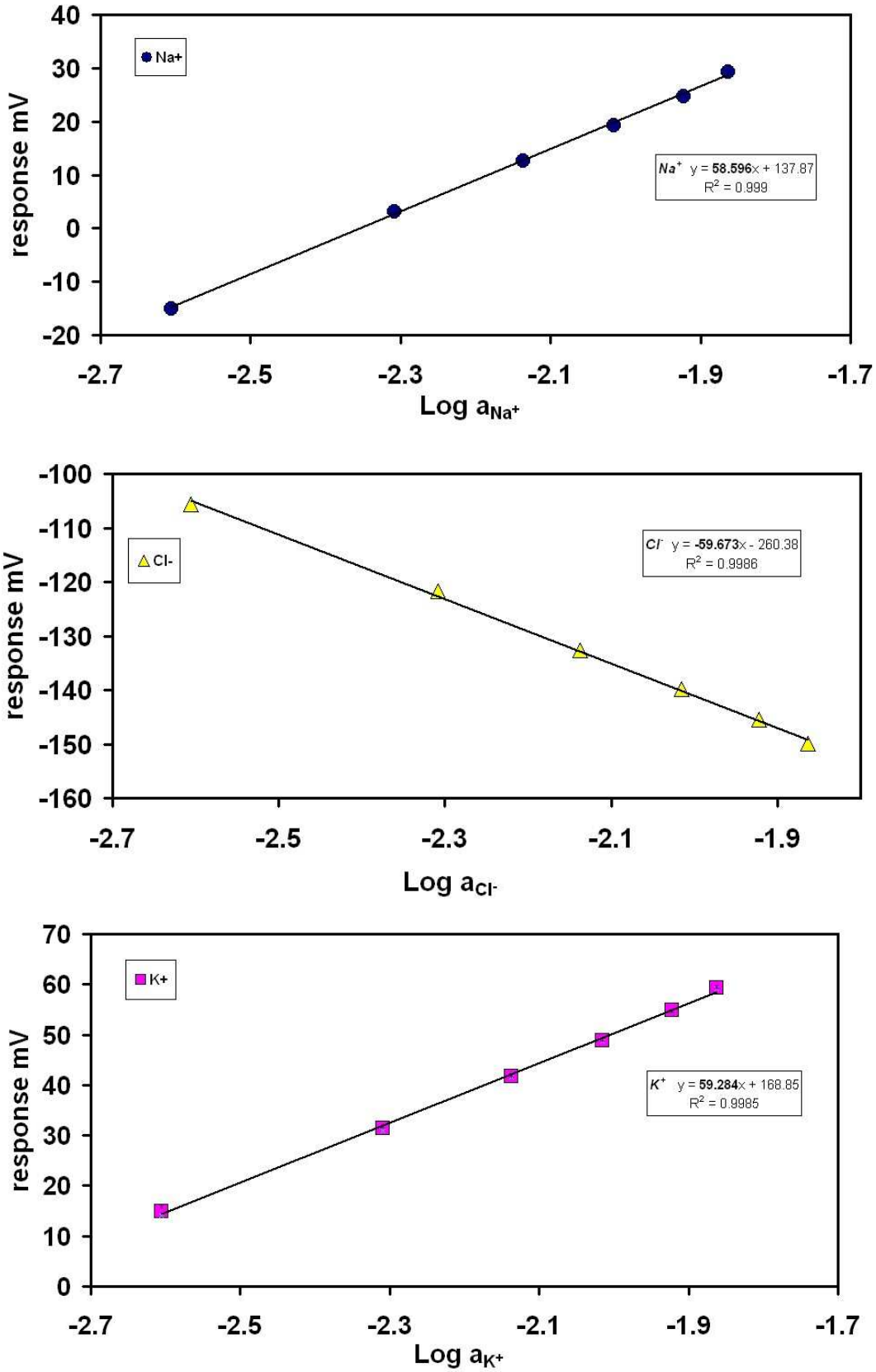

Figure 2.4 Standard curves from the 3 sensors. The responses are linear over the desired range, and Nernstian slopes are observed for the three electrodes.

	Electrode					
Sample	**K^+**		**Na^+**		**Cl^-**	
	response (mV)	activity (mol/L)	response (mV)	activity (mol/L)	response (mV)	activity (mol/L)
1	17.10	0.018	19.35	0.063	-113.61	0.023
2	21.12	0.021	19.00	0.062	-115.49	0.025
3	25.28	0.025	18.90	0.062	-126.49	0.038
4	-3.12	0.008	-0.32	0.029	-91.92	0.010
5	3.04	0.011	5.84	0.037	-98.50	0.013
6	21.40	0.022	9.12	0.042	-126.76	0.038
7	13.01	0.016	-7.52	0.022	-117.24	0.027
10	14.56	0.017	-0.87	0.029	-107.77	0.018
11	15.29	0.017	12.16	0.048	-109.72	0.020
12	2.96	0.011	-17.06	0.015	-91.19	0.010
13	-4.59	0.008	-10.73	0.019	-82.87	0.007
14	13.18	0.016	-18.42	0.014	-102.78	0.015
15	-4.26	0.008	-0.50	0.029	-84.57	0.008
16	-12.81	0.006	-9.74	0.020	-77.68	0.006
17	10.08	0.014	24.91	0.079	-106.26	0.017
18	20.63	0.021	17.05	0.058	-108.48	0.019
19	14.04	0.016	21.83	0.070	-113.75	0.023
20	12.30	0.015	20.39	0.066	-116.07	0.025
21	14.38	0.017	20.40	0.066	-116.89	0.026
22	1.37	0.010	5.80	0.037	-93.27	0.011
23	-3.19	0.008	-3.04	0.026	-90.10	0.009

Table 2.2 This table lists the mV responses to each sample for each electrode and the ion activities estimated from the standard curves. Sample volume was insufficient to allow duplicate analysis for calculation of standard deviations. The mV values do however represent a mean response over a 30 second monitoring period. The red colour indicates samples taken from the CF population, and the green represents samples taken from the normal population.

The sample ion activities in Table 2.2 were calculated from the sample millivolt responses (also listed in Table 2.2), and the standard curve trend-line equations for each electrode (Figure 2.4).

Example calculation: Sample #1, sodium ion.

The equation of the line from the sodium electrode calibration curve is:

$$y = 58.6x + 137.9$$

where "y" is the millivolt response of the electrode and "x" is the logarithm of the ion activity.

The mV response of the sodium electrode to sample #1 was 19.35 mV, and this value is substituted for "y" in the equation of the line:

$$x = \text{Antilog}\,[(19.35 - 137.9) / 58.6] = 0.00949\ M$$

The 6.67 dilution factor must also be taken into account (75 ul in 500 ul):

$$(0.00949)(6.67) = 0.063\ M$$

$$= \text{sample \#1 sodium ion activity}$$

To facilitate direct comparison of the array and reference method results, it was necessary to convert activity values obtained from the array, to actual concentrations. In anticipation of this, as outlined in the procedure, magnesium acetate was added to all standards and samples before analysis to buffer the ionic strength. For the 6 standards, the ionic strength "I" was calculated to range from 0.346 to 0.376, and the corresponding monovalent ion activity coefficients "f_i", calculated from the Davies equation (Equation 1), ranged from 0.687 to 0.683 respectively. The added magnesium acetate was assumed to also be the dominating contributor to ionic

strength in the samples. This is a reasonable assumption because of the expected similarity in ionic composition of the samples to the standards. Table 2.3 shows that the CF marker ions sodium and chloride are by far the most prevalent ions in sweat, and they are present within the range of the standard calibration. Samples were buffered in the same manner as the standards therefore it should be reasonable to assume the total ionic composition of the samples to be sufficiently similar to that of the standards to apply the same estimated activity coefficients to the sample calculations.

Ion	Sweat Concentration (mM)
Sodium	20 to 80
Potassium	4 to 18
Calcium	0 to 1
Magnesium	< 0.2
Chloride	20 to 60
Bicarbonate	0 to 35
Phosphate	0.1 to 0.2
Sulphate	0.1 to 2.0

Table 2.3 Principal ionic composition of sweat[5].

Converting activity to concentration:

(0.063) / (0.685) = 0.092 M

= Estimated sodium ion concentration for sample #1

Ion activities were similarly estimated for all samples and converted to concentration values. The results are tabulated in Table 2.4.

	Electrode		
Sample	K^+ (mM)	Na^+ (mM)	Cl^- (mM)
1	26.85	92.44	33.81
2	31.38	91.18	36.35
3	36.88	90.84	55.58
4	12.24	42.69	14.64
5	15.55	54.37	18.87
6	31.72	61.86	56.15
7	22.91	32.16	38.89
10	24.33	41.77	26.98
11	25.03	69.69	29.10
12	15.50	22.10	14.23
13	11.56	28.35	10.32
14	23.05	20.95	22.26
15	11.71	42.39	11.02
16	8.40	29.47	8.45
17	20.44	115.03	25.46
18	30.79	84.46	27.73
19	23.83	101.91	33.99
20	22.28	96.32	37.17
21	24.16	96.35	38.37
22	14.57	54.29	15.42
23	12.21	38.35	13.65

Table 2.4 Estimated concentration values for the three ions in each sample. The values are listed as mM concentrations. Once again, the sample numbers' colouration indicates the source population of the sample. Red is for the CF population and green for normal

The analytical performance of the array will be compared later by assessing these array results against the results obtained for the same samples via the reference

analytical techniques. For the moment, however, these results will be discussed in isolation and in assessed in terms of their diagnostic significance.

The marker ions for CF are sodium and chloride. The generally accepted diagnostic thresholds are 50mM sodium and 60mM chloride, above which is considered positively diagnostic of CF[6]. These values are, however, only valid for children. Sweating rates increase with maturity, which means that there is less time for reabsorption of ions in the sweat glands of healthy adults; therefore the sweat ion concentrations are higher. It is now accepted that due to increased sweating rates in adulthood, the threshold values used for children are not applicable to adults[7]. A higher threshold for both marker ions of 80 mM is recommended therefore to separate normal and CF adults[8,9]. In this study, all of the normal samples were taken from an adult population. For the normal samples therefore; a sodium and or chloride concentration of ≥80 mM should be considered diagnostic of CF. The CF population samples were taken from pre-pubescent children, and the Gibson and Cooke thresholds of ≥50 mM sodium and ≥60 mM chloride remain relevant.

Applying these diagnostic thresholds to the array results for sodium and chloride in Table 2.4, the results for sodium appear to be very good, while the chloride results do not. The sodium results correctly classify all samples in terms of the population from whence they came. The chloride results, however, are all lower than expected. Both the normal and CF chloride values are far lower than expected and in terms of the usual thresholds, provide no useful diagnostic information. The fact that all of the chloride values, both CF and normal, are depressed, seems to suggest a chemical interference on the chloride electrode, or some other phenomenon, masking the

chloride ion concentration. If the depression is general and not sample- or population-specific, then the expected separation of CF and normal samples should still be apparent. To investigate this separation, the sample values were projected onto their respective calibration curves, as shown in Figure 2.5, Figure 2.6 and Figure 2.7.

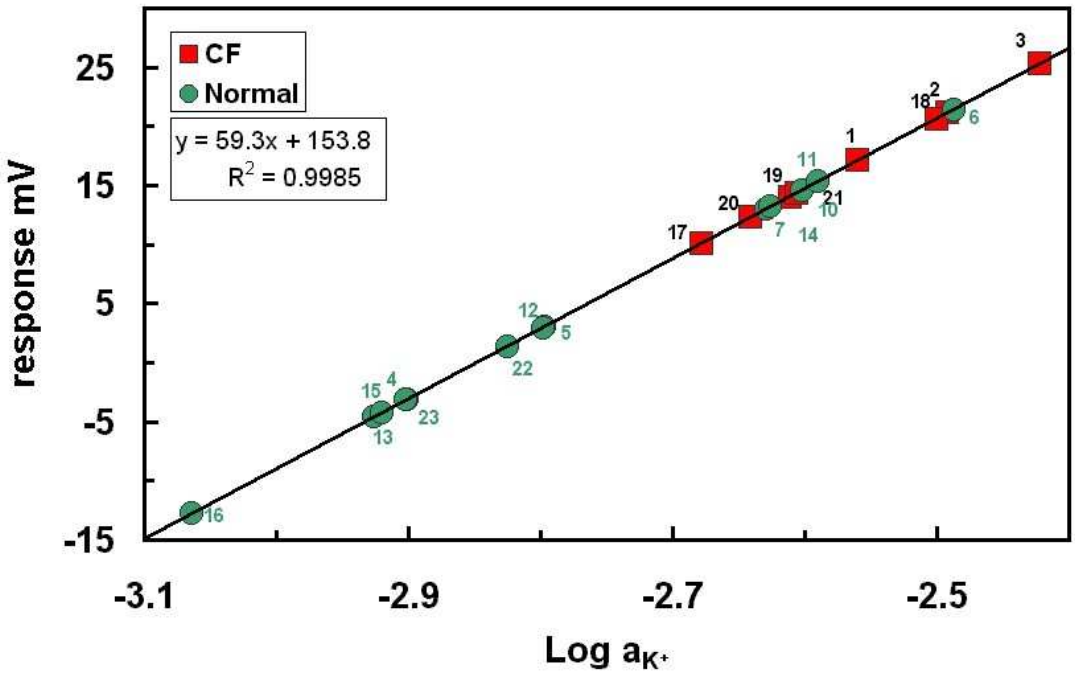

Figure 2.5 This illustrates the degree of separation exhibited by the potassium electrode on the CF positive and normal samples.

In Figure 2.5, the black line is the standard calibration curve. The green circles represent the potassium ion activities measured for the normal samples, and the red squares represent the CF samples. Potassium is not a marker ion for CF, so there is a certain amount of overlap, but there appears also to be a good degree of separation of the two sample populations. The CF samples are clustered in the upper half of the curve and 8 out of 13 of the normal samples are well separated from the CF ones. Potassium may provide some complementary diagnostic info therefore as part of a total array response.

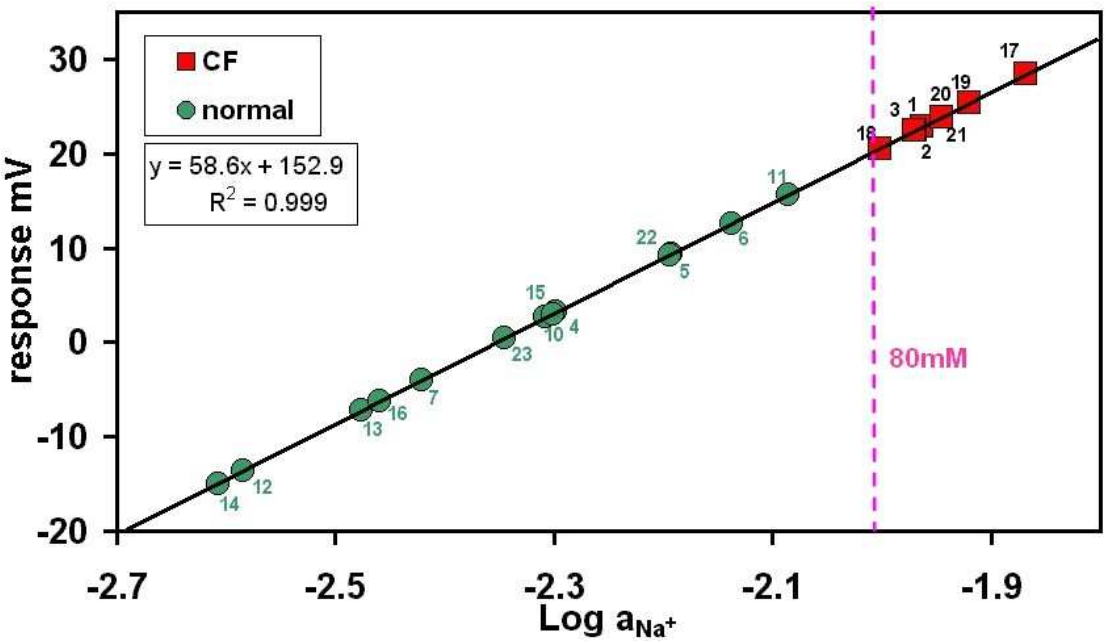

Figure 2.6 This illustrates the degree of separation exhibited by the sodium electrode.

Figure 2.6 clearly shows that the separation is much better for the sodium results. There is no overlap of positive and negative sample populations. The CF samples, indicated by the red squares are all tightly clustered together. The normal samples are more spread out but, as seen in Table 2.4, the normal values all fall below the 80mM threshold (log a_{Na}^{+} = -2.09), so they are all firmly diagnosed as negative, and the CF samples are all above the threshold. The sodium electrode therefore exhibits 100% diagnostic success for both the CF population and the normal population samples.

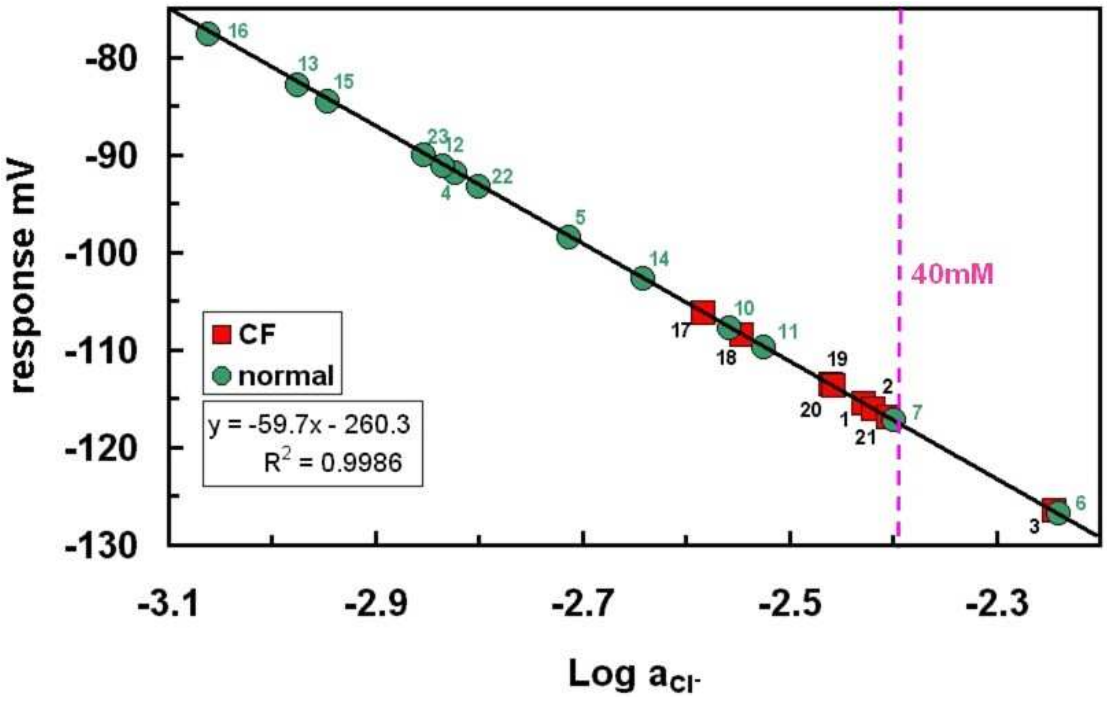

Figure 2.7 Here we see the degree of separation achieved on the chloride results alone.

As seen in Table 2.4, the chloride responses, illustrated graphically in Figure 2.7, are all considerably lower than the expected normal and usual CF values. Traditionally, chloride is considered the better diagnostic indicator because of the usually high degree of separation between positive and negative samples. Normal samples are usually expected to have a chloride concentration of less than 40 mM (log a_{Cl^-} = -2.39), and CF samples are expected to exceed 80 mM. The data here shows a disappointing degree of overlap between the CF and normal samples. There is still, however, quite a degree of separation. 9 out of 13 normal samples are not overlapping with the CF samples.

Cluster analysis of the array data was carried out with the aid of Dr. Brendan Duffy, using Minitab® software and is presented in Figure 2.8. Based on the array data for

the three ions, the samples were divided into two distinct groups. The CF samples were all grouped together and, with the exception of two samples, the normal samples were also grouped together.

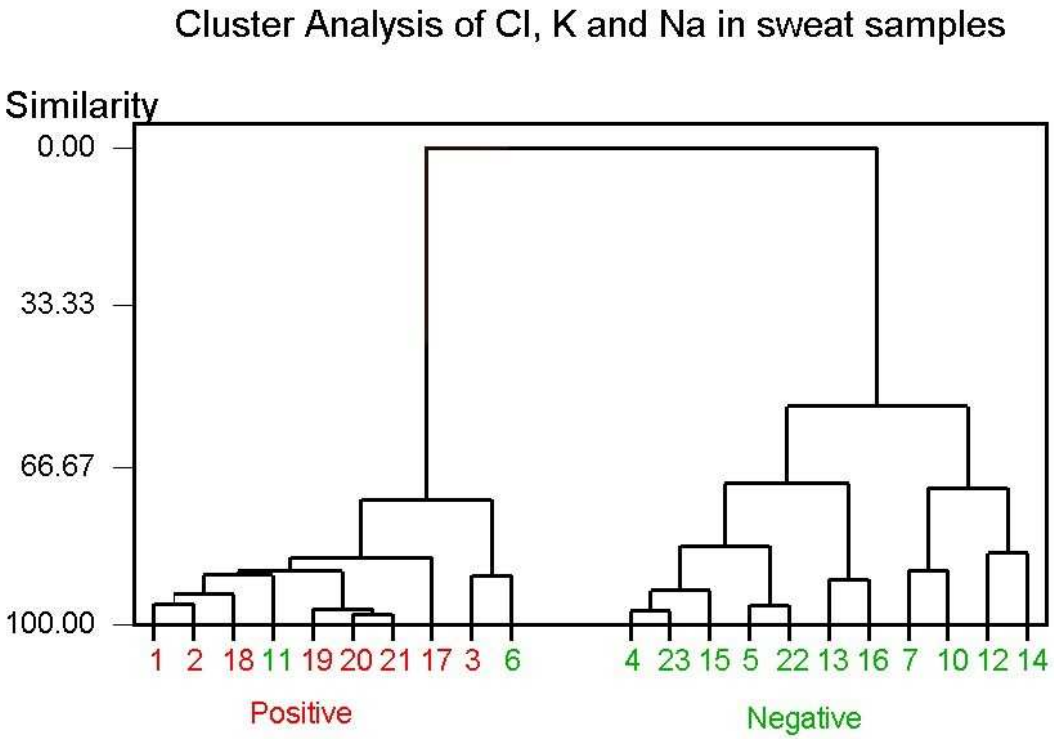

Figure 2.8 Cluster analysis dendrogram for Na, K and Cl in sweat samples, illustrating the separation of the two sample groups. Two of the normal samples (6 and 11) were falsely diagnosed as positive.

The reason for this misclassification of the normal samples 6 and 11 can be explained by closer examination of Figure 2.5, Figure 2.6 and Figure 2.7 which illustrate the degree of discrimination obtained from each of the three sensors, which ultimately contributed to the cluster analysis. Closer examination of these graphs, and indeed of Table 2.4 which lists the actual estimated concentrations, also provides an insight into the reason for the misclassification of the normal samples 6 and 11.

First of all the table and the graphs illustrate why two distinct groups emerge. In broad terms it is possible to say that samples taken from the normal population have lower potassium, sodium and chloride levels than samples taken from the CF population. Samples 6 and 11 were taken from a normal population but the cluster analysis software has grouped them with the CF population samples. Therefore according to the software, samples 6 and 11 are more closely associated with the CF samples than the normal samples. If one calculates mean and standard deviation values for the two populations, the following results are obtained (Table 2.5).

	K^+	Na^+	Cl^-
	Mean (stdev)	**Mean (stdev)**	**Mean (stdev)**
CF	27.08 (5.54)	96.07 (9.20)	36.06 (9.09)
Normal	17.60 (7.01)	41.42 (15.15)	21.54 (13.54)
Sample 6	*31.72*	*61.86*	*56.15*
Sample 11	*25.03*	*69.69*	*29.10*

Table 2.5 Group mean and standard deviation values calculated from the array results. Included for comparison are the values obtained for the cluster analysis misclassified normal samples, 6 and 11.

From this table one can see again that the population means for all three ions are higher for the CF population than the normal population. One also sees that the reason for the misclassification of the two normal samples is because the individual concentrations of the three ions are consistently high relative to the group means. Sample 6 in particular, though taken from a normal population, has a measured

potassium and chloride concentration in excess of the CF group mean. This is further illustrated in Figure 2.5 –samples 6 and 11 are the two highest placed normal samples in terms of potassium concentration; in Figure 2.6 which illustrates the sodium ion concentrations they are again the highest placed samples of the normal population samples; and in Figure 2.7 for chloride, where sample #6 is the highest placed of the normal samples and #11 is the third highest placed. This is what distinguishes the two samples 6 and 11 from the rest of the normal population. From Figure 2.7 sample #7 seems also to be grouped with the CF samples, but this does not lead to an overall misclassification. This is because the contribution from all three ions is taken into account in the cluster analysis, and the sodium ion concentration of sample #7 is low and clearly normal, which associates it with the normal population.

In this case, therefore, the use of an array of three sensors is counter-productive in a diagnostic sense, because the total array response yields two false positives, whereas assessment on the basis of the sodium results alone, yields 100 % diagnostic accuracy.

The poor performance of the chloride electrode was disappointing. Chloride is considered a better diagnostic indicator because the elevation in sweat chloride from CF is generally greater than that for sodium. This results in greater separation and less borderline diagnostic confusion. In all previous work involving standards and simulated samples the chloride response was as expected. Sweat is primarily a dilute saline solution so it seemed unlikely that some sweat-based component was causing the chloride electrode interference. The apocrine sweat glands, e.g. in the underarms release a thicker, yellowish, sweat secretion containing fatty acids and proteins as well as the usual electrolytes, but the primary thermoregulatory sweat glands, the eccrine

(or merocrine) glands, as found on the forearms and from where sweat was sampled in this study, secrete only an aqueous dilute electrolyte solution in which sodium and chloride are the primary ions. The only other constant to affect all samples is the pilocarpine nitrate used in the generation of the sweat samples by stimulation of the sweat glands. Anion-sensitive membranes based on organic ammonium ions (such as the SendX® chloride electrode, which is based on the ion exchanger tridodecylmethylammonium chloride (TDMAC)), follow a selectivity pattern described by the Hofmeister series (Table 2.6)[10].

ClO_4^- > SCN^- > I^- > Sal^- > NO_3^- > Br^- > Cl^- > HCO_3^- > OAc^- > SO_4^{2-} > HPO_4^{2-}

Table 2.6 Hofmeister Series. Decreasing lipophilicity from left to right

The nitrate ion therefore is a potential interferent on the chloride electrode response, and sample contamination from the pilocarpine nitrate may be the source of this interference. The SendX® array of course is designed for blood analysis, where nitrate interference is not expected. Fluka selectophore documentation provides selectivity coefficients for a similar TDMAC based solvent polymeric membrane cocktail for chloride activity determination in whole blood and serum. A $LogK^{Pot}_{Cl^-,NO_3^-}$ = 0.56 is quoted[11] (mixed solution method at 115 mM NaCl, 5 mM KOAc, 35 mM NaOAc) which suggests an electrode nitrate response that is 3 to 4 times greater than its response to chloride. The expected concentration chloride in blood is ca 115 mM, nitrate is not a major component of blood; therefore this preferential response to nitrate would not pose a problem in blood analysis. However, in this study nitrate

interference is an issue. A series of simple experiments were carried out therefore to investigate the effect of the nitrate ion on the SENDX(R) chloride electrode, and also to investigate the effect of the pilocarpine nitrate contained in the pilogel disks to the chloride response of the electrode.

In the first experiment, 3 standards solutions containing 40 mM, 50 mM and 60 mM NaCl respectively, were passed through the array, followed by a fourth solution that was 50 mM in NaCl and 50 mM in KNO_3. The real-time analytical trace is shown in Figure 2.9.

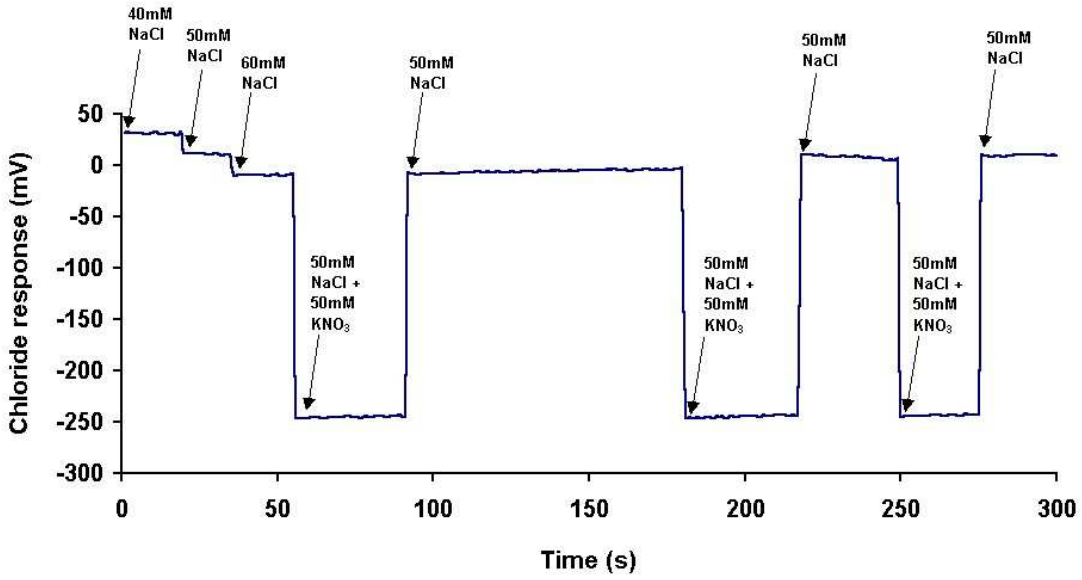

Figure 2.9 Analytical trace showing the mV response of the chloride electrode to the series of solutions as illustrated. Data capture was paused during solution changeover. Clearly the electrode is responding normally to the increasing chloride concentration, and then there is a huge change in the electrode response to the presence of similar concentrations of nitrate ion. The 50 mM NaCl solutions with and without nitrate present were re-analysed to illustrate the reproducibility of the nitrate response.

The chloride electrode clearly responds very strongly to the presence of nitrate. In a second experiment, three more NaCl standard solutions were made up that were 40, 60 and 80 mM in NaCl. Into the 60 mM standard was placed a fresh pilogel disc, which had been ground to a paste using a pestle and mortar. The mixture was sonicated for 5 minutes and then filtered. The 40 mM NaCl standard was passed thorough the array in the usual fashion, followed by the 80 mM standard, and then the filtrated solution from the 60 mM standard sonicated with the pilogel disc. The analytical trace is shown in Figure 2.10

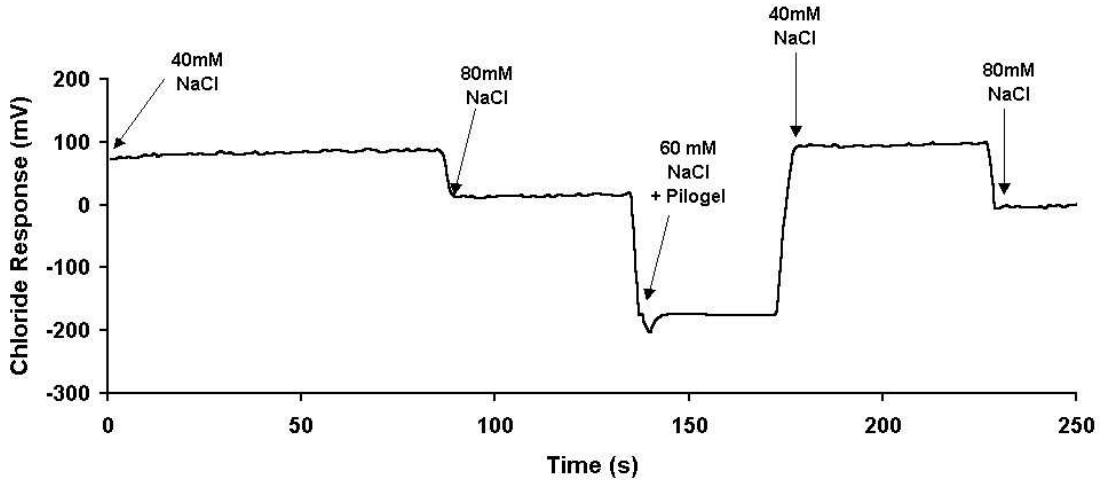

Figure 2.10 The trace shows the response of the chloride electrode to 40 mM and 80 mM standard solutions of NaCl, and then its response to a 60 mM standard after sonication with a pilogel disc (0.5% pilocarpine nitrate)

The trace clearly shows a large response to the pilogel infused sample, which may be attributed to nitrate from the disc. These experiments seem to suggest that the nitrate ion, which is the pilocarpine counter-ion present in the pilogel disc formulation, may indeed be the cause of the chloride electrode interference. Pilocarpine iontophoresis is the standard method of sweat stimulation and is unlikely to change; therefore the

investigation of other chloride electrode formulations that are less susceptible to interference from nitrate ion, or the use of other pilocarpine formulations where nitrate is not the counter-ion, are pointers for the future.

Reference methods

As described earlier, ion chromatography (IC) and atomic absorption spectroscopy (AAS) were used as reference methods to compare to the sample concentrations calculated from the array data. The calibration curves obtained from these two reference methods for each of the ions under investigation are illustrated below in Figure 2.11 to Figure 2.15. These calibration curves were also used to calculate sample concentrations and the results obtained by the two reference methods were tabulated alongside the results from the array for comparison purposes – see Table 2.7

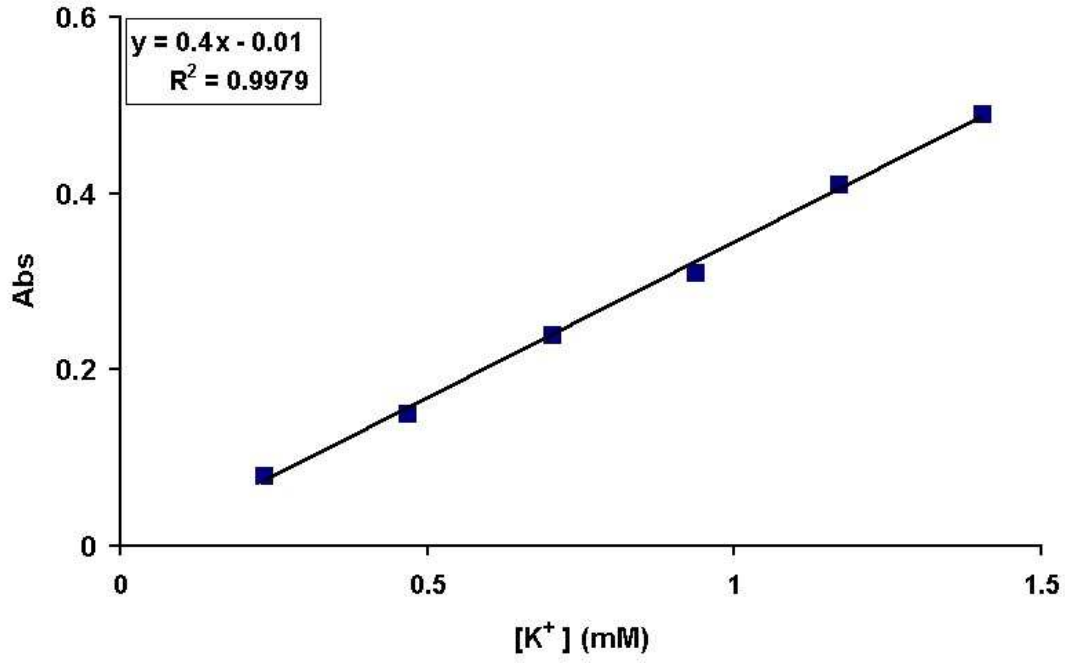

Figure 2.11 AAS Calibration curve for potassium

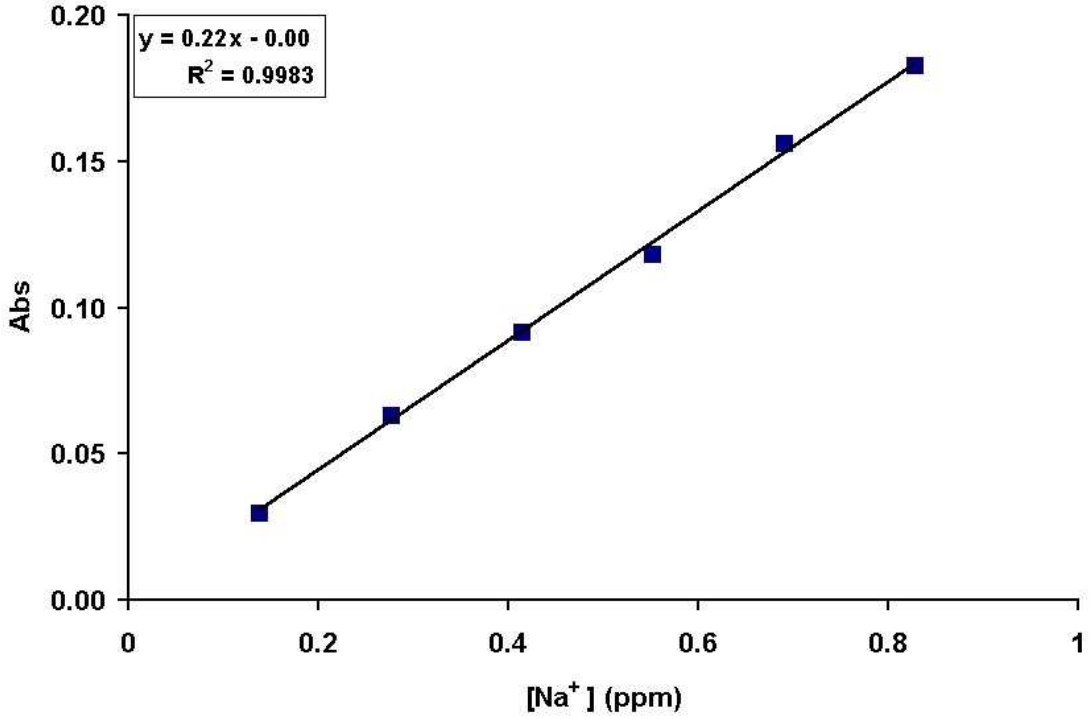

Figure 2.12 AAS Calibration Curve for Sodium

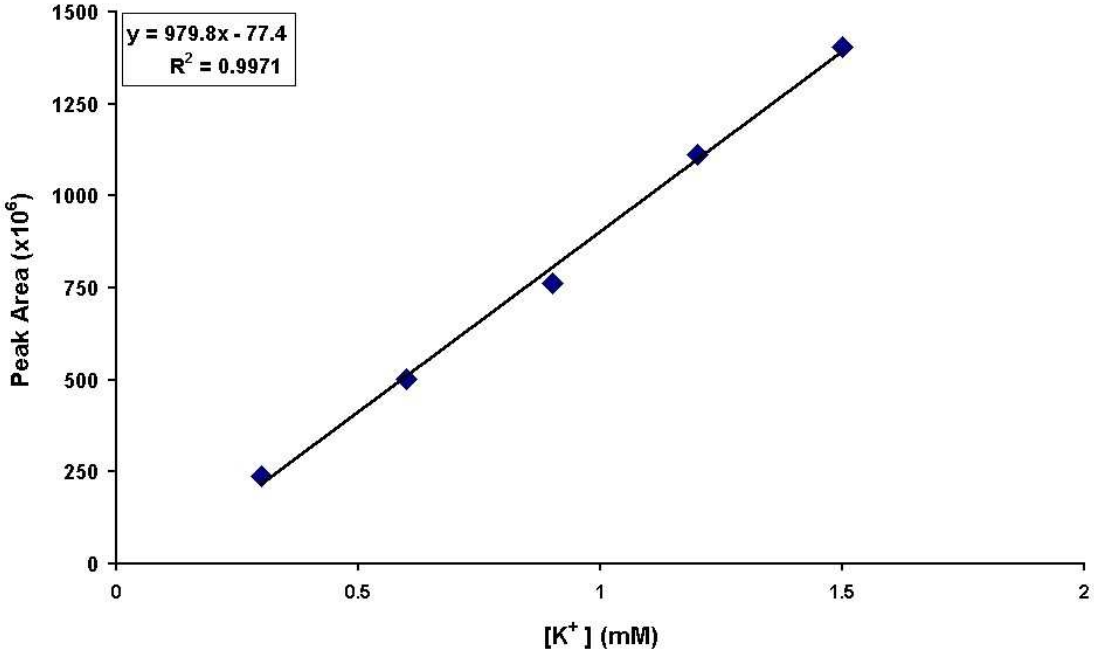

Figure 2.13 IC calibration curve for potassium

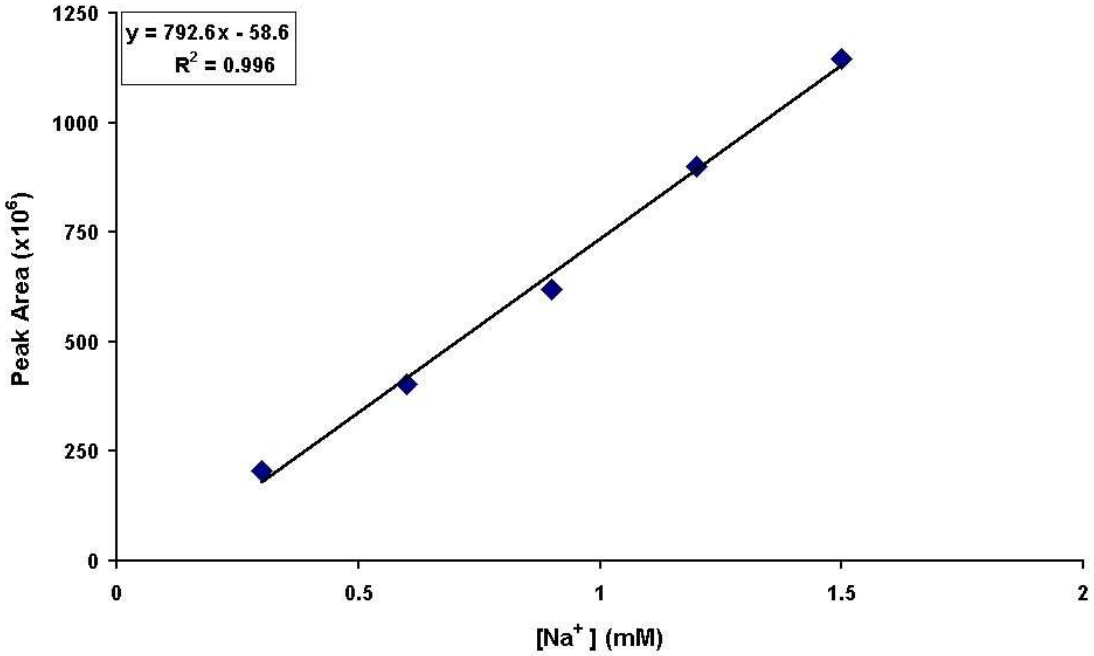

Figure 2.14 IC calibration curve for sodium

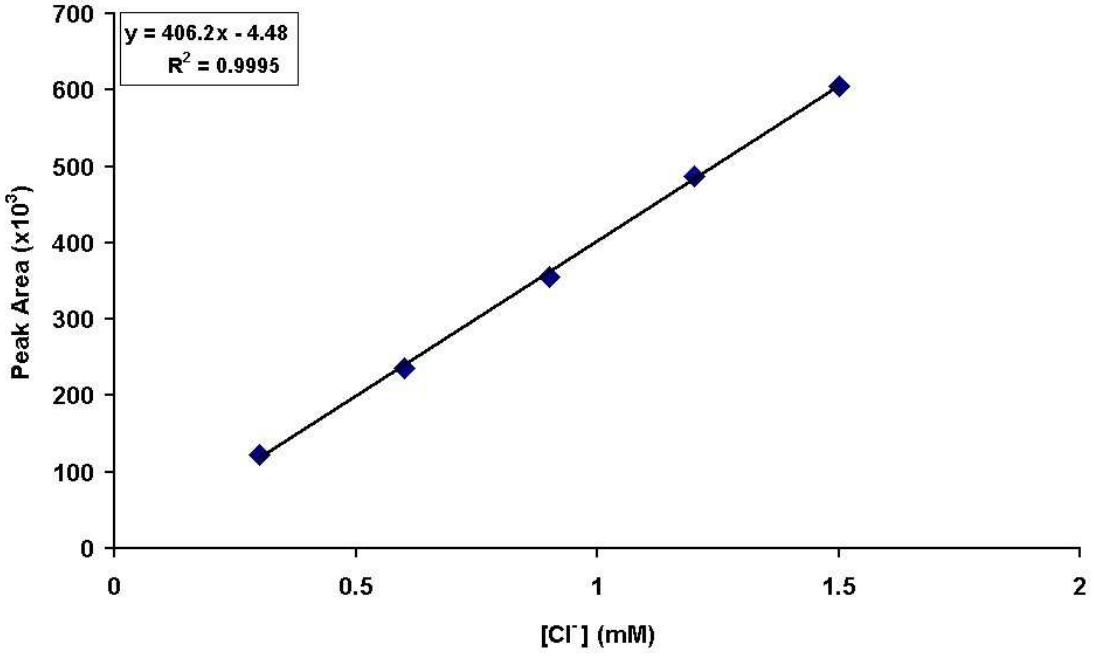

Figure 2.15 IC calibration curve for chloride

	K+				Na+				Cl-			
	Array (mM)	Ref. (mM)		Error (abs)	Array (mM)	Ref. (mM)		Error (abs)	Array (mM)	Ref (mM)		Error (abs)
1	26.85	24.14	(AAS)	2.71	92.44	95.10	(AAS)	-2.66	33.81	101.62	(IC)	-67.81
2	31.38	28.96	(AAS)	2.42	91.18	93.43	(AAS)	-2.25	36.35	78.32	(IC)	-41.97
3	36.88	36.21	(AAS)	0.68	90.84	95.14	(AAS)	-4.30	55.58	90.47	(IC)	-34.89
4	12.24	12.07	(AAS)	0.17	42.69	40.11	(AAS)	2.58	14.64	15.58	(IC)	-0.95
5	15.55	14.48	(AAS)	1.07	54.37	43.49	(AAS)	10.88	18.87	2.17	(IC)	16.71
6	31.72	28.96	(AAS)	2.76	61.86	61.72	(AAS)	0.14	56.15	12.27	(IC)	43.88
7	22.91	24.14	(AAS)	-1.23	32.16	36.77	(AAS)	-4.60	38.89	18.26	(IC)	20.64
10	24.33	16.90	(AAS)	7.43	41.77	43.30	(AAS)	-1.53	26.98	-	(IC)	-
11	25.03	19.31	(AAS)	5.72	69.69	65.20	(AAS)	4.49	29.10	23.32	(IC)	5.77
12	15.50	14.48	(AAS)	1.02	22.10	21.75	(AAS)	0.35	14.23	43.21	(IC)	-28.97
13	11.56	12.07	(AAS)	-0.51	28.35	28.40	(AAS)	-0.05	10.32	-	(IC)	-
14	23.05	19.31	(AAS)	3.74	20.95	20.10	(AAS)	0.85	22.26	-	(IC)	-
15	11.71	7.24	(AAS)	4.47	42.39	48.34	(AAS)	-5.95	11.02	-	(IC)	-
16	8.40	9.65	(AAS)	-1.25	29.47	31.78	(AAS)	-2.31	8.45	-	(IC)	-
17	20.44	19.92	(IC)	0.52	115.03	128.22	(IC)	-13.19	25.46	97.59	(IC)	-72.12
18	30.79	26.80	(IC)	3.99	84.46	83.41	(IC)	1.05	27.73	85.68	(IC)	-57.95
19	23.83	22.90	(IC)	0.94	101.91	95.11	(IC)	6.80	33.99	112.53	(IC)	-78.53
20	22.28	19.99	(IC)	2.29	96.32	98.00	(IC)	-1.68	37.17	117.30	(IC)	-80.13
21	24.16	19.27	(IC)	4.88	96.35	93.33	(IC)	3.02	38.37	88.54	(IC)	-50.17
22	14.57	15.15	(IC)	-0.58	54.29	55.90	(IC)	-1.61	15.42	30.04	(IC)	-14.62
23	12.21	12.79	(IC)	-0.58	38.35	40.15	(IC)	-1.80	13.65	33.47	(IC)	-19.83
mean	27.08	24.77		1.94	96.07	97.72		-0.56	36.06	96.50		-28.81
stdev	5.54	5.77			9.20	13.06			9.09	13.44		
Mean	17.60	15.89			41.42	41.31			21.54	22.29		
stdev	7.01	5.92			15.15	14.06			13.54	13.04		

Table 2.7 Comparison of the estimated concentrations calculated from the array data, with the "true" concentrations calculated from the reference methods' data. For each ion the array value and reference value is listed, along with the reference method used to analyse the sample, and the absolute error is also quoted. As before, the coloration indicates the population from the sample was taken – red for CF and green for normal. The population means and standard deviations as well as the mean error values were also calculated and listed in the lower half of the table at the foot of each column of data. Five of the samples (10 & 13-16) could not be analysed for chloride by any reference method due to instrumental difficulties.

Table 2.7 compares the array results with the reference methods used. For diagnosis, a sodium concentration greater than or equal to 80 mM is considered a positive indication of CF. All of the CF samples are above and all of the normal samples fall

below this threshold for both the array and the reference methods. Diagnostic accuracy is therefore 100% and diagnostic agreement between the array and the reference methods is also 100 %. The analytical accuracy of the sodium electrode appears also to be acceptable with, in general, excellent agreement between the calculated array sodium concentrations and the "true" reference values (mean absolute error of -0.56 mM).

The chloride diagnostic threshold is 60 mM, above which is suggestive of CF. From the reference (IC) data we can see that, diagnostically, 100% accuracy is again achieved and we can see the magnitude of the separation between normal and CF samples. All of the CF samples show a chloride concentration of over 80 mM and all of the normal samples are below 50 mM. The population means also show that the separation for chloride is greater than for sodium. Unfortunately, the apparent pilocarpine nitrate interference on the chloride electrode means that the quality of the chloride data from the array is poor and the agreement between the array and reference results is poor.

Besides this, however, the array results for potassium appear to be in good agreement with the reference methods. Although potassium is not a diagnostic indicator for CF, from the population mean values, CF-related elevation in sodium and chloride levels appears to be accompanied by a general increase above normal of potassium concentration. Potassium levels therefore may provide useful information in terms of an overall array response, or as an internal marker to confirm diagnosis.

2.4 Conclusions

Overall the results obtained were very encouraging. The SendX® device was purpose designed and built for a very specific and very different application, i.e. whole blood analysis, but it was adapted here for the diagnosis of CF, with some degree of success. A custom designed unit could incorporate a number of platform improvements to address the compromises inherent in the use of a device not specifically designed for the application: the size of the array and subsequent dead volume, required dilution of the sweat samples; the fact that most of the sensors in the array are superfluous for this application. The interference exhibited by the chloride electrode is also problem for this application, but not in blood analysis of chloride levels as blood should certainly not contain appreciable levels of nitrates. The sodium and potassium electrodes performed much better, with excellent accuracy exhibited by both sensors, diagnostically and analytically, comparing well with much more sophisticated, much more expensive bench top instruments such as AAS and IC. Also the ability of a miniature array, such as this, to analyse multiple ions at once with similar levels of accuracy to the 2 larger instruments, is impressive. Overall (with the exception of chloride) the errors are small, given the differences in the two methods. Clearly, the array approach offers comparable results in a much more compact, portable instrument. It was not possible to run replicates owing to the small volume of the samples gathered, but the precision of the method is evident from the quality of the data.

Portable instruments capable of rapid multi-component analysis can be produced by coupling sensor arrays to portable PCs fitted with data acquisition cards. This

configuration, in conjunction with the Labview software development environment enables portable analytical instruments to be rapidly customised for particular applications. This approach has been employed for the rapid diagnosis of cystic fibrosis with an encouraging degree of success, despite interference by nitrate on the chloride electrode response. The integration of the sampling and measurement process into a single miniaturised unit that can be used at point-of-need is desirable. The lifetime of the devices is excellent. For example, the array used in this was still functioning after approximately 3 months of regular use, with no noticeable decrease in performance. The coupling of such portable sensor-based analytical instruments with rapidly developing wireless (rf or Bluetooth®) communications technologies presents the exciting prospect of much more compact autonomous sensing systems, which are capable of making sophisticated analytical measurements for extended periods of time at point-of-need without human intervention[12].

2.5 References

1 C. Davies, Ion Association, Butterworth London 1962

2 J. Weiß, S, Reinhard, C. Pohl, C. Saini, L. Narayaran; Journal of Chromatography, 1995, 706, 81-92

3 C. Saini, C. Pohl, L. Narayaran; "An improved ion exchange phase for the determination of fluoride and other common anions by ion chromatography." Presentation at Pittsburgh Conference, New Orleans, LA, USA, 1995.

4 H. Small; Ion chromatography, New York: Plenum Press, 1989

[5] Oxford Textbook of Sports Medicine; Ed's: M. Harries, C. Williams, W.D. Stanish, L.J. Micheli, New York Oxford University Press, 1994.

[6] L.E. Gibson, R.E. Cooke; Pediatrics, 1959, 23, 545-549.

[7] B.J. Rosenstein; Clinics in Chest Medicine; 1998, 19, 423-441

[8] J.M. Kirk, M. Keston, I. McIntosh, S.A. Essa; Annals of Clinical Biochemistry, 1992, 29, 145-152

[9] S.K. Hall, D.E. Stableforth, A. Green; Annals of Clinical Biochemistry, 1990, 27, 318-320

[10] W.E. Morf, "The Principles of Ion-Selective Electrodes and of Membrane Transport"; Elesevier 1981; p213

[11] H.J. Marsoner, Chr. Ritter, M. Ghahramani; TFCC Workshop, Helsinki, 1985.

[12] K. MacAteer, D. Raftery, D.Diamond; Trends in Food Science and Technology, 2000, 11, 291-295.

Chapter 3

3 CF Watch

3.1 Introduction

This chapter follows the steps taken in the development of a wearable, watch-type device for the rapid on-line diagnosis of Cystic Fibrosis (CF). It was to be based on the standard, and universally accepted Gibson and Cooke sweat test[1], which has been in existence since the 1960's and is still regarded as the gold standard test for CF as well as being one of the most reliable tests in modern medicine[2]. The device was designed to be compatible with modern, commercially available, and widely used, sweat sampling equipment, and the construction of the sensors was based on tried and tested formulae to ensure reliability in the finished prototype. A number of different materials were assessed in the construction of the device, and compatibility of materials as well as assessment of the devices at various stages of production involved a number of surface visualisation techniques from bench-top microscopy to scanning electron microscopy. A test-well was also constructed to facilitate construction and testing of the sodium and chloride sensor designs and to assess their performance against a standard reference electrode.

Finally a working 2-sensor prototype was constructed consisting of one miniature sodium PVC membrane electrode and one Ag/AgCl electrode. The Ag/AgCl electrode takes the place of the usual standard reference electrode, i.e. an electrode that would not, by definition, respond to changes in the concentration of the sample.

The Ag/AgCl electrode, however, was expected to respond to changes in the chloride concentration, but in the opposite "direction" to that of the sodium ISE. Both electrodes therefore would be contributing to the overall cell potential E_{cell} where:

$$E_{cell} = E_{Na+} - E_{Cl-}$$

It was hoped that this arrangement would provide the optimal discrimination of monitoring both of the CF marker ions, while using the minimum number of sensors.

Following testing, a prototype working device was employed in a clinical trial involving the analysis of real sweat samples from a confirmed CF population and a normal population to assess its usefulness as a possible real-world diagnostic / screening device.

3.2 Equipment and Reagents

3.2.1 Equipment

Prototype devices were constructed in-house using a CAT3d drilling and milling machine. Membrane and sub-membrane solutions were deposited using WPI glass micro-litre syringes compatible with an Ultra Micro Pump II syringe pump and micromanipulator also obtained from WPI (World Precision Instruments www.wpiinc.com.). Sub-membrane hydrogel solutions were cured using an ELC403

UV-Light Curing Gun manufactured by the Electro-Lite Corporation (43 Miry Brook Road, Danbury, CT, USA) and purchased from Edmund Scientific www.edsci.com. Visualisation and inspection of devices and of dispensed layers before, during and after dispensing and post-curing etc, was carried out using a standard bench top microscope with a black and white camera attachment (obtained from WPI), linked to a PC to allow microscopic image capture. Scanning Electron Microscopy was carried out using a Hitachi S3200N SEM microscope.

3.2.2 Materials and reagents

Substrate plastics (PVC, Perspex, and Polycarbonate) and silver wire (0.5 mm diameter) were all obtained from Goodfellow GmBH (www.goodfellow.com). The sodium ionophore (4-tert-Butylcalix[4]arene-tetraacetic acid tetraethyl ester) was synthesised and purified in-house by Dr. Kieran Nolan. Reagent grade (99.8% pure) NaCl and $AgNO_3$ were purchased from Fluka. Acrylamide, TEMED (N,N,N',N'-Tetramethylethylenediamine), N'N"-methylene-bis-acrylamide, Glycerin, and (-)-Riboflavin were all electrophoresis grade and were purchased from Sigma-Aldrich. Selectophore® grade Potassium tetrakis(4-chlorophenyl) borate (KTpCIPB), 2-nitrophenyl octyl ether (2-NPOE), high molecular weight PVC, and cyclohexanone were purchased from Fluka. Sodium hypochlorite (NaOCl, 10-13% active chlorine) was purchased from Sigma-Aldrich. Silver-loaded epoxy was purchased from Loctite.

Sodium Sub-Membrane Solution

A salt-doped polyacrylamide hydrogel was utilised as the sodium sub-membrane solution. Hydrogels are polymeric materials with the ability to swell and absorb appreciable quantities of water without dissolving and to retain the water within their polymeric structure. They leave no residue, they are repositionable, relatively non-drying and they make a firm electrical contact[3]. They have been used successfully in place of internal filling solutions in similar solid-state devices such as are employed here[4]. Polyacrylamide gels are also used in protein and nucleic acid electrophoresis for the separation of macromolecules. TEMED (N,N,N',N'-Tetramethyl ethylene-diamine) is used as an accelerator for free radical polymerisation and N'N"-methylene-bis-acrylamide is employed as a cross-linking agent. Glycerol is present as a water-soluble hydrating agent, while riboflavin functions as a depolariser in membranes[5]. The chemical structures of these additives are given in Figure 3.1. Ammonium persulphate is often added as an initiator in the production of polyacrylamide gels but it was more convenient here to dispense the mixture as an unpolymerised solution and to photo-initiate polymerisation *in situ* using ultra violet light (described in Figure 3.2 and Figure 3.3).

1 g of acrylamide monomer, 5 g of $1x10^{-3}$ M NaCl (saturated with $AgNO_3$), 15 µl of TEMED, 0.2 g of N'N"-methylene-bis-acrylamide, 0.004 g of Riboflavin, and 5 g of glycerol were mixed together thoroughly in an aluminium-foil-covered vial. The purpose of the foil was to prevent photo-initiation of polymerisation by ambient light. The clear yellow solution was stored at 4 °C until required.

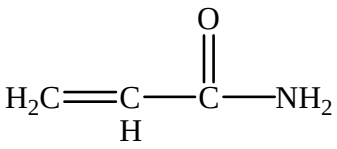

Acrylamide

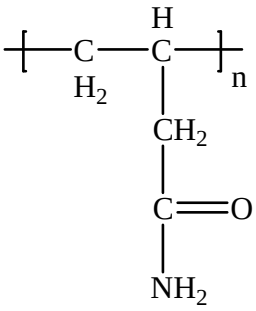

Polyacrylamide

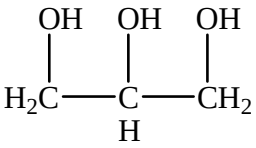

Glycerol

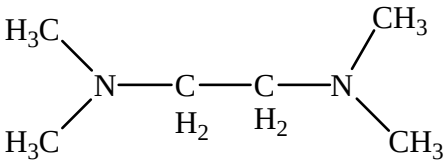

N,N,N',N',-Tetramethylethylenediamine (TEMED)

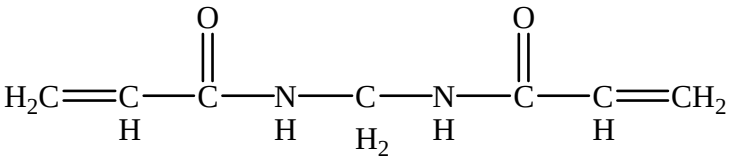

N,N'-Methylenebisacrylamide

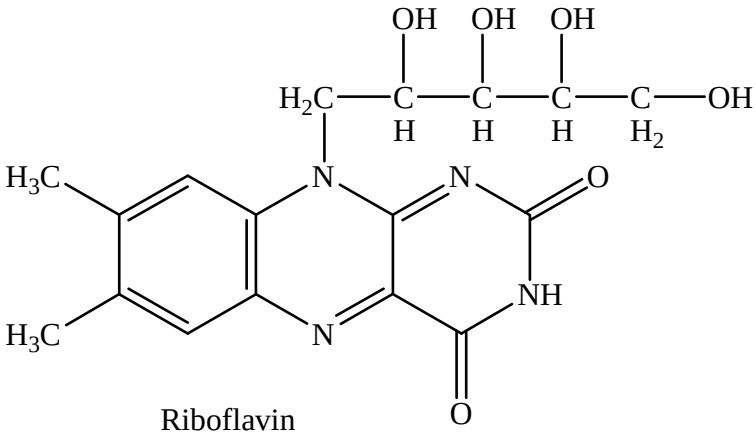

Riboflavin

Figure 3.1 Sodium submembrane solution components and their structures

Sub-membrane hydrogel polymerisation mechanism

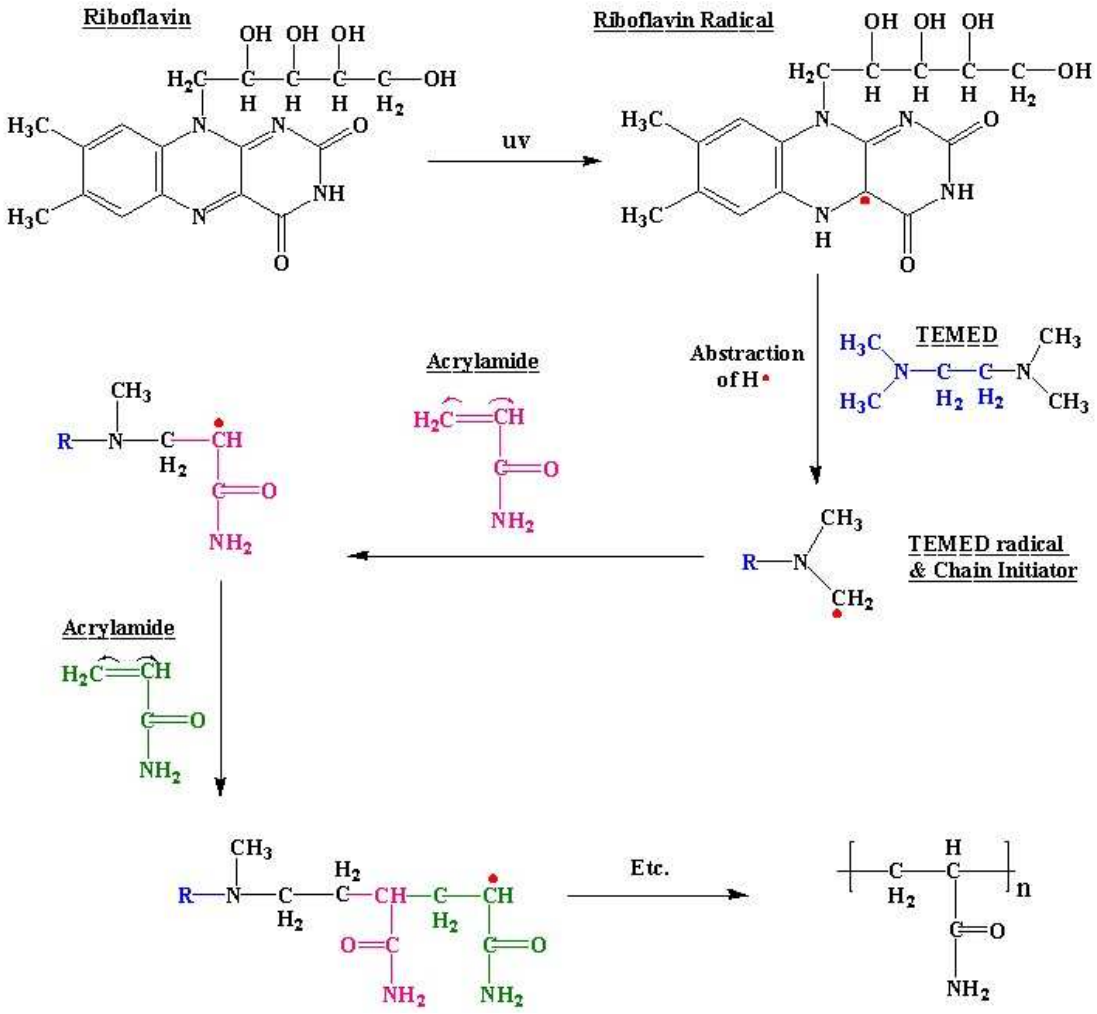

Figure 3.2 Light sensitive riboflavin molecule interacts with ultra-violet light to form riboflavin radicals. These radicals attack the TEMED molecules, removing a hydrogen atom to form a TEMED radical, which initiates the acrylamide polymerisation reaction to form long chains of polyacrylamide.

Cross-linking

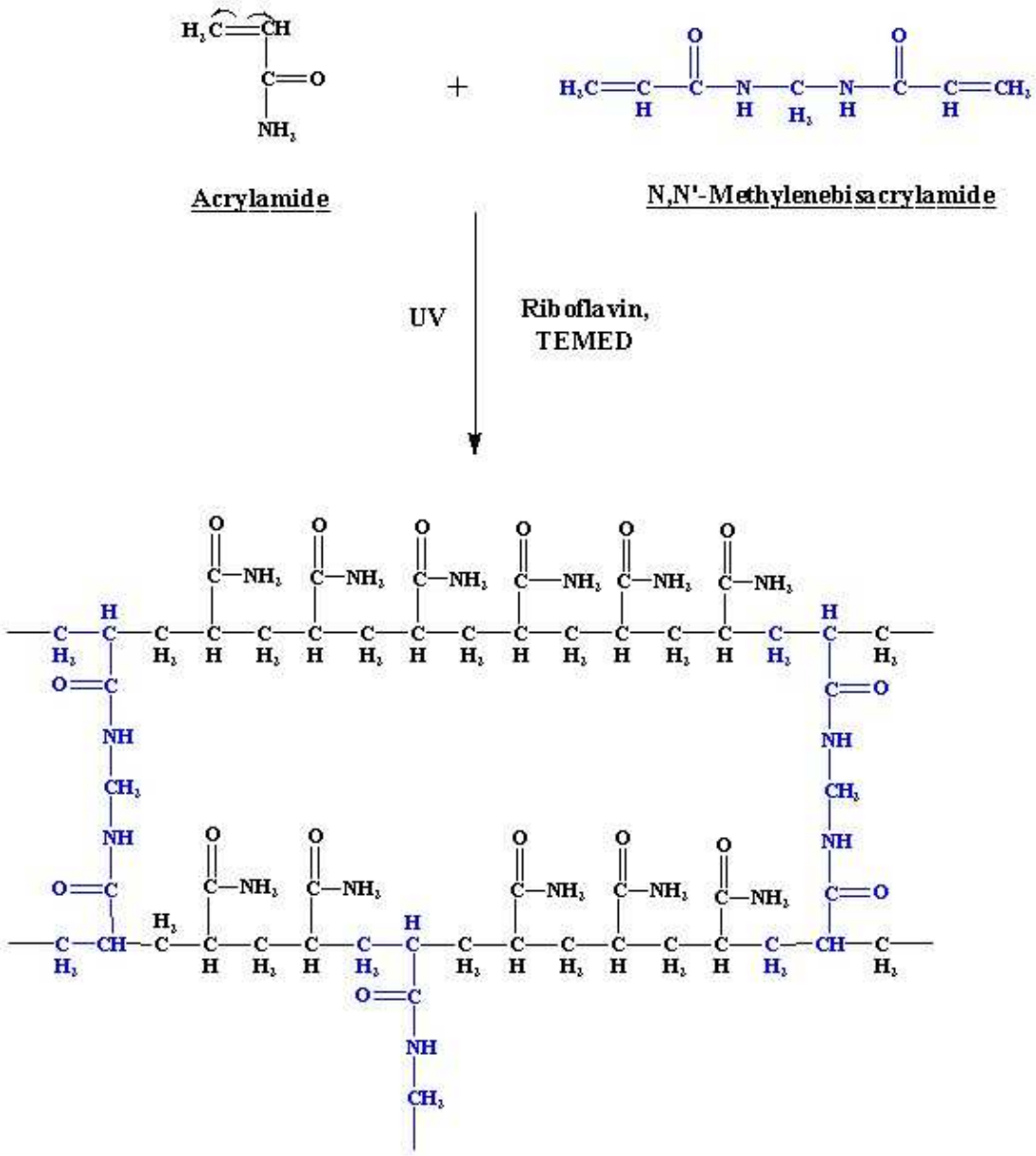

Figure 3.3 N'N"-methylene-bis-acrylamide, the cross linking agent, is almost like two acrylamide monomer groups stuck together. It has a reaction-propagating carbon-carbon double bond at both ends, which serves to link neighbouring chains together as they form, as illustrated here.

PVC Membrane

10 mg ionophore and 2 mg ion exchanger (KTpClPB) were dissolved in 1g plasticiser (2-NPOE). 0.5 g of high relative molecular mass PVC was added to produce a slurry. 3-5 ml of cyclohexanone solvent was then added and the mixture allowed sit overnight with stirring to allow complete dissolution. The resultant clear solution was then refrigerated at 4 °C until it was required. THF was initially used as solvent but was found to be problematic during the PVC membrane solution dispensing stage as it evaporated too quickly leading to clogging of the microsyringe needles. Cyclohexanone, another solvent commonly quoted for the preparation of PVC membranes and less volatile than THF, was employed and the problem was resolved with no noticeable effect on the performance of the membranes.

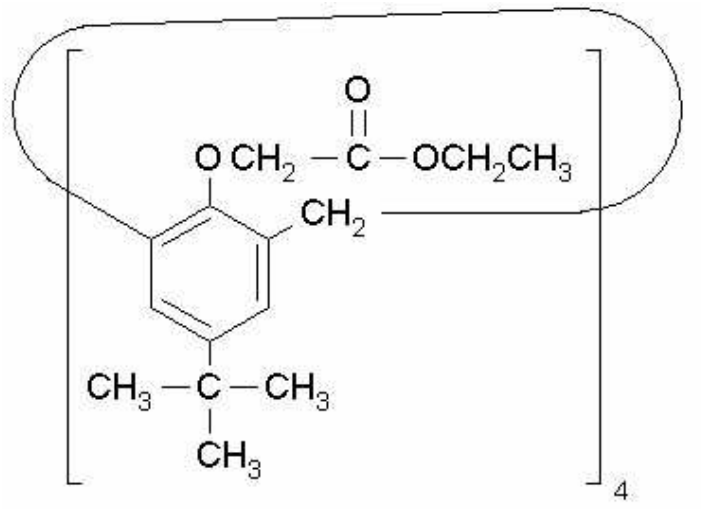

4-tert-Butylcalix[4]arene-tetraacetic acid tetraethyl ester

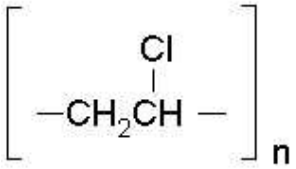

Poly (vinyl chloride)

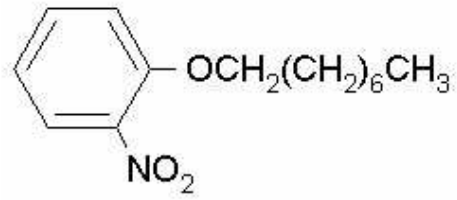

2-Nitrophenyl octyl ether

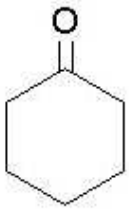

Cyclohexanone

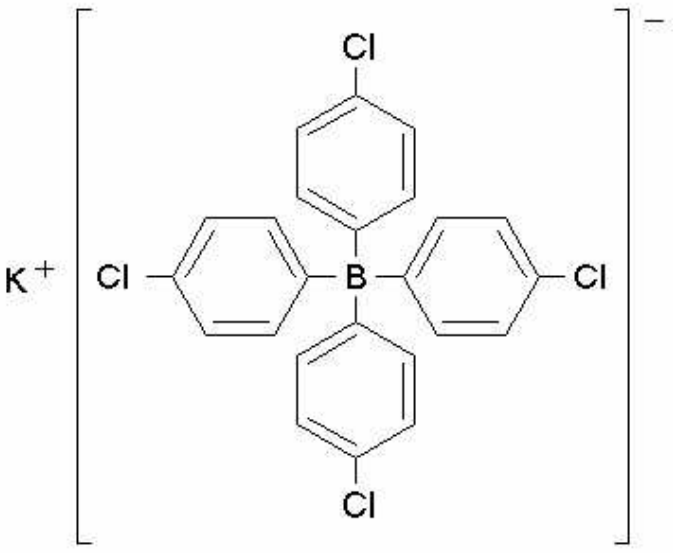

Potassium tetrakis (4-chlorophenyl) borate

Figure 3.4 PVC Membrane components and their structures

3.3 Watch design

The physical design of the analytical device was to be based around the Wescor Macroduct sweat collection system, with which it was to be compatible. The Macroduct, pictured here again in Figure 3.5, is available commercially, and is a very simple and reliable method of liquid sweat collection[6,7] and has been accepted by the scientific and CF community for use as a sweat collection device.

Figure 3.5 Wescor Macroduct Sweat Collection System (image reproduced from www.wescor.com) as used and described previously. The cut-away shows the Wescor device, which is the size and shape of a wristwatch. The arrow points to a small hole in the underneath of the device through which the sweat enters the coiled capillary tubing where it is collected.

As seen in Figure 3.5, a capillary hole in the underneath of the Macroduct allows the sweat, which has been stimulated by pilocarpine iontophoresis to collect in the coiled tubing with minimal evaporation. In its intended guise the Macroduct therefore is a sweat sample collection device. When the tubing is full, sampling is ceased and the

sample is removed from the device for analysis. Equally however, the same device could potentially be used in a sample delivery mode. By using the length of capillary tubing as a sample delivery line to an appropriate flowcell analytical device, and utilising the sweat glands as a bio-pump to pump the samples through the flowcell, the Macroduct adopts the role of sample collection and delivery.

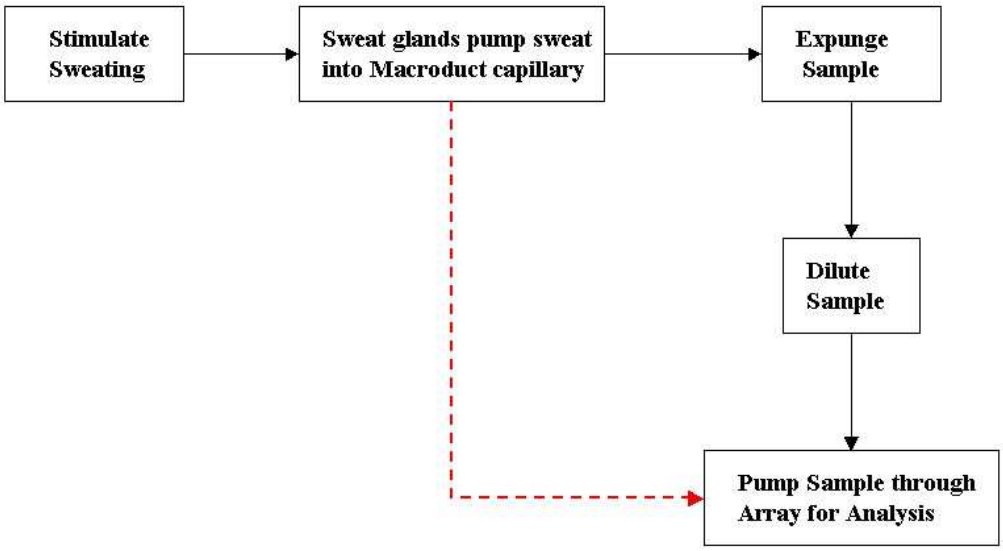

Figure 3.6 Flowchart 1

Figure 3.6 shows a flowchart for the basic analytical procedure followed in the previous chapter's clinical trial using the SendX® array. It also shows how the CF watch device could simplify the procedure. The 5 basic steps of the original procedure and their sequence may be followed via the solid black arrows in the flowchart. The procedure, however, can be short-circuited and simplified considerably, as indicated by the dashed red arrow, by bypassing the intermediate sample-handling steps between sample collection and sample analysis. Essentially the original procedure requires each sample to be expunged from the length of

capillary tubing (in the Macroduct) into which it has been pumped by the sweat glands, only for it to be re-injected into another piece of capillary tubing shortly afterward and pumped into the sensor array flowcell for analysis. The reason for this is that the Macroduct and the array could not be linked to each other directly because they were not compatible due to excessive dead volume demands. The Macroduct allows the collection of up to 75 µl of sweat, but often sample volumes as low as 15µl only are collected. The dead volume of the SendX® array is too large therefore at >40 µl. The SendX® array, however, is a multi-sensor array, and most of the sensors in it are redundant for the CF application. A similar device containing only the relevant sensors (sodium and chloride) could therefore be made much smaller, greatly reducing the dead volume of the analytical device. Quite clearly if a device compatible with the Macroduct could be used, then it would no longer be necessary to remove the samples for dilution, and they could simply be directed into an analytical device via the Macroduct capillary line. And if the device was small and compact enough it could be fully integrated into the Macroduct during post iontophoresis sweat collection, creating a "CF watch" capable of one-shot sweat sample collection and analysis.

The Macroduct devices are sold with a removable transparent plastic cap (not shown) that covers and protects the coiled capillary tubing. This snap-on cover fits into the circular central cavity (the white circular central portion seen below in Figure 3.7). The fact that the Macroduct was already designed to accommodate a plastic mounting was an advantage therefore and the size and fit of this plastic cap was utilised in the design of the analytical device.

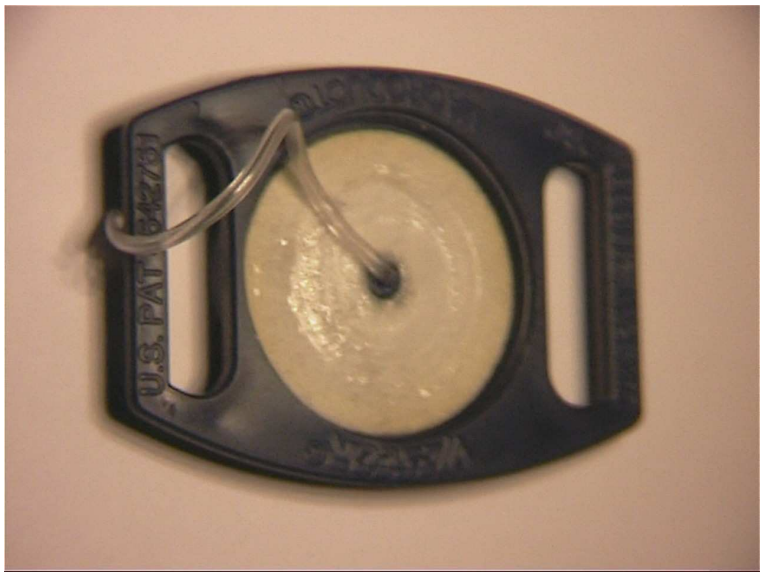

Figure 3.7 Adapted Wescor Macroduct. This is the same basic device pictured in Figure 3.5 except the plastic cover has been removed and the capillary tubing uncoiled and trimmed back leaving a small section of the tubing.

Figure 3.7 shows a dismantled and adapted Wescor Macroduct with the plastic cap removed, along with the majority of the coiled tubing. A short section of the capillary tubing is retained for use as a sample delivery line to the analytical device proposed in Figure 3.8.

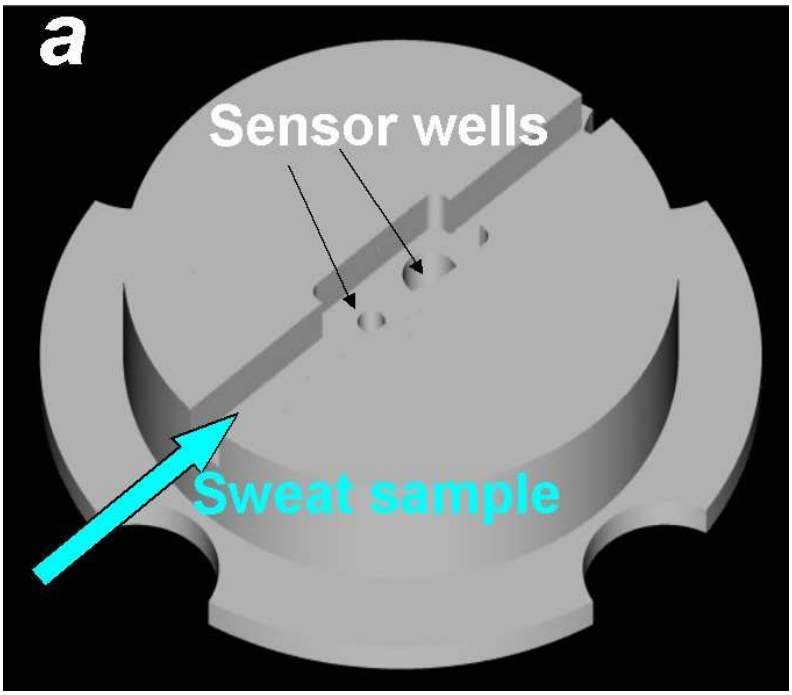

Figure 3.8 CAD drawing of proposed design

Figure 3.8 shows a CAD drawing of a proposed design for the device. It consists of a plastic disk, small enough to sit on top of the Macroduct, with a flow-through channel into which the capillary tubing from the Macroduct delivers the sweat sample as it is being collected. The sweat enters and fills the analytical chamber where it passes over a number of sensors before continuing on to waste. The sensor signals are to be taken out from underneath and to the side of the device to facilitate connection to a portable PC for on-line monitoring of the sweat as it flows through the device.

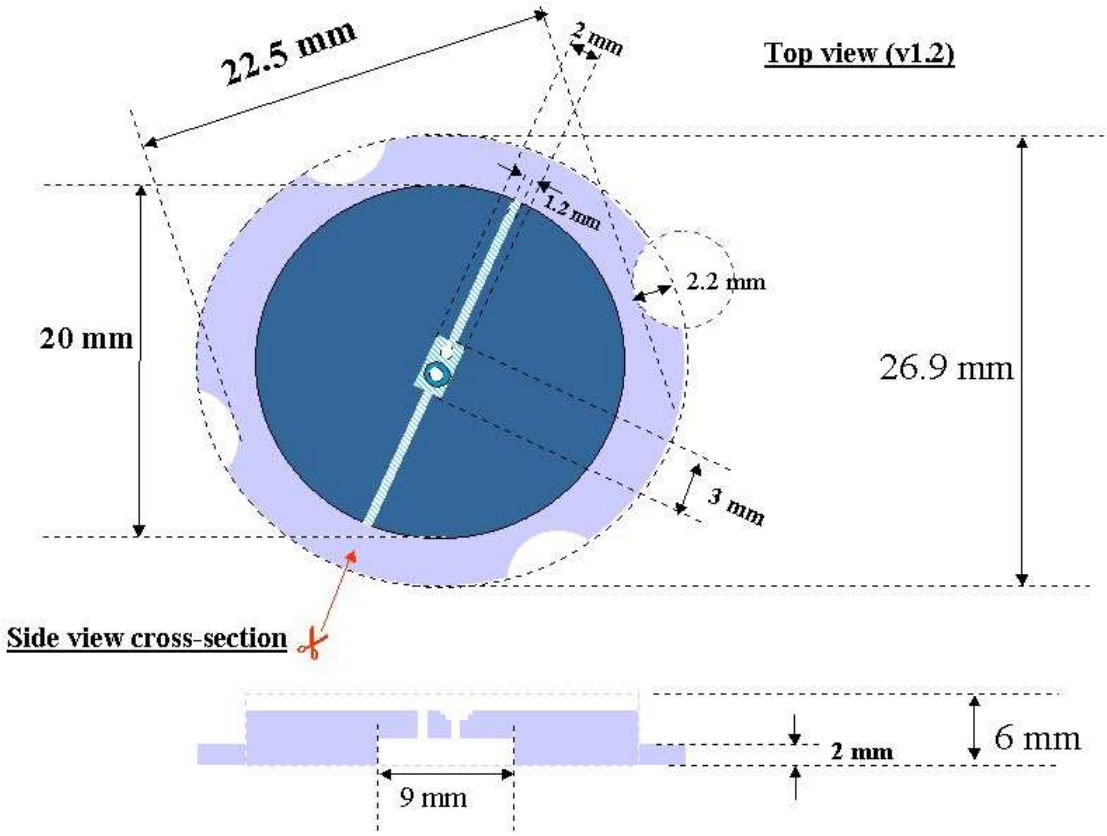

Figure 3.9 2D top-down and side-on cross-sectional views of the proposed device and its dimensions

The dimensions and proportions of the proposed device are shown in the two dimensional drawings in Figure 3.9. The basic size and shape of the device were dictated by the Macroduct, on which it must sit. The flow channels leading to the central chamber are designed to accommodate the Macroduct capillary tubing. The side view is a cross section along the central flow-channel. There is a cavity milled in the underneath of the device also, to accommodate the capillary tubing at the centre of the Macroduct. The next figure (Figure 3.10) shows a close-up of the central chamber.

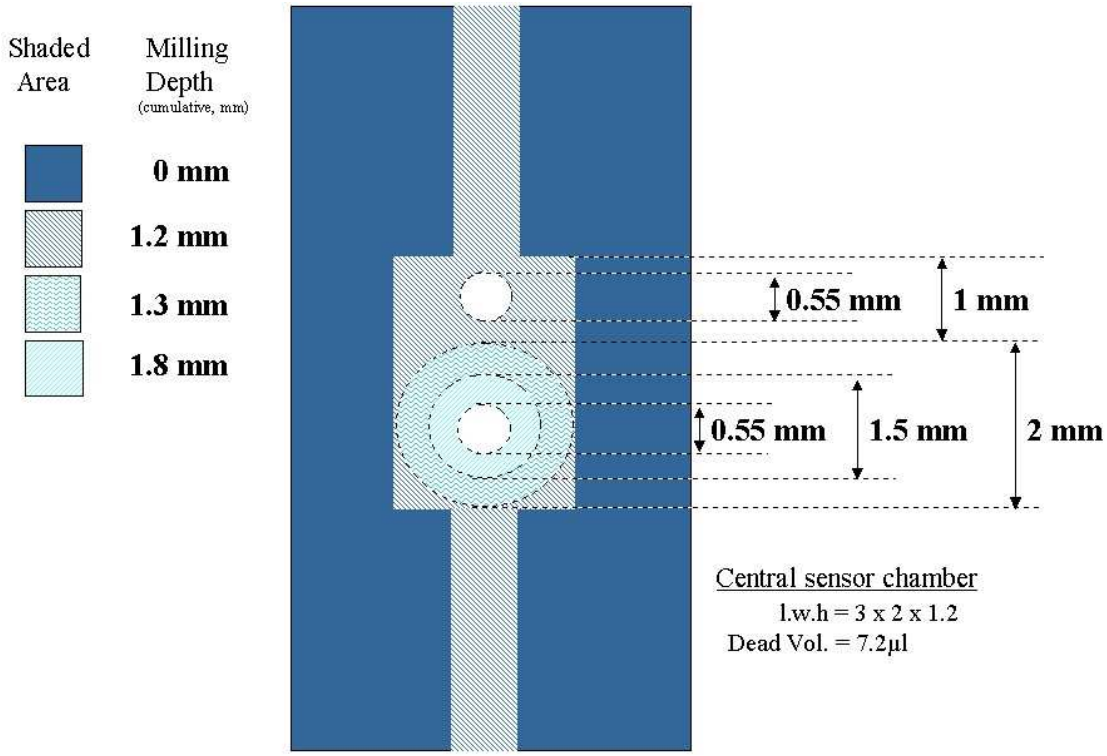

Figure 3.10 Central flow-chamber and sensor well dimensions.

Figure 3.10 shows a close-up of the central chamber and the sensor wells inside. 0.55 mm diameter holes were drilled to accommodate 0.5mm silver wire, to be chloridised in situ. The top sensor well is for an Ag/AgCl chloride electrode and the bottom sensor well is for a sodium electrode. The latter has additional layered wells for a hydrogel layer and a PVC layer. The individual sensor construction is described in detail later in this chapter. From the dimensions of the cell, the dead volume of the sensor chamber was calculated at 7.2 µl.

Figure 3.11 Prototype device based on CAD design to assess its physical size and fit to Wescor Macroduct “throne”.

Figure 3.11 shows a sample device milled from the CAD design shown in Figure 3.8, mounted onto the adapted Wescor Macroduct as seen in Figure 3.7. The section of capillary tubing, which was retained, fits into the milled flow channel to allow the collected sweat sample to proceed into the central analytical, which will house the analytical sensors. One problem, which quickly became apparent with this design, was the relative complexity of the shape of the device with respect to the repeated milling of small numbers of devices one at a time for the purposes of testing. For each device, as well as milling the flow-channels on the top of the device, milled features were also required on the underneath to allow it to fit snugly to the Wescor Macroduct. This creates practical difficulties in terms of turning the piece around and

repositioning it in the CAT3D machine so that it is properly and accurately lined up to continue precision milling on the opposite side. It also means unnecessary repeat milling work for every fresh pair of sensors. To simplify the procedure, it was decided to use an adapter base plate onto which would sit a much simpler device to mill, requiring only top-down milling of the flow channels, sample chamber and sensor wells. This would allow the design of a much simpler-to-mill flow through cell to house the analytical sensors and speed up the milling process, and the base-plate would serve as an interface between the flowcell and the Wescor Macroduct. In this way, one base-plate would serve many Macroducts and flow-cell iterations.

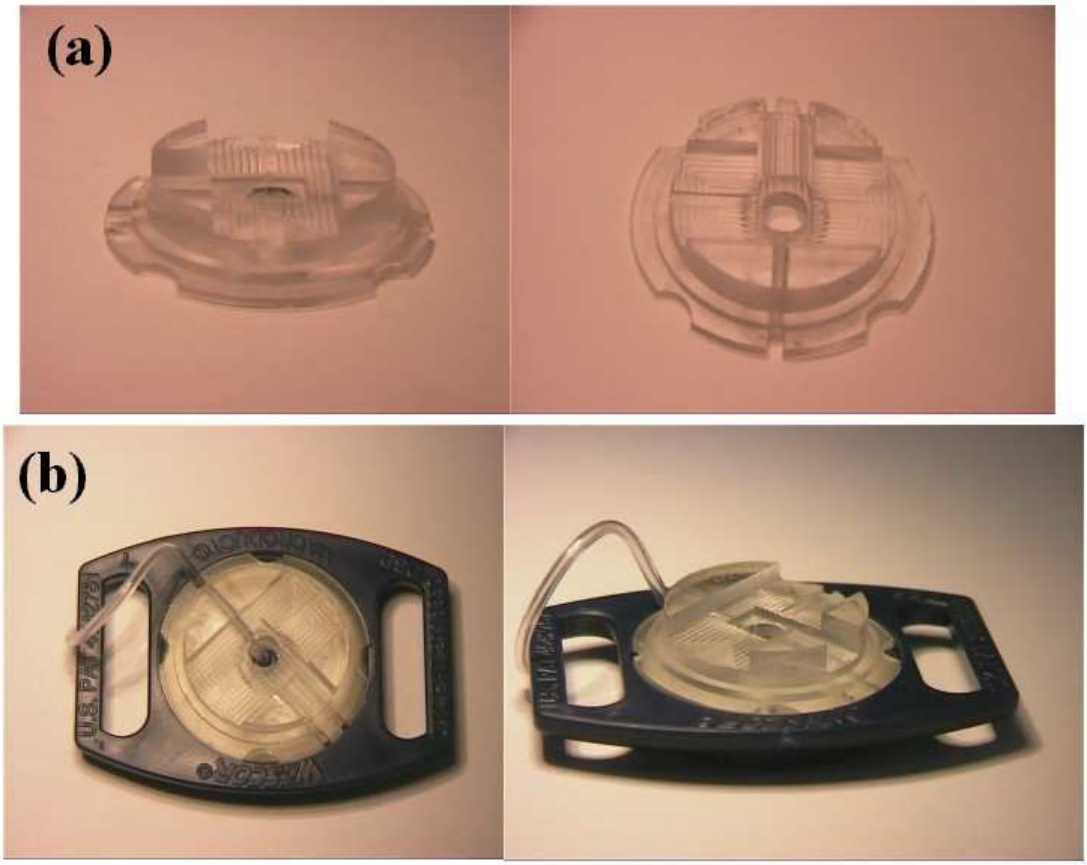

Figure 3.12 (a) base-plate and (b) base-plate plus Macroduct.

With reference to Figure 3.11 one can see that the base-plate in Figure 3.12 incorporates all the basic features of the prototype except that a rectangular section has been removed, where the flow-channels etc would normally be. Into this hollowed out rectangular section a plain rectangular analytical module (Figure 3.13) was fitted.

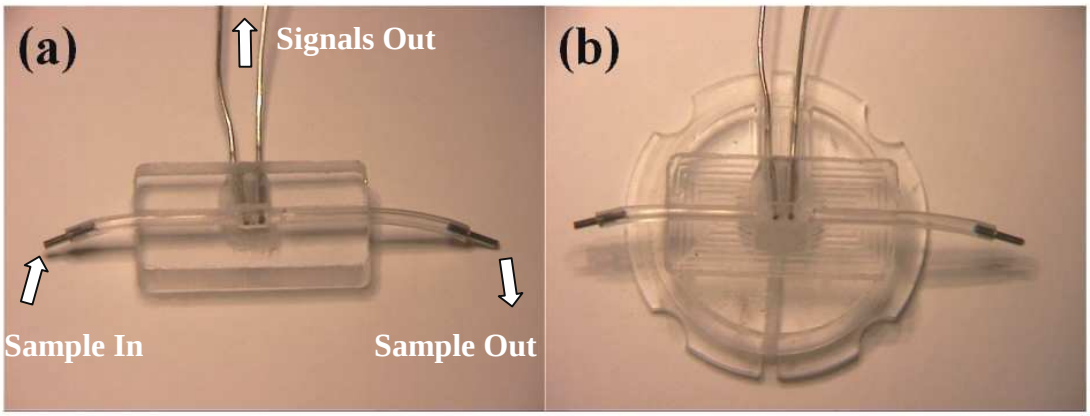

Figure 3.13 (a) Analytical 2-sensor flow cell and (b) flow-cell pictured with base-plate.

The analytical device is a simple rectangular piece, designed to fit the base-plate (Figure 3.12a) as shown here in Figure 3.13b. The flow-channel runs the length of the piece from left to right. In the centre a wider chamber has been milled out to accommodate two sensor-wells in which the sensors will be constructed. All that is required therefore is milling from one side, of the flow-channel, sample chamber and sensor wells. The picture also shows the silver wires used to take the signals out from the two sensors. Sections of the Macroduct capillary tubing were also used to direct the samples into and out of the sample chamber, and short sections of a hypodermic

syringe were cut and inserted into the capillary tubing to connect up to the sample delivery line in the Macroduct (see Figure 3.7).

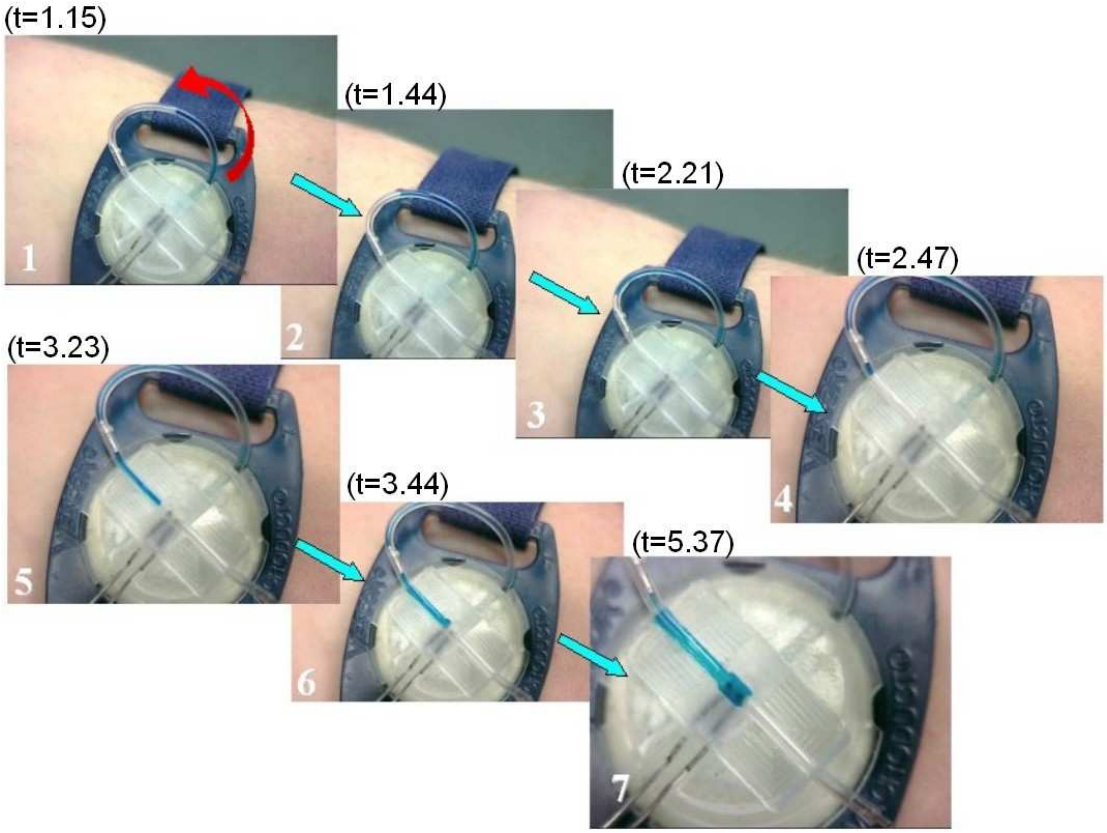

Figure 3.14 On-line and on-skin sweat analysis.

Figure 3.14 features a sequence of video stills (1 to 7) showing the completed device strapped to the arm of an individual who has undergone sweat stimulation by the standard pilocarpine iontophoresis method. The Macroduct fulfils its normal function of trapping the sweat produced and channelling it through the capillary hole in the back of the device where it enters the capillary tubing. However, instead of merely collecting in the coiled tubing, the adapted Macroduct carries the sweat sample through the short section of tubing and on into the analytical device where the sweat is passed over the sensors in the central chamber. The red arrow in still #1 shows the

progress and the direction of travel of the sweat sample front. The sweat sample itself is a blue colour and its progress can be easily traced through the rest of the sequence. The blue dye is a sample visualisation aid and is a normal feature of the Wescor Macroduct – the sweat takes up the blue dye on the underneath of the device as it enters the capillary. The time-line for the sequence is also detailed in Figure 3.14, taking approximately 6 minutes for the commencement of sample collection to the sample chamber being filled completely. The video from which these stills were taken will be made available on-line as supplementary material at http://doras.dcu.ie.

Figure 3.12 and Figure 3.13 show the piece-by-piece construction of the analytical system. One can see the adapter and the manner in which it fits on top of the Macroduct to act as a cradle for a simple 2-sensor flow cell. The wires protruding from underneath the device are lengths of 0.5 mm silver wire, used both in the construction of the individual sensors and as electrical contact wires to take the signals out.

Wescor provide a syringe with their commercial sweat test kits, the cross-sectional diameter of which (ca 0.3 mm) is designed to fit neatly into the Macroduct tubing forming an airtight seal. After collecting a sweat sample with the Macroduct, the unit is designed to be dismantled by removing the plastic cap, inserting the syringe needle into the open end of the capillary tubing and then uncoiling and removing the tubing, which is then snipped at the opposite end (the end attached to the plastic disk –the point of sample entry). The sweat can then be expelled into an appropriate vial, using the syringe as a pneumatic pump. Because this syringe needle is designed to provide a perfect fit with the Macroduct tubing, short sections of the needle were cut and

utilised as connectors to hitch up the sample tubing in the flowcell with that of the adapted Macroduct as shown in Figure 3.13 and Figure 3.14.

Figure 3.14 shows the finished device in its intended mode of use. The images show the device strapped to the arm of a "patient" (in this case a willing volunteer from a non-CF population) following pilocarpine iontophoresis. The time-line for the sequence from #1 to #7 is approximately 4 minutes 20 seconds. The entire procedure involves pilocarpine iontophoretic stimulation for 5 minutes followed by sample collection / analysis for 20 to 30 minutes. The important points illustrated by Figure 3.14 are that:

(1) The device is sufficiently small to cope with the typical volumes of sweat, which the Macroduct is capable of collecting and delivering. In its original form as simply a collection device the sample volume upper limit was determined by the length of capillary tubing inside the Macroduct, which had a maximum dead volume of ca 75µl. After iontophoresis some patients produce <20µl of sweat, whereas others may produce several times the volume of one Macroduct. The tubing in the adapted Macroduct used here is not used for collection, it is used as a sample delivery line to the analytical device. The sample may be monitored continuously therefore as long as sweat is being produced. The patient's sweat glands, and not the Macroduct therefore now limit the maximum sample volume. Wescor recommend a minimum of 15µl of sweat for a valid sample. As shown in Figure 3.10 the dead volume of

the sensor chamber is 7.2µl, i.e. less than half of the minimum sample. Most samples collected will be more than this and are generally >50µl. Compared to the SendX® device dead volume of ca 40µl, the new device is clearly more compatible.

(2) The sample is delivered to the analytical sensors in a reasonably short space of time. With reference to Figure 3.14, from the point at which the device was strapped to the patients arm after iontophoresis to the point where the sweat sample front reaches the sensors thereby giving an analytical reading, is ca 5 minutes. In previous trials described in this thesis, and indeed in many CF centres worldwide, there is a lapse of a period of days between sample collection and sample analysis. With conductivity meters such as those manufactured by Wescor themselves to accompany the Macroduct the sample collection period of 30 minutes must first be carried out, then the device must be unstrapped, dismantled, the capillary tubing removed and a syringe employed to pump the sweat sample into the conductivity meter, before a reading can be taken. The time and labour saving seen here is, therefore, a significant improvement.

(3) The hydraulic pressure of the sweat glands and capillarity of the tube are sufficient to push the sweat sample through the flowcell and to fill the analytical chamber to facilitate analysis. This is obvious from the images in Figure 3.14.

(4) The dimensions of the flowcell (see Figure 3.10) and in particular the construction of the sensor well and the sensors themselves exhibit very encouraging flow dynamics. As the sequence shows there are no air gaps, no air bubbles or air traps at any stage in the flow system. This is quite significant as trapped air was consistently a major problem with the SendX flow cell. Air bubbles would frequently invade the system through tubing junctions and connections and entrap themselves in the concaves and convexes of the soft polymer membrane ISE's. These air bubbles caused large spikes in the analytical signal trace, and were often very problematic to remove, requiring high speed flushing and agitation of the array, activities which ran the risk of the introduction of still more air to the system.

This high degree of compatibility with the Macroduct was very encouraging. The next section describes the construction of the device itself and the sensors within. The device was then employed in a clinical trial involving the analysis of CF positive and negative samples.

3.4 Construction of Analytical Device

3.4.1 Choice of Material / Substrate

Three common and easily available plastics were selected as possible substrates from which the devices could be made. The primary requirements were:

1. Physical compatibility of substrate with drilling and milling machinery.

2. Chemical compatibility of substrate with membrane components

The physical compatibility of the substrate refers mainly to how easy it was to work with the material with respect to making small batches of test devices for the purposes of this research; however, compatibility with larger scale processes such as injection-moulding is also an important consideration for the possible future manufacture of many devices. The principal chemical requirement is the quality of adhesion of the PVC membrane to the substrate. The submembrane hydrogel can swell considerably exerting not inconsiderable pressure on the cap PVC membrane leading to delamination of the membrane and sensor failure if the adhesion is poor[8] (see Figure 3.15).

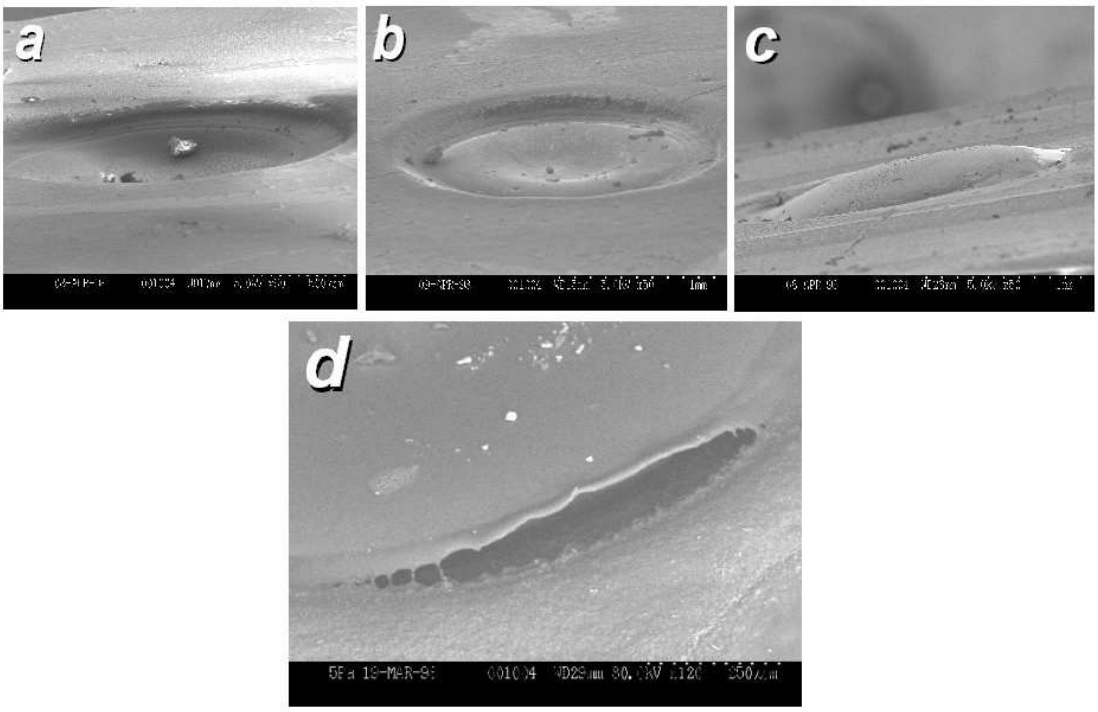

Figure 3.15 Examples of the effect of hydrogel swelling, taken from SEM swelling study on solid-state PVC-membrane ISEs in a SendX array, such as was used in this research (earlier in this thesis). (a) A newly made unconditioned sodium membrane; (b) a sodium membrane left to hydrate for one day; and (c) after eleven days hydration. The hydrogel swells to accommodate the water molecules, which exerts an upward pressure on the cap membrane, which can occasionally lead to rupture of the membrane itself[8] (d).

Three common and easily available plastics were selected for testing: Perspex, PVC and Polycarbonate. Test devices based on the CAD design in Figure 3.8 were milled from each of the substrates to assess the physical attributes of the materials as shown in Figure 3.16.

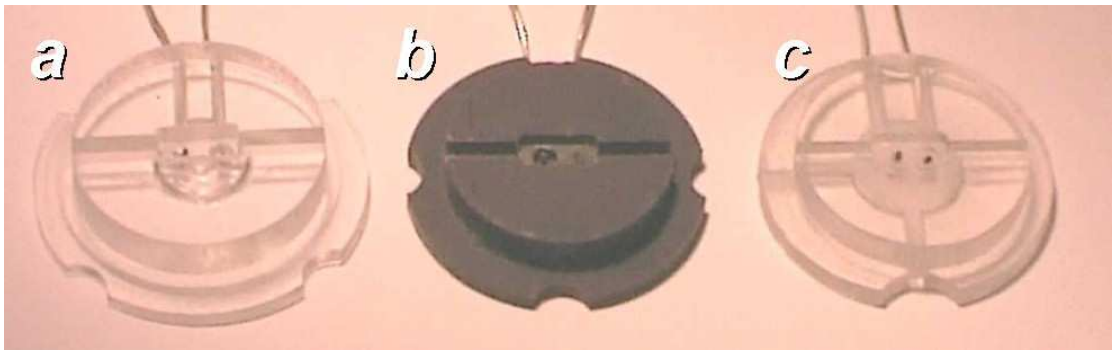

Figure 3.16 The three test substrates: (a) Perspex, (b) PVC and (c) Polycarbonate

From the test milling, it was possible to mill devices from all three materials (see Figure 3.16). Initially, Perspex and polycarbonate posed a problem for the CAT3d milling machine as the heat generated by the cutting tools during high spindle speed operation caused the substrates to melt and to fuse to the tool. These problems were overcome, however, by decreasing the spindle speed and increasing the feed rate, which can be done through the XCAD software package used to control the CAT3d machine. The CAT3d also has a tool-cooling feature, which pumps a continuous flow of coolant (such as water) over the tool during operation. This is generally intended for use when milling much harder materials such as metals, when slow feed rates and high spindle speeds and consequently high heat generation are the order of the day. This facility was not required here.

All of the materials required a certain amount of post-milling clean up under a microscope with a sharp blade to remove “crusts” or “lips” from milled edges. Perspex was found to be the most problematic in this regard, followed by PVC, with

polycarbonate being the easiest substrate to mill cleanly and with a good quality finish.

Basic adhesion testing was carried out by dispensing micro-litre quantities of the PVC membrane solution onto 5 cm square pieces of each substrate and leaving overnight to dry. These were inspected the following day and a simple "lift-off" adhesion test carried out using a thin, sharp scalpel-type flat blade (Figure 3. 17). The substrates were then immersed in an aqueous 0.1M NaCl solution overnight and re-inspected in a similar manner the following day.

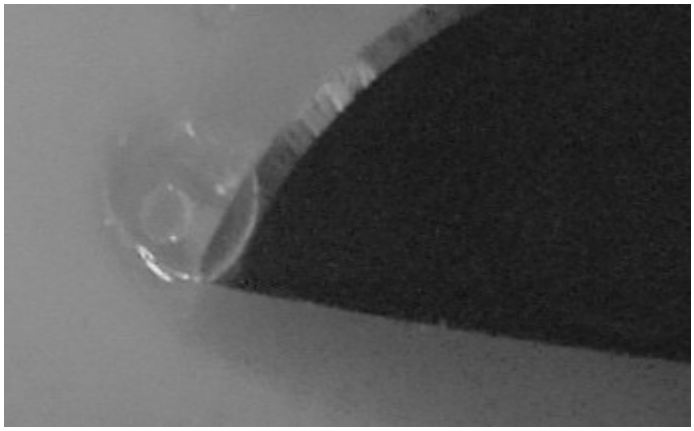

Figure 3. 17 PVC membrane lifting off Perspex surface using a flat blade

Post immersion examination of substrates eliminated Perspex, which showed little or no adhesion under the conditions investigated. The deposited membrane peeled off with little encouragement required as shown in Figure 3. 17. This ease of removal was not exhibited by the remaining two substrates, which both exhibited strong adhesion to the PVC membrane. On visual examination the deposited membrane

solution on the PVC substrate appeared to have been absorbed rather than adsorbed by the PVC, whereas in the case of the polycarbonate substrate the adhesion of the membrane seemed very strong while still retaining its shape and autonomy as a discernable cap membrane. The polycarbonate was selected for a number of practical reasons:

(1) The polycarbonate was easier to mill.

(2) The transparent nature of the polycarbonate substrate greater facilitated the development of the device through easy visualisation of milled features, dispensed layers and electrical contacts, at all levels of manufacture and testing compared to the opaque PVC substrate.

(3) Polycarbonate is very suited to injection moulding, a useful process for the batch analysis (and indeed mass production) of many devices and available in-house to the research group. Injection moulding of PVC requires special safety considerations because of the dangers of liberation of toxic HCl gas at temperatures over 230 °C.

For these physicochemical and practical reasons, polycarbonate was considered to be the most suitable of the three materials investigated. In its subsequent use, no adhesion difficulties arose and delamination of PVC layers was therefore not an issue.

3.5 Watch Sensors

The marker ions for cystic fibrosis are sodium and chloride and it is generally recommended that both ions be monitored for optimum reliability[9]. It was desirable in this case to keep the sample chamber as small as possible to allow efficient analysis of the small volumes of sweat ($\leq$ 15 µl) generally collected via the Macroduct. The sample chamber is potentially the biggest contributor to the dead volume of the device, therefore it needed to be kept as small as possible. This was done by keeping the individual sensors themselves small, and by minimising the number of sensors. Fewer sensors also make for a simpler device, which is desirable in terms of manufacture and ease of use as a potential one-shot screening device. The possibility of using a simple 2-electrode system was therefore investigated, whereby a solid-state sodium-ISE would be referenced against an Ag/AgCl electrode, which would act as both a pseudo-reference and a chloride electrode.

3.6 Electrode manufacture and testing

This section details the construction of the sodium solid-state PVC membrane ISE and the Ag/AgCl electrode within the sensor wells.

3.6.1 Milling of the flow-cell

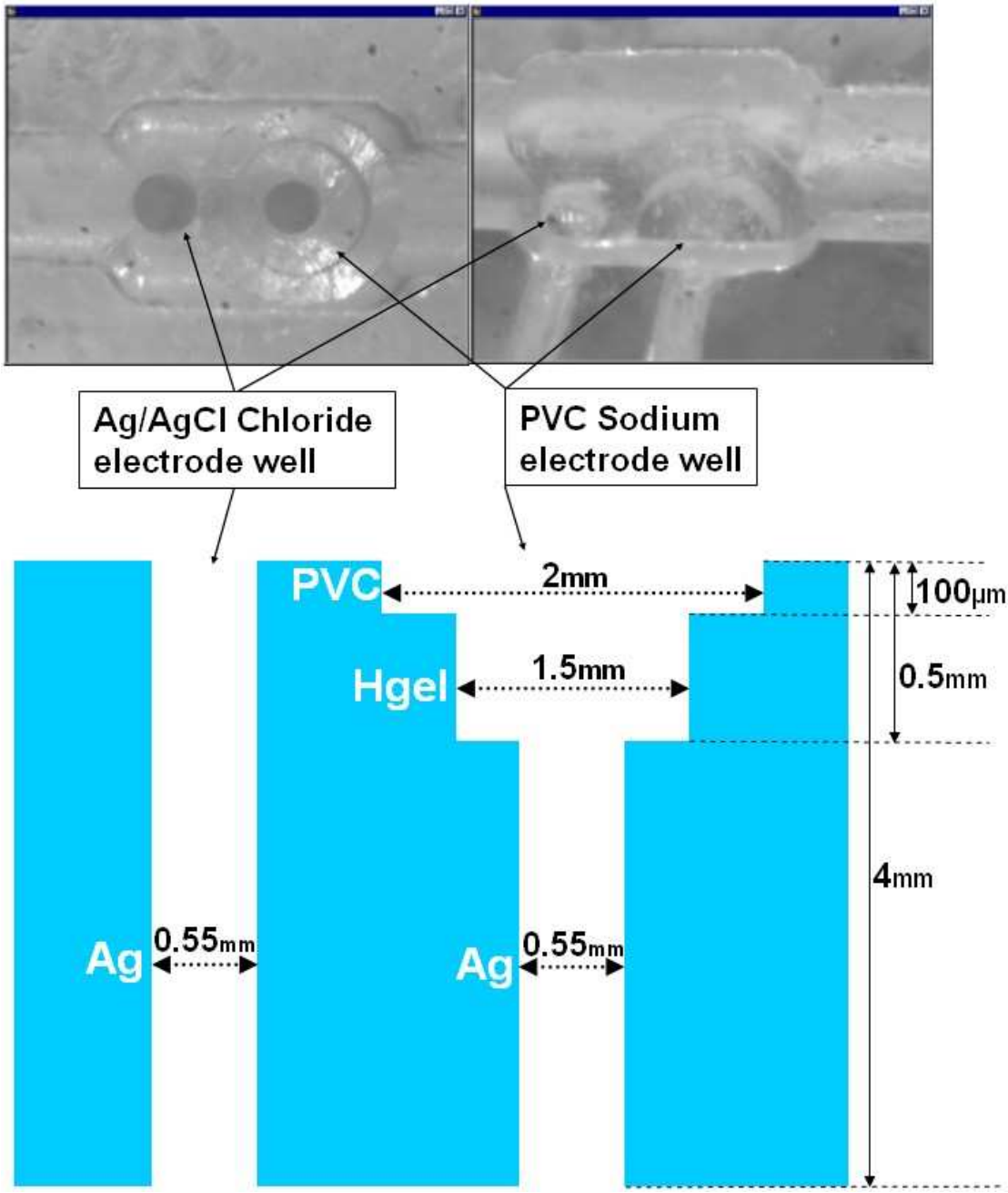

Figure 3.18 Flow-cell sample chamber and empty sensor wells.

The two photographic images in Figure 3.18 were taken using a microscope with a camera attachment, connected to a PC to allow on-screen visualisation and screen capture of microscopic images. They show the central chamber from the top down

and at a slight angle. The schematic below the photographs is of the sample wells and helps to explain the photograph images. The central chamber (as described earlier in Figure 3.9 and Figure 3.10) is 2 mm by 3 mm and it is 1.2 mm deep. The images show the sample flow channels leading to and from the chamber. Inside in the chamber are two sample wells. The one on the left is designed to accommodate a silver-silver chloride electrode. The one on the right is for the sodium electrode construction. It has a similar hole drilled for an Ag/AgCl internal reference electrode, there is a larger well to accommodate a hydrogel layer, which acts as the internal filling solution, and finally an additional well for the PVC sensing layer. The construction of these sensors is described in detail further on in Figure 3.19 to Figure 3.23.

The structural features of the flow-cell and sample chamber shown in Figure 3.18 were milled into the surface of the polycarbonate substrate using a CAT3d milling and drilling machine. The controlling software for this machine is an MS-DOS-based package, which requires each movement of the tool and spindle to be inputted manually prior to each movement's execution. For lengthy and repeat procedures it is also possible to pre-program the step-by-step movements of the cutting tool prior to execution of the entire sequence of instructions. In this case, relatively few commands were involved, but a number of tool changes were required, which proved to be more reliable if carried out manually. The machine command sequence was as follows:

(1) After basic machine, tool, and substrate set-up, a channel was milled (22 mm x 1.2 mm x 1.2 mm) (X,Y,Z) using the "Mill Rectangular Cavity From

Centre" command and a 1.0 mm (diameter) ball-end milling tool. These channel dimensions were defined by the external diameter of the Macroduct tubing (1.2 mm) used to pass the sample in and out of the device, and by the total length of the device (20 mm). The 2 mm overrun was to account for the diameter of the tool used and to ensure a thorough cut at either end of the channel.

(2) The tool was re-centred and the "Mill Rectangular Cavity From Centre" command again used to mill the central sample chamber (3 mm x 2 mm x 1.2 mm). An incremental movement instruction (+1 mm in the X direction) was performed and the "drill" instruction used to drill a hole 2 mm in diameter and 1.3 mm in the Z direction, resulting in a cavity 2 mm in diameter, and 100 µm deep. This cavity was intended for the PVC cap membrane.

(3) The tool was exchanged for a 1 mm drill. This was first used to drill a cavity into which the hydrogel would be dispensed. The "drill" command was again used to drill a hole 1.5 mm in diameter and 1.8 mm in the Z direction, resulting in a cavity 0.5 mm deep. The CAT3d has a "spiral" feature, which facilitates the drilling of holes larger than the diameter of the drill bit being used by spiralling the drill bit to increase the cutting radius. This feature was employed here.

(4) The tool was exchanged once more for a 0.5 mm drill bit. The "drill" command was used with the "spiral" feature to drill a 0.55 mm diameter hole, 8 mm deep. This hole was to house the silver wire.

(5) The tool was re-centred, moved incrementally –0.5 mm in the X direction, and the previous “drill” command recalled to drill another hole for the Ag wire for the Ag/AgCl electrode.

(6) The tool was again re-centred and exchanged for a 1 mm cutting tool. To cut the finished piece from the polycarbonate substrate the “Mill Square From Centre” command was used (20 mm x 10 mm x 8 mm).

Following milling the piece was cleaned and examined under a microscope to remove any debris or imperfections.

3.6.2 Deposition of Sensing Layers

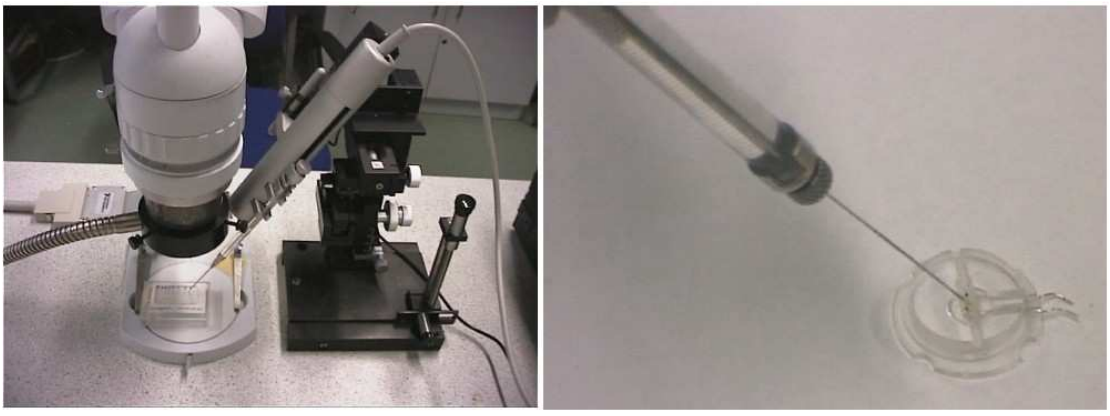

Figure 3.19 Visualisation and dispensing set up.

Figure 3.19 shows the equipment used for visualisation and dispensing of sensing layers. The image on the left shows the bench-top microscope and a 50µl glass syringe held in a motorised WPI Ultra Micro Pump, which is in turn clamped into a WPI Micro-Manipulator. The Micro-Manipulator allows precise motorised or manually controlled micrometer movement of the syringe needle tip, in the X, Y and Z directions, with a Vernier scale for each vector. Not pictured is a camera attachment, which allows image capture of what is being observed through the eyepieces from above. This camera was used to obtain the close-up images of the flowcell features and the dispensed layers in Figure 3.18, Figure 3.20, Figure 3.21, Figure 3.22, and Figure 3.23.

Step 1.

Sections of 0.5 mm diameter pure silver wire were inserted into the drilled holes from the top of the device and pulled through from the back and cut to the appropriate length. A small amount of silver loaded epoxy was used to seal the wire into place at the back end of the device. As shown in the photographs and the accompanying graphic image in Figure 3.20, the silver wires were allowed to protrude a certain distance, inside the sample well in the case of the sodium sensor to ensure adequate contact with the hydrogel, and into the sample chamber in the case of the chloride electrode to ensure contact with the sample stream.

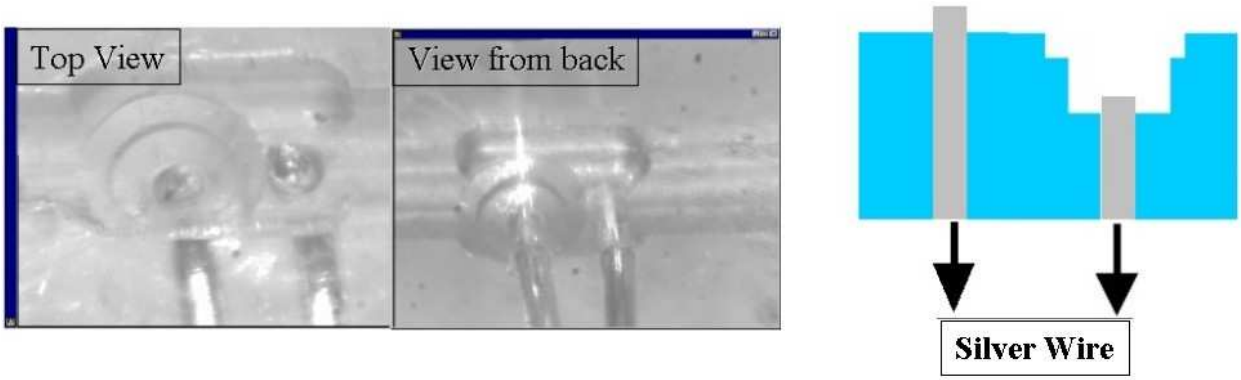

Figure 3.20 Insertion of Ag wires

Step 2

The silver wires were chloridised *in situ* by immersing them in Sodium Hypochlorite for approximately 40 to 60 minutes. Visual examination of the electrodes confirms the formation of an AgCl layer as shown in Figure 3.21. Gone is the bright silver sheen, replaced by a blackish layer of silver chloride.

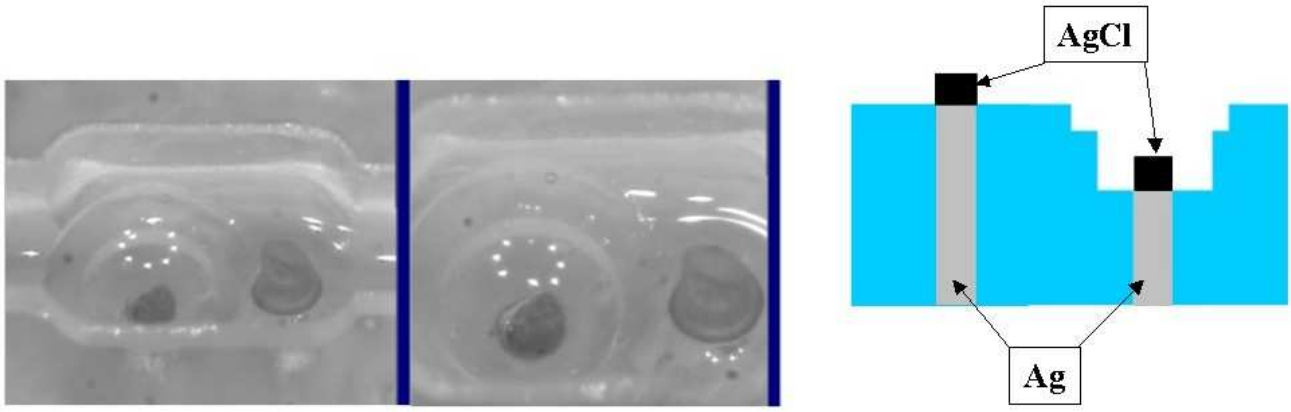

Figure 3.21 Ag wires after chloridisation by exposure to sodium hypochlorite for 60 minutes. Visual examination confirms the formation of a blackened layer of silver chloride.

Step 3

Using the dispensing set-up in Figure 3.19, the hydrogel cavity was filled with the uncured hydrogel solution. The amount was estimated visually rather than volumetrically. The approximate volume of the cavity is ~0.8 µl. The solution was then cured using the ELC403 UV-Light Curing Gun, for 30 minutes at an intensity of 80mW/cm^2. Successful curing was confirmed by visual examination, clearly illustrated by Figure 3.22 in which can be seen the gelled / rippled surface of the cured hydrogel.

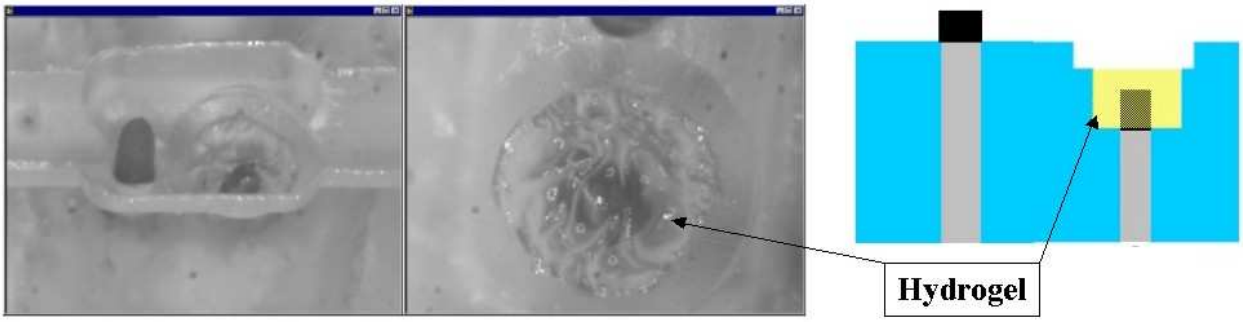

Figure 3.22 Hydrogel layer after curing

Step 4

The PVC solution described earlier was made up and dispensed in a similar fashion to the hydrogel. In the case of the PVC, however, it was necessary to repeat the dispensing procedure a number of times to build up the thickness of the membrane and fill the cavity, allowing time for the solvent to evaporate off between each dispensing. As shown in Figure 3.23, the provision of a defined cavity for the PVC layer is quite neat and provides a definite and consistent contact area for the PVC and the substrate to ensure good quality adhesion and minimise failure of the sensors.

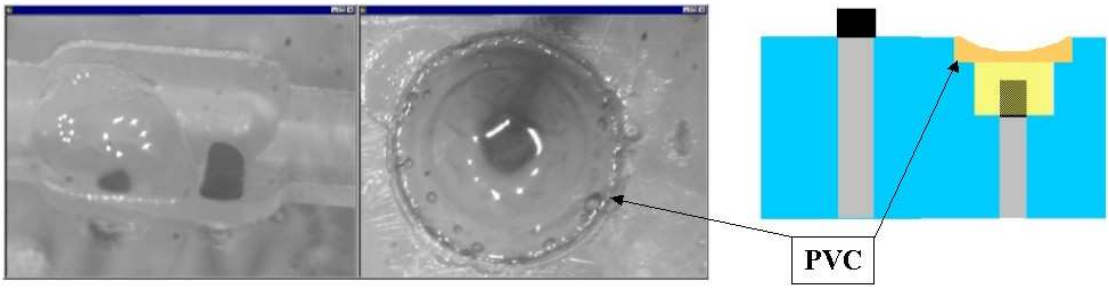

Figure 3.23 PVC membrane layer.

3.6.3 Electrode Test Well

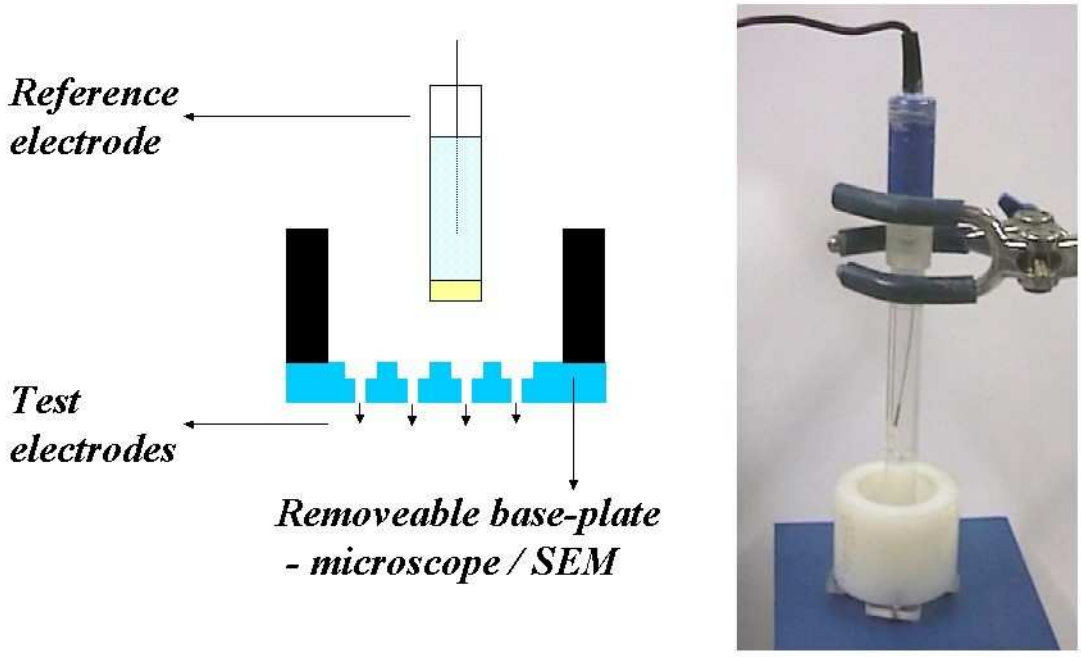

Figure 3.24 Electrode Test Well used to test sensor construction and performance before prior to their incorporation into finished device design.

To facilitate testing of the individual sensors against a standard reference electrode, the set up illustrated in Figure 3.24 was constructed. A cylindrical block of nylon was hollowed out and four locking nuts attached to the underneath to allow the attachment of a cylindrical base plate, sealed with a rubber O-ring. This set up allows the simultaneous construction and potentiometric investigation of several sensors at once. After potentiometric investigation the base-plate containing the sensors can then be removed and the sensors visualised using an SEM.

A number of sodium sensors therefore were constructed in the same manner as described in steps 1 to 4 earlier. The construction stages are illustrated in Figure 3.25 to Figure 3.29. SEM analysis was also carried out and the completed array was used in a series of potentiometric experiments to assess sensor performance. An Ag/AgCl electrode was also made up and its response to changing concentrations of chloride investigated.

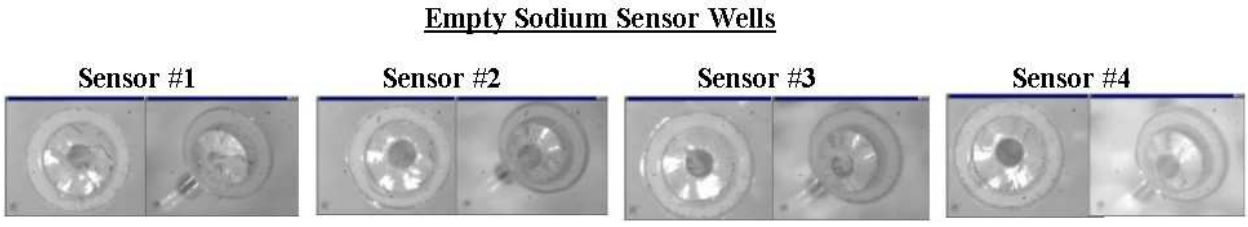

Figure 3.25

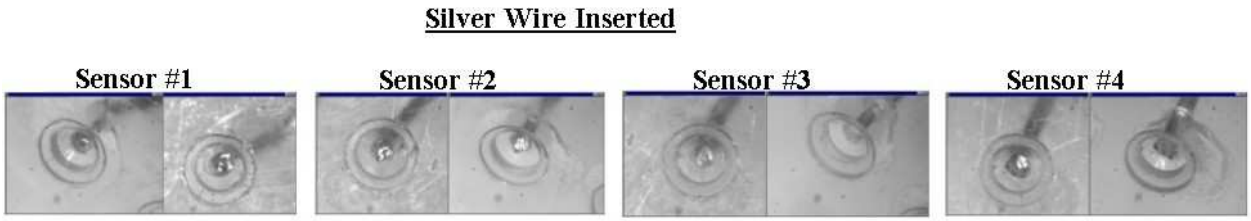

Figure 3.26

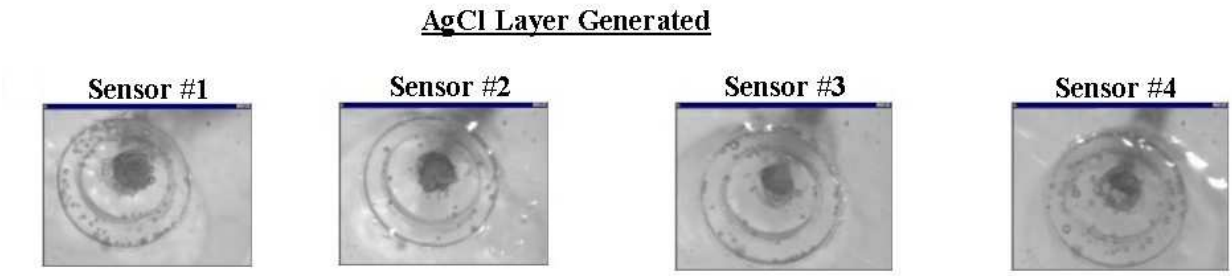

Figure 3.27

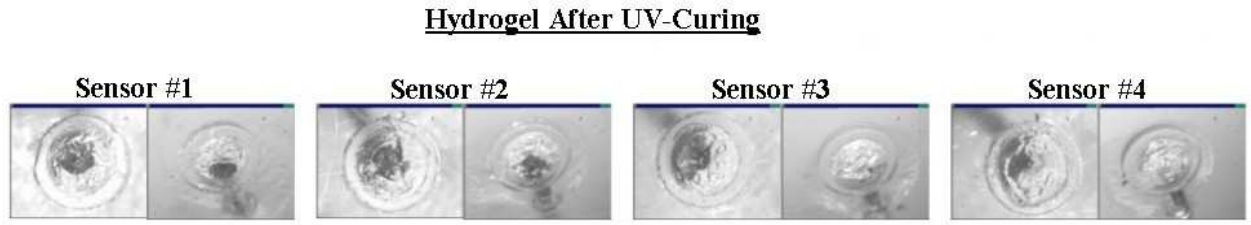

Figure 3.28

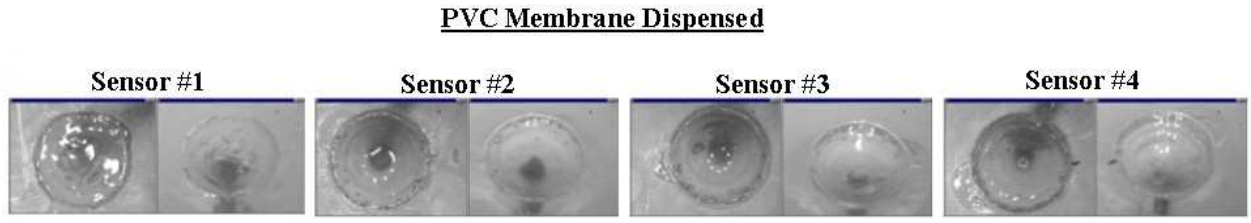

Figure 3.29

Figure 3.25 to Figure 3.29 show a sequence of microscopic screen-capture images to illustrate the stages of construction of the test bed array of sodium sensors: Empty

milled sensor wells (Figure 3.25); Silver wire (Figure 3.26); Chloridisation of Ag wire to form AgCl layer (Figure 3.27); Cured hydrogel layer (Figure 3.28); and the PVC cap membrane (Figure 3.29).

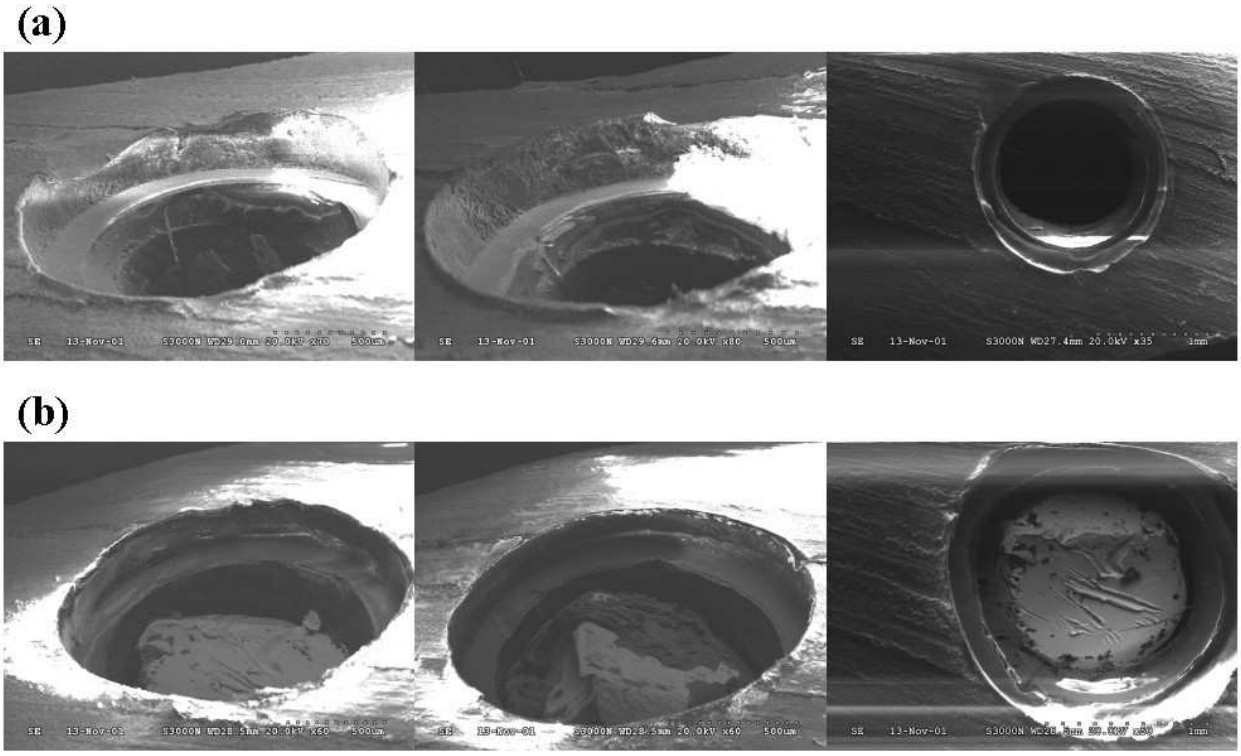

Figure 3.30 SEM images of the empty milled wells (a), and chloridised silver wire (b). (SE, 20kV, WD 28.5-29.6, Magnification 60-80).

Comparison of the benchtop microscopic images with those obtained by SEM in Figure 3.30, illustrates how the higher magnification SEM images can highlight structural faults and details that are invisible to the bench-top microscope. The milled surfaces appear rather crude at these higher magnifications, but they are fit for purpose in the development of a prototype. Once a prototype design was established, it was then prudent to use a milling machine such as the CAT3d to manufacture a precision mould, from which many devices of high quality could be cast.

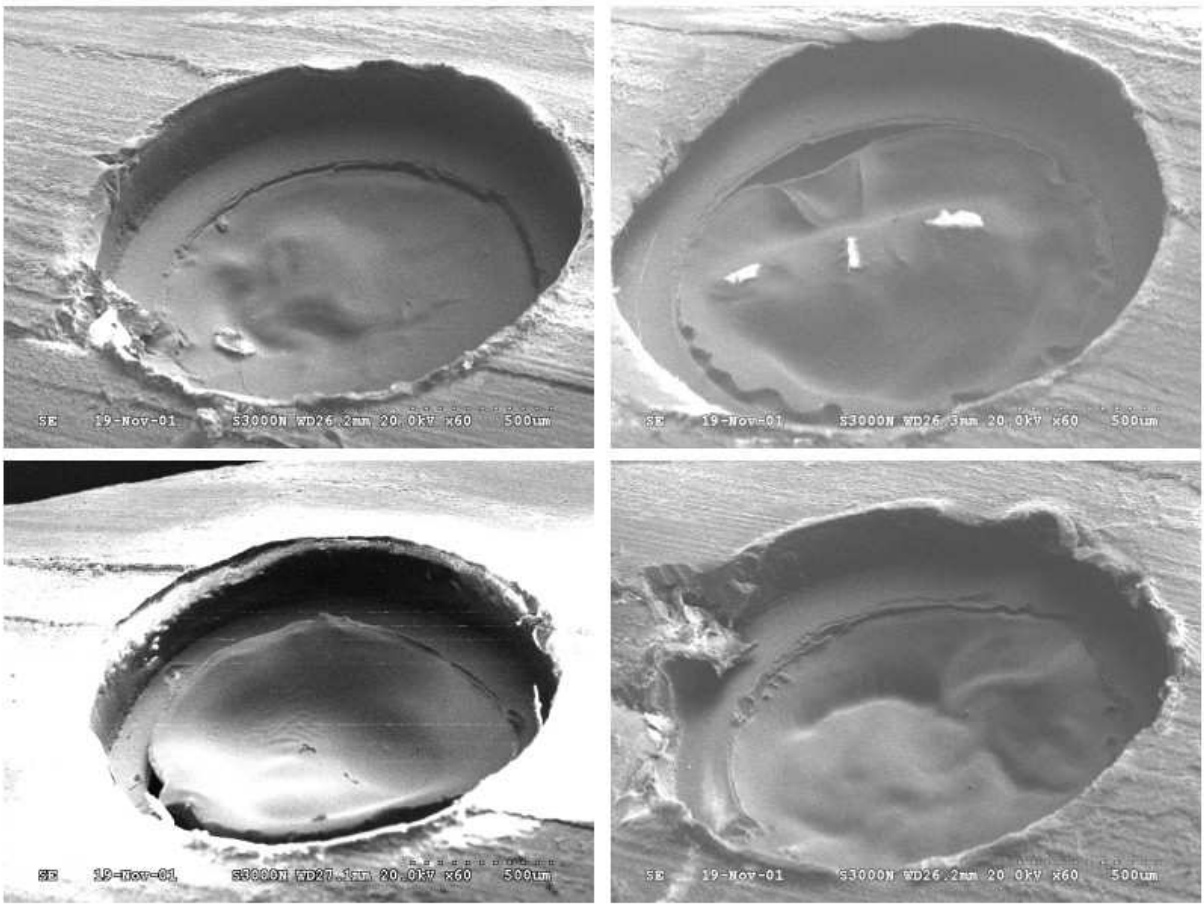

Figure 3.31 SEM images of cured hydrogel layer. (SE, 20kV, WD 28.5, Magnification 50-60). The 100µm deep PVC well is also plainly seen, inside in which the PVC membrane will be cast.

As seen earlier in Figure 3.15, Scanning Electron Microscopy can be a very useful tool for trouble-shooting failed or non-functioning sensors[8]. Errors during the manufacturing and dispensing process can result in problems such as: poor quality, non-uniform deposition of the PVC membrane layer and structural weaknesses in the membrane itself, leading to rupture; or poor adhesion of the PVC membrane layer to the substrate leading to de-lamination of the membrane at the edges. Such weaknesses, if present, can be exposed by internal pressure from the sub-membrane

hydrogel, which swells in volume as it hydrates, exerting pressure on the membrane above it. Hydrogels have the ability to absorb large amounts of water without dissolving. They have three dimensional cross-linked polymer structures, which allow them to swell to accommodate water molecules. The swelling properties of a given hydrogel are influenced by the nature the polymer itself, by the nature of the cross-linker molecule used, and by the density of the cross-linking. Polymers and cross-links with more polar groups absorb more water and swell more than those with fewer polar groups. The more polar the polymer network, the more attractive it is to water molecules. Greater polarity also increases the electrostatic repulsion within the polymer itself, promoting swelling to increase the distance between neighbouring polar groups.

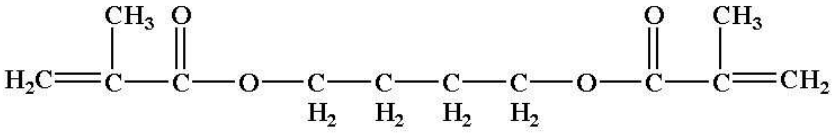

1,4,-Butanediol Dimethacrylate

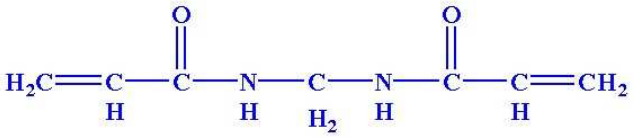

N,N'-Methylenebisacrylamide

Figure 3.32 these are two examples of cross-linker molecules used in the preparation of polyacrylamide-based hydrogels. Both molecules have the same reaction-propagating C=C groups at both ends, and therefore serve the same function, but they differ in terms of polarity. Bisacrylamide, the cross linker used in this study, is a more polar cross-linker than dimethacrylate.

Figure 3.32 shows two different cross-linker molecules capable of cross linking chains of polyacrylamide. Both are tetra-functional cross-linking agents, so classed because they can attach to the main polymer chain at four locations. There is a carbon-carbon double bond at both ends of each molecule and attachment can occur at any of these four unsaturated carbons. The equilibrium swelling of acrylamide polymers cross-linked with bis acrylamide has been shown to be greater than acrylamide polymers cross-linked with dimethacrylate[10]. The reason for this is the greater polarity of the CO-NH-R groups of bisacrylamide over the CO-OR groups of the other cross-linker. Cross linking density also decreases swelling ratio, e.g. if a trimethacrylate (hexafunctional) cross-linker is used, it has more cross-linking sites, cross linking density will be higher, and the degree of swelling will be decreased[11]. Similarly, using a higher concentration of cross-linker also increases the cross-linking site density, there are more links, making the polymer more rigid and less able to swell. The hydrogel preparation and curing recipe used here was obtained from SendX and had been previously optimised therefore further swelling studies were not carried out.

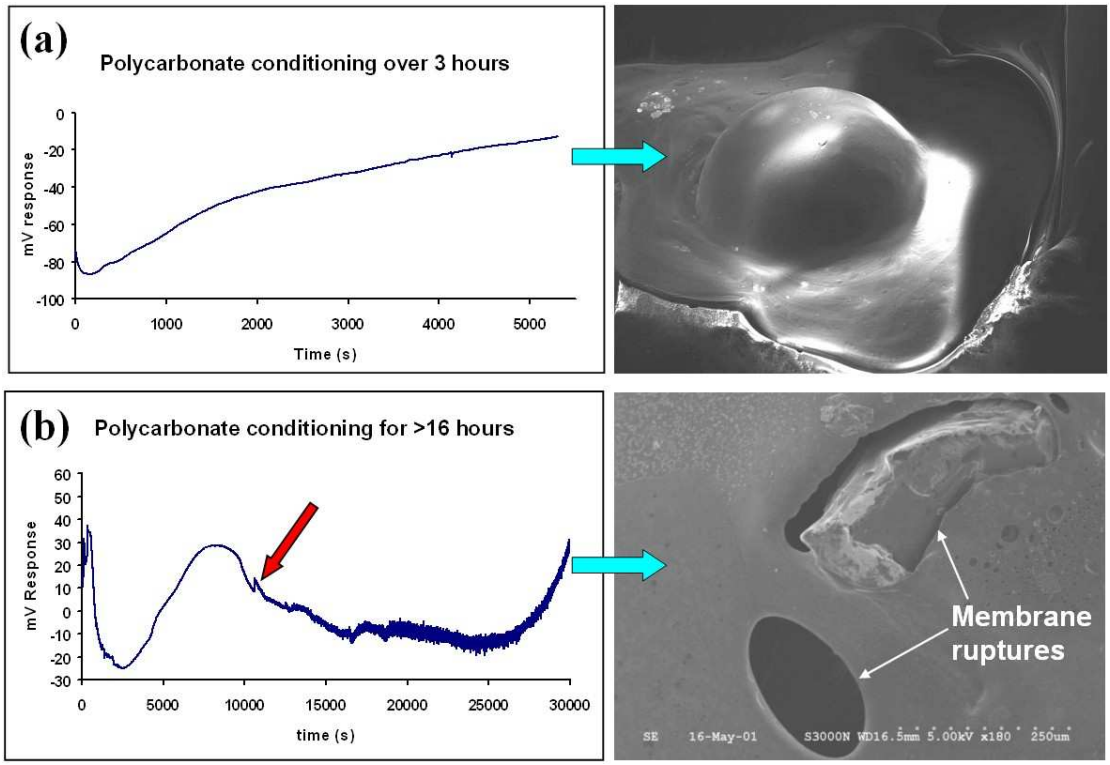

Figure 3.33 SEM images of sensors conditioned in 100 mM NaCl.

Figure 3.33 shows two different sodium sensors from the polycarbonate test bed left to condition in 100 mM sodium chloride for a period of time, after which they were visualised by SEM. The graphs show how the mV response of the electrodes changes during conditioning as the dry hydrogel gradually becomes more hydrated, and the SEM photographs show what the membrane looks like at the end of each conditioning period. Figure 3.33(a) is an extreme example of swelling which illustrates the extent to which the sub-membrane solution can sometimes swell through the absorption of water, and also the flexible nature of the PVC cap membrane in its ability to distort to accommodate this swollen sub-membrane hydrogel. Figure 3.33(b) is an SEM image of a sodium ISE left to condition overnight in 100mM sodium chloride. At the point indicated by the red arrow on graph (b), something has happened to the signal and from then on it is extremely noisy. SEM investigation shows a tear in the surface of

the PVC membrane. This may have resulted from the pressure exerted from underneath by the swelling hydrogel, or it may have been punctured by the silver wire beneath it.

3.7 Potentiometric Experiments

Characterisation of Sodium Sensors

Four electrodes were made up as described and calibrated by a number of methods. Initially calibrations were carried out using a Metrohm® 644 bench-top pH meter, which was the simplest method of confirming that the sensors were functioning correctly. A 5-point calibration was carried out from 10^{-5} M to 10^{-1} M NaCl using a standard calomel electrode as a reference as per the setup illustrated in Figure 3.24. The pH meter only allows the monitoring of one electrode at a time so the calibration was repeated for each electrode. The electrodes were each allowed to stabilise for about 15 seconds and the response was then monitored for a period of about 30 seconds during which time the highest and lowest readings were recorded (see Table 3.1). The average reading was graphed against the log of the activity of the sodium ion.

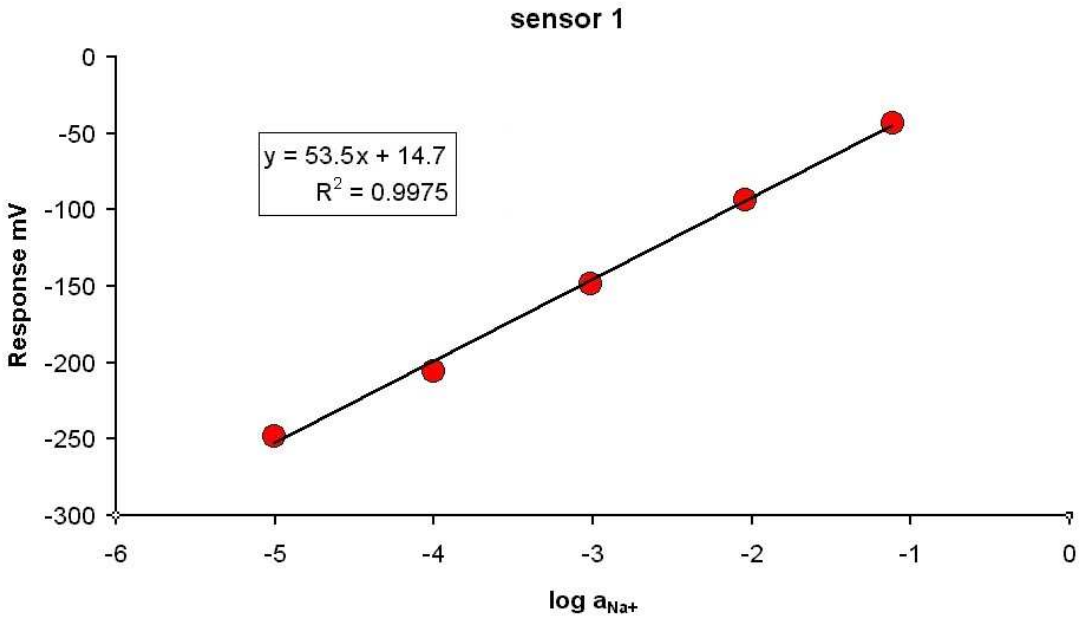

Figure 3.34 Calibration curve for sodium sensor #1

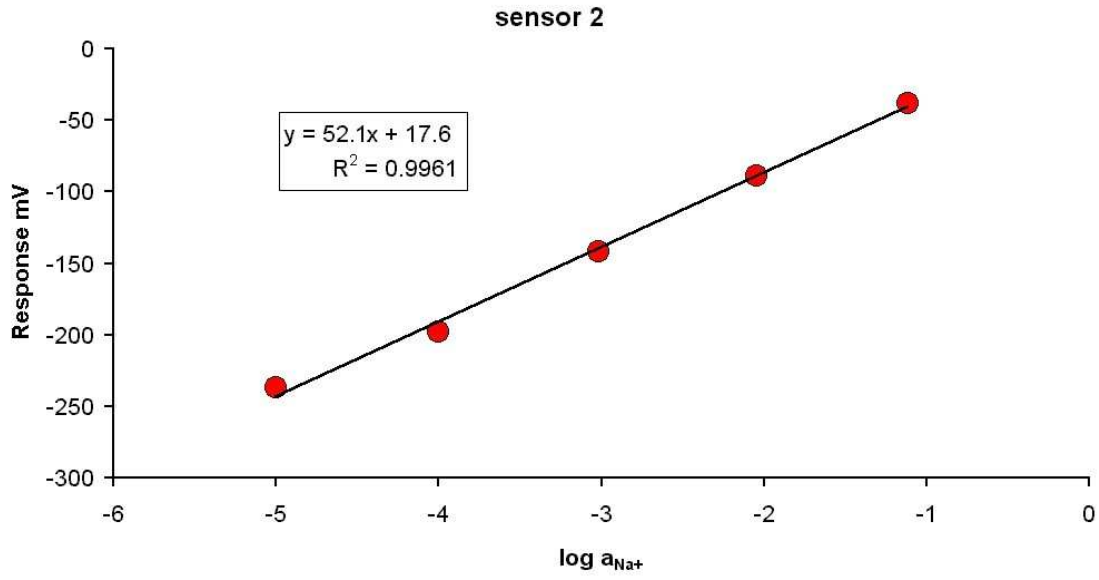

Figure 3.35 Calibration curve for sodium sensor #2

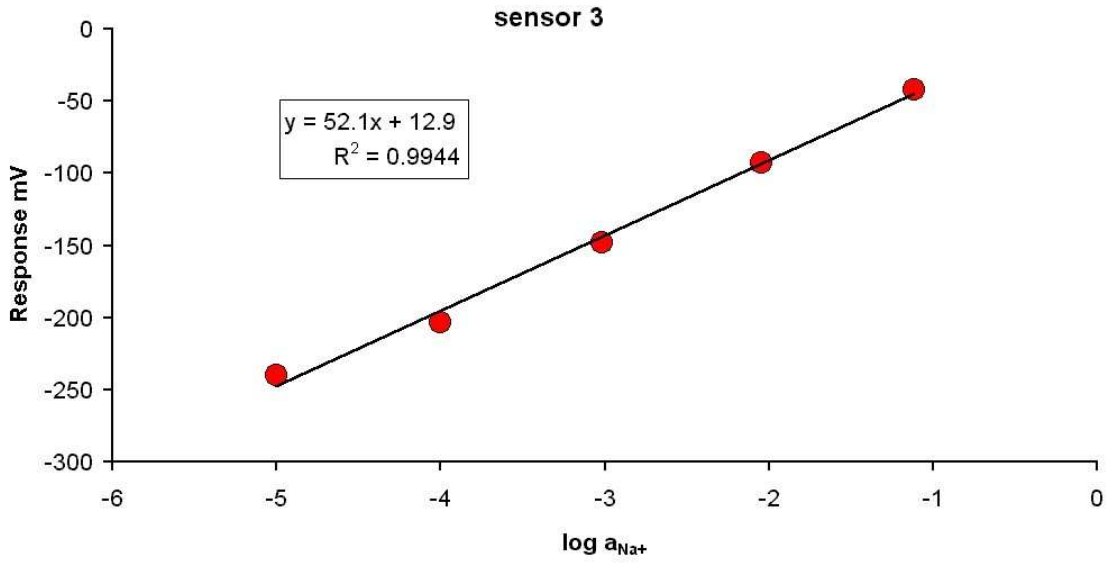

Figure 3.36 Calibration curve for sodium sensor #3

The three calibration curves in Figure 3.36, Figure 3.35, and Figure 3.36 show three of the sensors performing well. The slopes (53.5mV, 52.1mV and 52.1mV respectively), though slightly sub-Nernstian, show good consistency and reproducibility, particularly for handmade devices. Reproducibility could be further improved by using more sophisticated and automated manufacturing techniques such as would be employed in the large scale production of many devices. The fourth electrode was found to be non-functioning due to PVC membrane rupture (see Figure 3. 37).

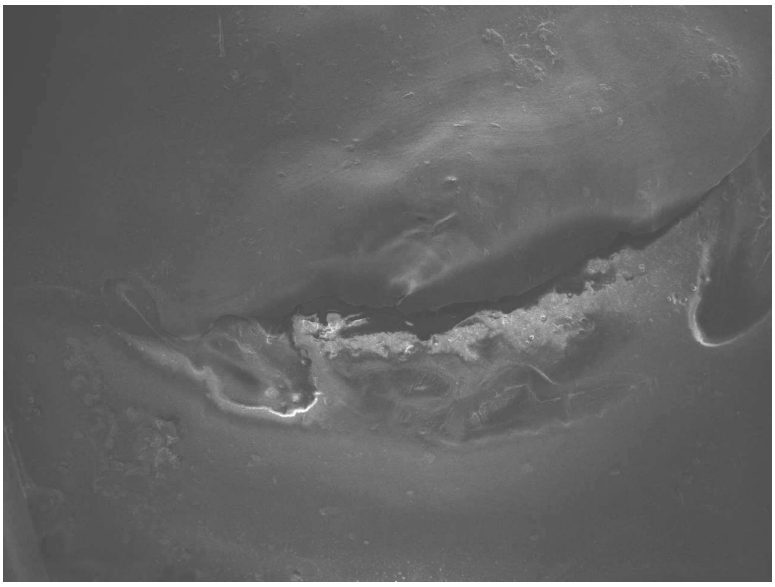

Figure 3. 37 SEM image of a non-functioning sensor with a ruptured PVC cap membrane

Subsequent SEM analysis of sensor 4 explains its non-functionality. As shown in Figure 3. 37 the PVC membrane is clearly torn at the outer edge. SEM facilitates easy diagnosis of the problem, but it is rather more difficult to ascertain the reason behind it. It is most likely attributable to a fault in the construction of the sensor to begin with. Perhaps a sharp or roughly milled edge affected the surface adhesion of the PVC, or the membrane may not have been built up sufficiently during the deposition process to withstand the swelling of the hydrogel layer. In general throughout this work the adhesion and structural integrity of the PVC membranes were found to be very good and sensor failure was not a serious issue.

Solution (M)	sensor 1		sensor 2		sensor 3	
0.00001	(-247.8, –248.2)	-248.0	(-237.3, -236.3)	-236.8	(-240.7, -239.9)	-240.3
0.0001	(-205.5, -205.2)	-205.4	(-198.2, -198.0)	-198.1	(-203.5, -203.5)	-203.5
0.001	(-148.6, -148.8)	-148.7	(-141.8, -141.2)	-141.5	(-148.1, -148.2)	-148.2
0.01	(-93.7, -93.8)	-93.8	(-88.7, -88.5)	-88.6	(-92.6, -92.6)	-92.6
0.1	(-43.2, -43.1)	-43.2	(-37.8, -37.9)	-37.9	(-41.9, -42)	-41.2
Slope	53.52		52.09		52.11	
Intercept	14.76		17.63		12.94	

Table 3.1 Calibration data used to generate the three sodium ISE calibration curves (Figure 3.34, Figure 3.35, and Figure 3.36). All values in mV.

Table 3.1 shows the calibration data for the three sensors over the 10^{-1} M to 10^{-5} M range. Measurements were made in duplicate and the mean values calculated and plotted. The slopes were slightly lower than the expected Nernstian response in each case, but the general performance of the electrodes was good, and the responses were quite rapid and stable. A similar test calibration was carried out in the CF-relevant sodium ion range (20 to 100 mM). The resultant calibration curves are shown in Figure 3.38, Figure 3.39, and Figure 3.40.

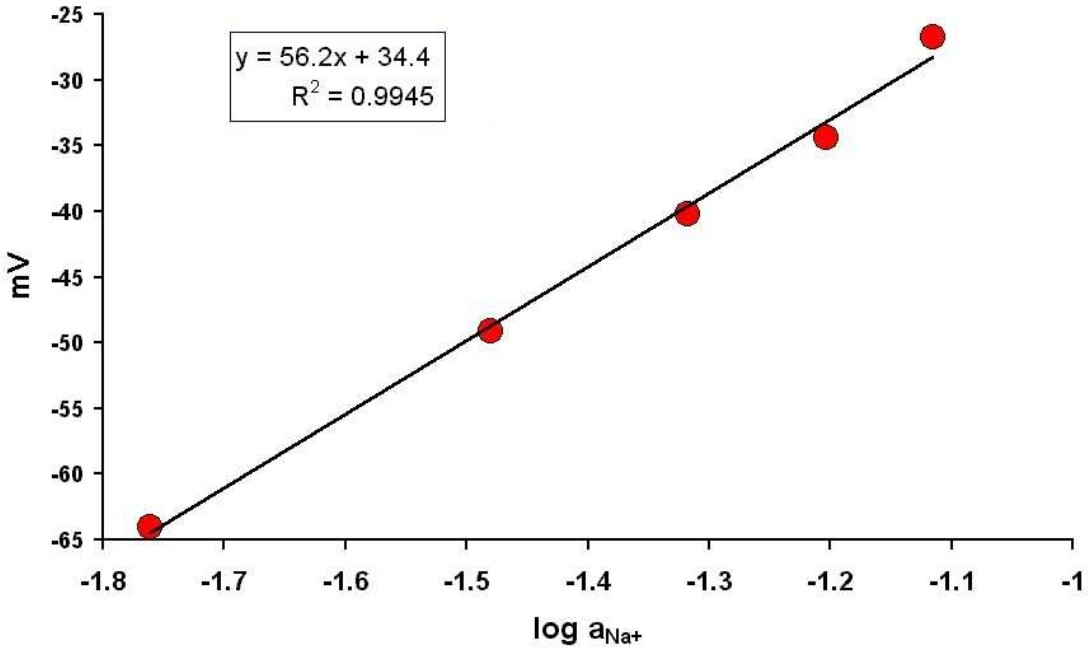

Figure 3.38 Calibration curve for sodium sensor #1 over CF-relevant range, 20-100mM.

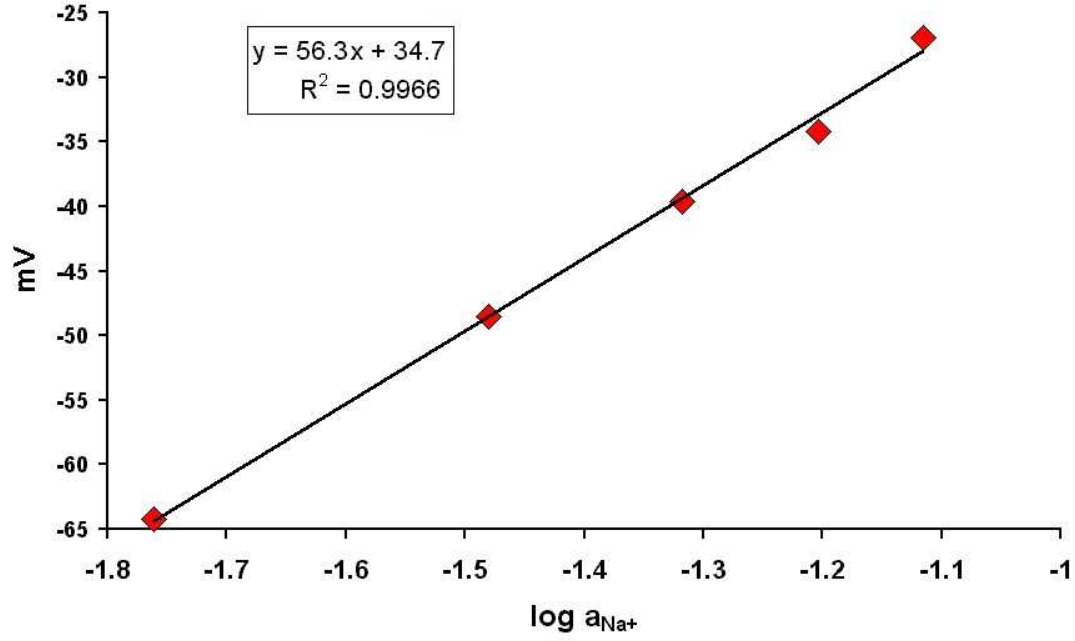

Figure 3.39 Calibration curve for sodium sensor #2 over CF-relevant range, 20-100mM.

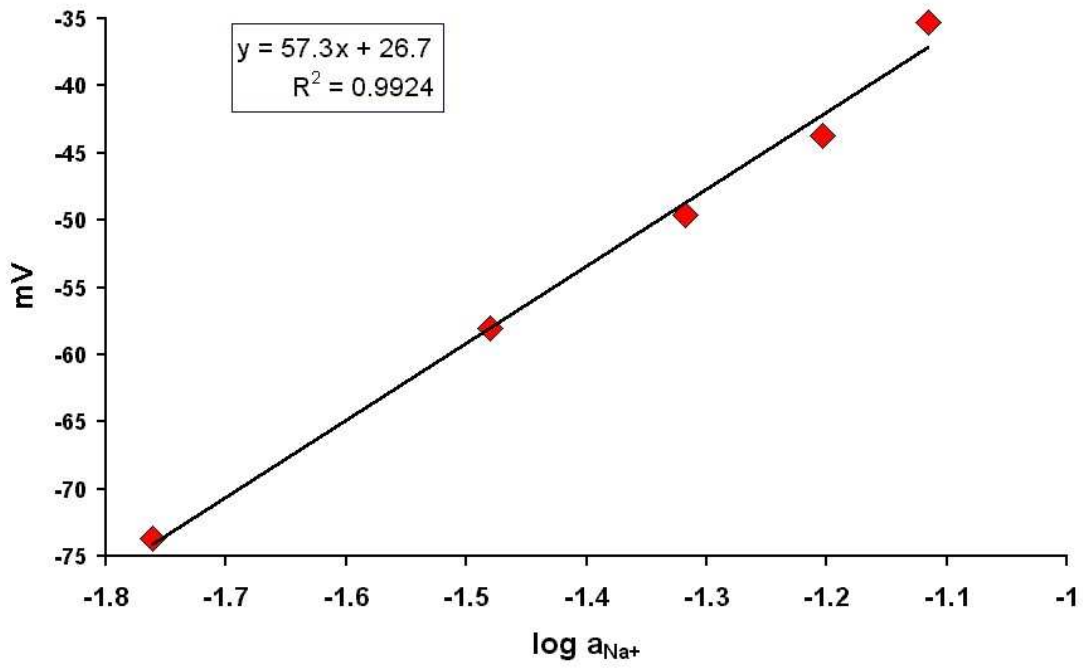

Figure 3.40 Calibration curve for sensor #3 over CF-relevant range, 20-100mM.

Solution (mM)	sensor 1	sensor 2	sensor 3
20	-64.0	-64.2	-73.7
40	-49.1	-48.5	-58.0
60	-40.2	-39.6	-49.6
80	-34.4	-34.2	-43.7
100	-20.1	-26.7	-26.9
Slope	56.2	56.3	57.3
Intercept	34.4	34.8	26.8

Table 3.2 Calibration data (in mV) used to generate the three sodium ISE calibration curves (Figure 3.38, Figure 3.39, and Figure 3.40) over the CF relevant range of 20-100mM

The test calibrations over the expected sodium CF range yield near Nerstian slopes and excellent linearity. Repeat calibrations carried out on a different day, this time in triplicate, assessed the reproducibility of the sensor responses.

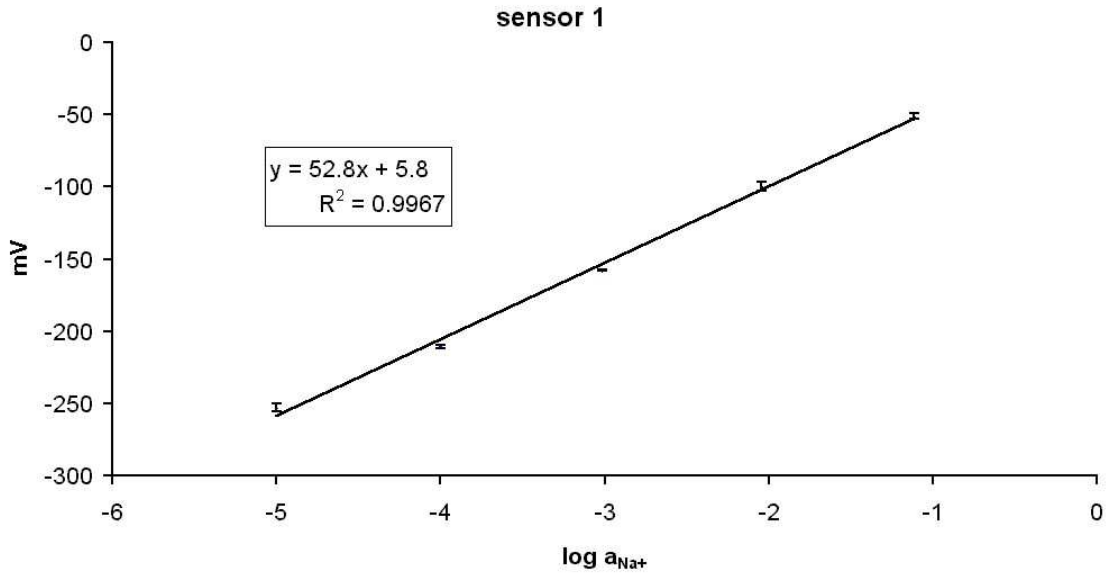

Figure 3.41 Repeat calibration curve, sodium sensor #1

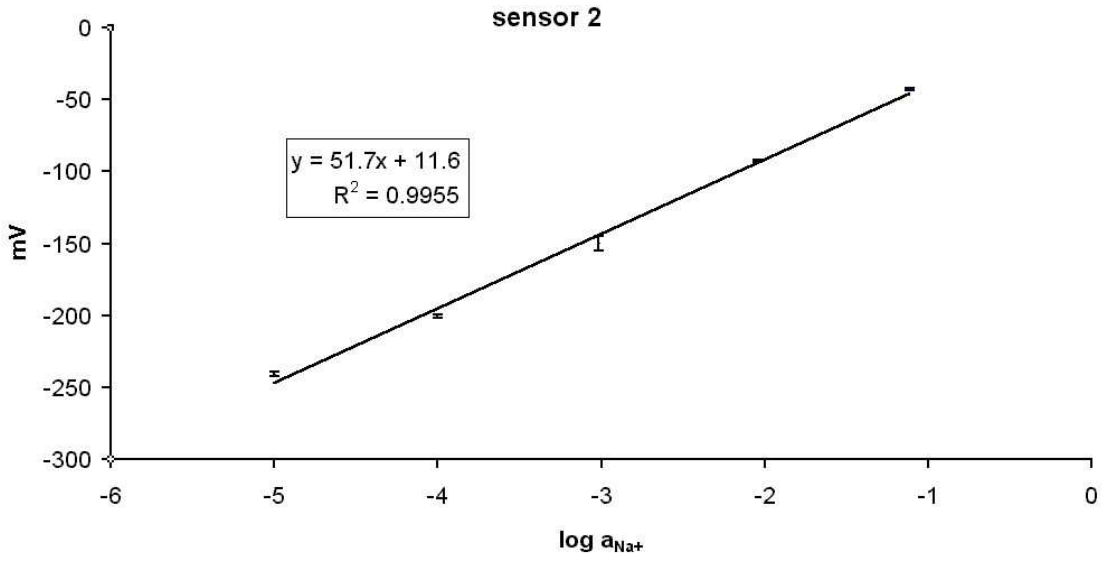

Figure 3.42 Repeat calibration curve, sodium sensor #2

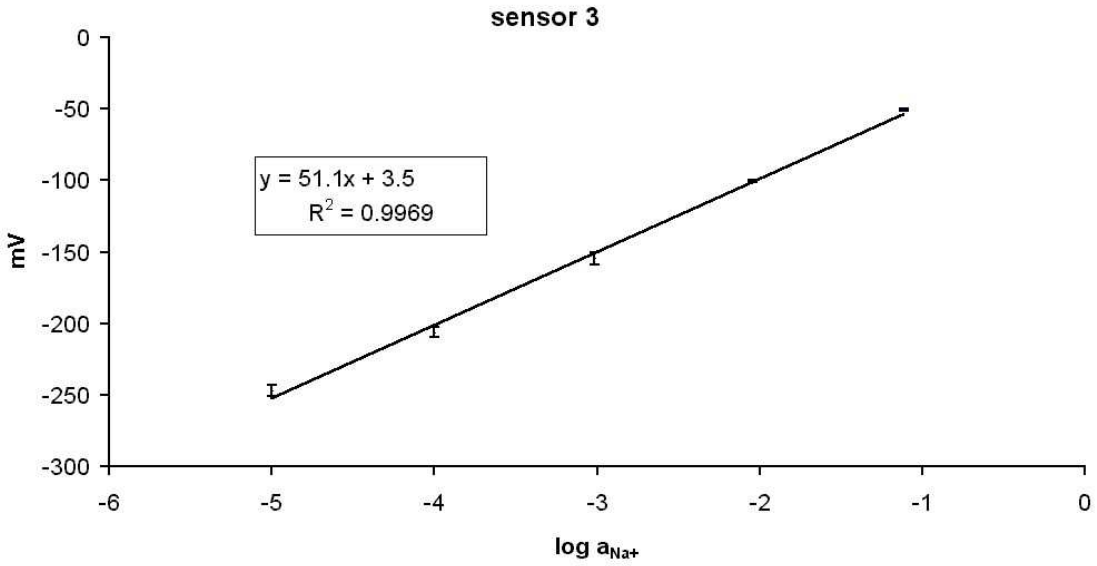

Figure 3.43 Repeat calibration curve, sodium sensor #3

Figure 3.41 to Figure 3.43 shows three calibrations carried out once again over a full 5-point calibration range from 10^{-5} M to 10^{-1} M NaCl using a standard calomel electrode as a reference. The electrodes were each allowed to stabilise for about 15 seconds and the response was then monitored for a period of about 30 seconds during which time the highest and lowest readings were recorded (see Table 3.3). This was repeated three times for each electrode. The average of these three readings was graphed against the log of the activity of the sodium ion. N=3 standard deviations were also calculated and are listed in Table 3.3. From the graphs it can be seen that once again the slopes are slightly sub-Nernstian but good linearity over the range is observed and the results are consistent.

Solution (M)	sensor 1		sensor 2		sensor 3	
0.00001	(-252.3, -252.5)	-252.4	(-240.7, -240.9)	-240.8	(-243.1, -243.1)	-243.1
0.0001	(-210.6, -210.5)	-210.6	(-200.3, -201.1)	-200.7	(-202.1, -202.4)	-202.3
0.001	(-157.6, -157.7)	-157.7	(-155.2, -155.1)	-155.2	(-149.4, -149.4)	-149.4
0.01	(-96.1, -96.0)	-96.1	(-93.0, -92.7)	-92.9	(-99.7, -99.8)	-99.8
0.1	(-49.1, -49.2)	-49.2	(-42.6, -42.7)	-42.7	(-49.7, -49.7)	-49.7
0.00001	(-255.8, -256.1)	-255.9	(-242.1, -241.9)	-242.0	(-251.0, -250.6)	-250.8
0.0001	(-212.1, -212.1)	-212.1	(-202.1, -201.9)	-202.0	(-208.3, -208.1)	-208.2
0.001	(-158.3, -158.5)	-158.4	(-145.5, -145.7)	-145.6	(-157.3, -157.2)	-157.3
0.01	(-102.3, -102.3)	-102.3	(-92.3, -92.3)	-92.3	(-101.0, -101.0)	-101.0
0.1	(-52.4, -52.5)	-52.5	(-42.6, -42.6)	-42.6	(-51.1, -51.1)	-51.1
0.00001	(-250.6, -250.7)	-250.7	(-239.0, -239.2)	-239.1	(-246.9, -247.0)	-247.0
0.0001	(-209.6, -209.7)	-209.7	(-199.7, -199.7)	-199.7	(-207.9, -208.1)	-208.0
0.001	(-158.2, -158.1)	-158.2	(-148.8, -148.9)	-148.9	(-156.8, -156.9)	-156.9
0.01	(-100.7, -101.7)	-101.2	(-93.1, -92.2)	-93.2	(-101.4, -101.5)	-101.5
0.1	(-52.2, -52.5)	-52.4	(-43.4, -43.4)	-43.4	(-51.1, -51.2)	-51.2

Standard deviations (n=3)			
0.00001	2.70	1.46	3.85
0.0001	1.24	1.15	3.35
0.001	0.38	4.86	4.42
0.01	3.34	0.43	0.88
0.1	1.88	0.45	0.82

Table 3.3 Calibration the data used to generate the calibration curves in Figure 3.41 to Figure 3.43. The results are given in the format *(1st reading, 2nd reading) average reading.* Standard deviations n=3 were calculated from the average values from the triplicate calibrations and used to construct the error bars as illustrated

Having established using the pH meter that the sodium electrodes were functioning satisfactorily, further experimentation was simplified by interfacing the electrodes with a PC via a National Instruments MIO-16 data acquisition card. This allowed the simultaneous monitoring of all electrodes using an in-house written LabVIEW program which also facilitated visualisation of the response trace of the electrodes over time, and was the intended data capture and monitoring system for use with the CF watch.

The Ag/AgCl electrode

The external reference electrode for the cell was to be a simple silver-silver chloride electrode. It was prepared in exactly the same way as the internal Ag/AgCl internal reference electrodes incorporated into the sodium ISE's, i.e. by immersing a length of silver wire in sodium hypochlorite solution for 40 to 60 minutes to form a layer of silver chloride on its surface. In the analysis of aqueous sodium chloride solutions however, this Ag/AgCl "reference" electrode will be expected to respond to changes in the chloride ion concentration as an electrode of the second kind. To investigate its performance as a chloride ISE, this electrode was subjected to the same 5-point calibration (10^{-5} M to 10^{-1} M NaCl) as the sodium test electrodes, using a standard calomel electrode as a reference.

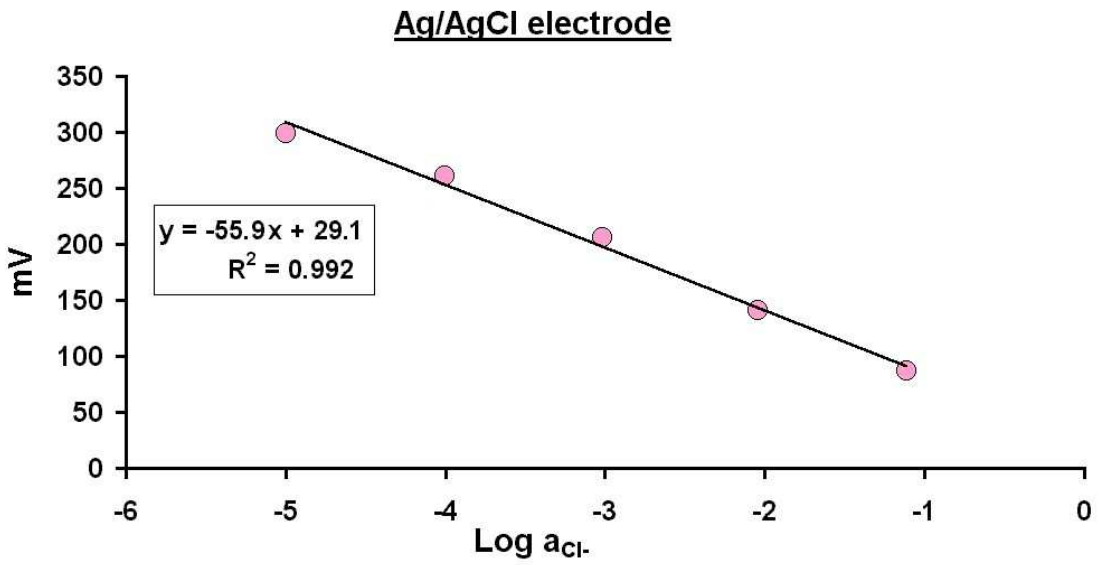

Figure 3.44 Calibration curve for Ag/AgCl, 10^{-5} M to 10^{-1} M NaCl.

From the Ag/AgCl electrode calibration curve in Figure 3.44 it can be seen that the slope of the curve, though slightly sub-Nernstian, is adequate, and is on a par with the responses obtained from the sodium electrodes to the same calibration regime. Table 3.4 below shows that stability of the response is best in the 10^{-1} to 10^{-2} M range, which is the concentration range of interest for sweat analysis.

Solution (M)	Ag/AgCl avg response	Standard Deviation
0.00001	299.4	1.47
0.0001	261.3	0.79
0.001	205.5	0.68
0.01	141.3	0.99
0.1	87.1	0.09
Slope	-55.94	
Intercept	29.08	

Table 3.4 Ag/AgCl electrode data, used to generate the calibration curve in Figure 3.44.

Sodium and Chloride ISE Combined Response

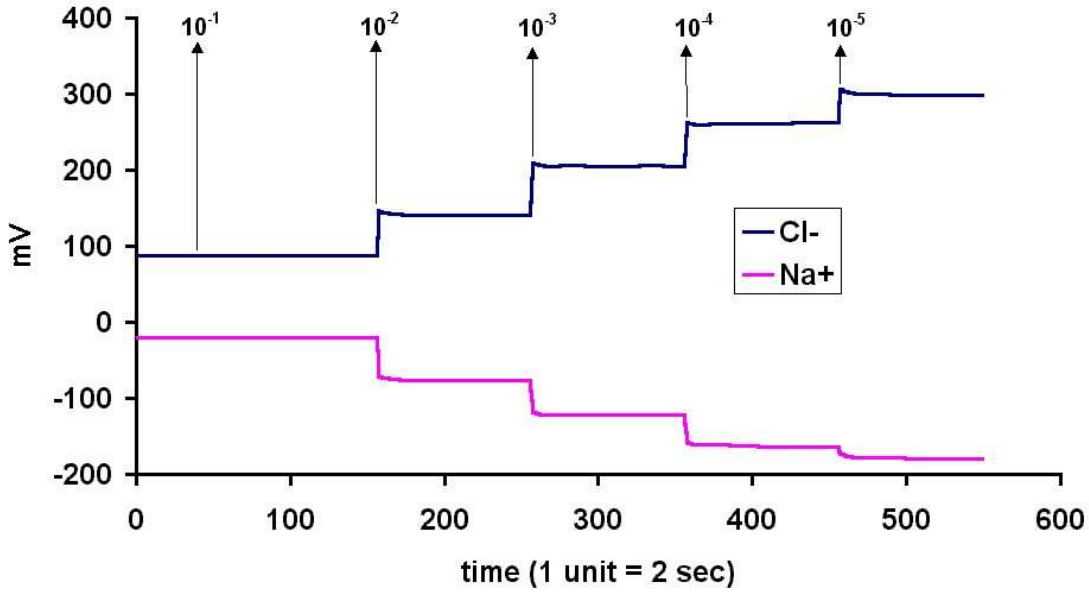

Figure 3.45 Comparison of both electrodes response to the same calibration, using a standard calomel reference electrode.

Figure 3.45 compares the response of the Ag/AgCl electrode (see Figure 3.44) and sodium sensor #1 (see Figure 3.43). The electrode responses were monitored using a LabVIEW virtual instrument interface and a 5-point calibration (10^{-1} M to 10^{-5} M NaCl) for each of the two electrodes was carried out, using a standard calomel reference electrode. The test set-up pictured and described in Figure 3.24 was used to analyse the standard. As usual, each horizontal portion of the graph represents the mV response (x-axis), measured and recorded automatically every two seconds, over a period of time (approximately 3 minutes). After monitoring the response for this period of time, the data monitoring software was paused while the test well was emptied and rinsed and an aliquot (ca 10ml) of the next standard pipetted into the well. The trace is not intended to represent a real time flow injection analysis trace therefore, and while each horizontal portion does represent a real time response, data collation was paused between standards. The graphs illustrate therefore the relative responses of the two electrodes to the same standards, it shows that the responses are stable and not excessively noisy or prone to excessive drift, and it illustrates also how the chloride response mirrors the sodium response but in an opposite direction. Referencing the sodium electrode against this “moving reference” chloride electrode has the effect of adding the slopes of the electrodes together to give an overall response. This is further illustrated in Figure 3.46.

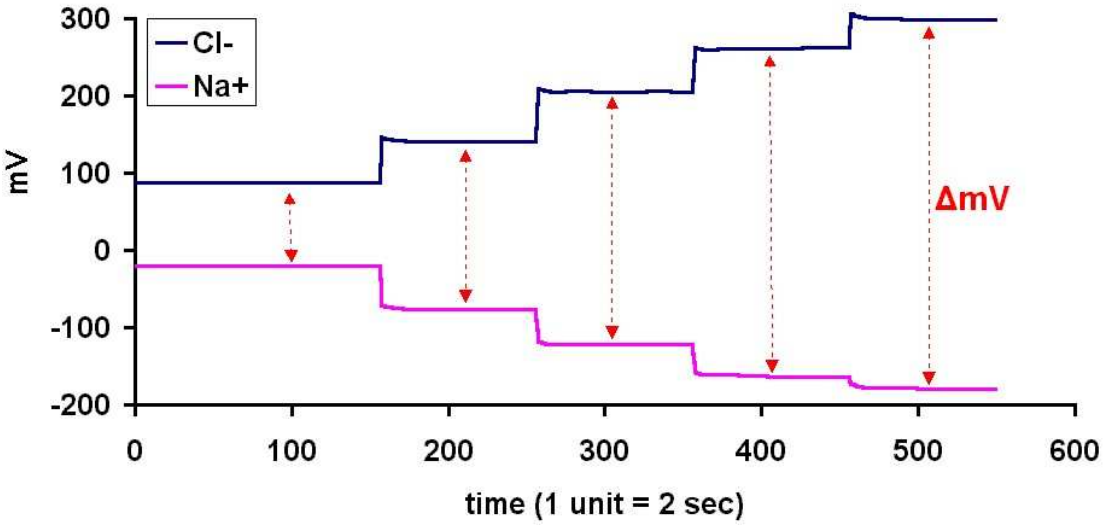

Figure 3.46 Response of the two ISE's relative to each other.

Figure 3.46 shows the same graph as in Figure 3.45 but with the relative response between the two indicator electrodes highlighted by the red dotted arrows. As the sodium and chloride concentrations increase from left to right ΔmV increases with both electrodes contributing to the overall response.

The 5 point calibration was repeated again but without the external calomel reference electrode. Instead the sodium electrode response was measured with the chloride Ag/AgCl electrode acting as the reference electrode. Only one signal was obtained therefore, so there is only one signal trace. The slope of the response is equal to the sum of the slopes of the individual electrodes. The calibration trace is shown in Figure 3.47

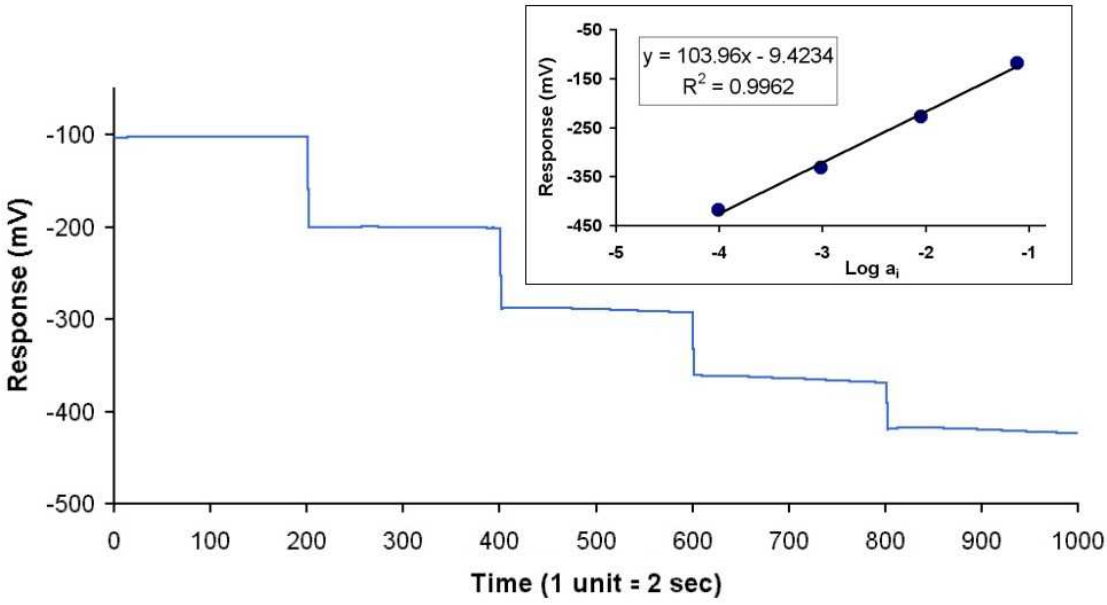

Figure 3.47 Combined E_{cell} response where $E_{cell} = E_{ise} - E_{ref} = \Delta mV$ and the Ag/AgCl Chloride electrode is employed as a reference.

Figure 3.45, Figure 3.46 and Figure 3.47 illustrate the magnification of the overall signal obtained by referencing the sodium electrode against an Ag/AgCl electrode. A CF diagnosis is given by elevated sodium and chloride concentrations; therefore a positive CF sample value will evoke a sodium concentration–related response from the sodium electrode in a positive direction (E_{ise}), while the same sample will evoke a chloride concentration-related response from the Ag/AgCl electrode in a negative direction E_{ref}. The net measured response $E_{cell} = E_{ise} - E_{ref}$ will effectively be the sum of the responses of the individual electrodes.

Figure 3.47 is a graph of the response obtained when the Ag/AgCl electrode is used in place of a standard reference electrode. There are two electrodes but only one response trace, and the slope of the cell as shown is the sum of the slopes of the individual electrodes. In Figure 3.43 the slope of the sodium electrode (#1) is

51.1mV, and the chloride electrode slope from Figure 3.44 is –55.9 mV. The overall cell response in mV per decade change in activity =

$$
\begin{aligned}
E_{cell} &= E_{ise} - E_{ref} \\
&= E_{Na^+} - E_{Cl^-} \\
&= 51.1 - (-55.9) \\
&= 107.0 \text{ mV}
\end{aligned}
$$

When measured separately against an external reference, the sum of the slopes is ca 107 mV. When the electrodes were referenced to each other, the combined slope was calculated at 104 mV (Figure 3.47 inset). Some variation in the slopes is expected, but the overall response, as with the individual responses, is lower than the predicted Nernstian response (118mV). A reasonable level of reproducibility was exhibited by the individual electrode slopes considering that the devices are hand made, and it is important that this reproducibility should carry through to the combined response.

The results obtained so far suggest that the sensors are operational. The response is satisfactory and reasonably consistent and reproducible. A “CF Watch” device was therefore constructed following the design brief already described (Figure 3.18 to Figure 3.23) and using the same dimensions, materials and construction methods as were used in the manufacture of the test electrodes. The device was utilised in the analysis of real sweat samples in a simulated clinical screening trial

3.8 Clinical Trial

A mixed 1.00 mol l^{-1} stock standard solution of sodium chloride was prepared by dissolving 5.85g of NaCl in water and making up to volume in a 100ml volumetric flask. This was diluted with ultrapure water to give 0.02, 0.04, 0.06, 0.08, and 0.1 mol l^{-1} standard solutions (= 20, 40, 60, 80 and 100 mM). 21 sweat samples were collected, 15 from a normal population, and 6 from a CF positive population. Samples were collected on-site at the following locations: Our Lady's Hospital Crumlin CF clinic; Beaumont Hospital CF clinic; and Dublin City University. For ethical and sensitivity reasons the hospital trials did not involve on-skin collection & analysis. Samples were instead collected on-site by pilocarpine iontophoresis and stored at 4˚C until all of the samples were collected and could then be analysed together in a laboratory environment. As well as being more ethically sensitive to the patients involved, it enabled a more controlled trial to be carried out in the DCU laboratory environment. The on-line situation was mimicked as closely as possible, the sweat samples were analysed un-diluted and untreated and a peristaltic pump was used to pump the samples through the flow-cell.

The compatibility of the Macroduct and the analytical device in an on-line analysis situation is demonstrated later in Figure 3.54.

AAS was used as a reference method for sodium as in previous trials. The Mohr titration method was used as a reference method for chloride.

Mohr Method

The Mohr method is a titrimetric method for the quantitative analysis of chloride by silver nitrate titration. The use of silver nitrate in volumetric analysis depends on the fact that silver halides are quantitatively precipitated from solution:

$Ag^{+}_{(aq)} + X^{-} \rightarrow AgX_{(s)}$ X= Cl^{-}, Br^{-}, I^{-}

The reaction is self-indicating, as precipitation will cease when all the chloride is precipitated. However this method is slow and the endpoint is difficult to ascertain therefore potassium chromate is used as a colour indicator to assist in the determination of the endpoint of the titration. The chromate anion forms a brick red precipitate with silver ions:

$2AgNO_3 + K_2CrO_4 \rightarrow Ag_2CrO_4 + 2KNO_3$

Silver nitrate is available in a high state of purity and is suitable as a primary standard. If silver nitrate is added to a solution containing Cl^{-} ions and a few drops of potassium chromate indicator, silver chloride is selectively precipitated before silver chromate. The first trace of excess silver ions reacts with the chromate ions present forming a brick red precipitate, which marks the end point of the titration. The Mohr method can only be used in neutral solution because silver chromate is soluble in acid solution and silver oxide is precipitated from alkaline solution. The silver nitrate reacts with

chloride ions in a 1:1 stoichiometry. When all the chloride is spent, the first sign of a persistent brick-red colour signals the endpoint of the titration.

$(\text{Vol } AgNO_3)\ (\text{M } AgNO_3) / (n) = (\text{Vol } Cl^-)\ (\text{M } Cl^-) / (n)$

The molar concentration of Cl^- therefore $= (V_{AgNO3}).(M_{AgNO3}) / (V_{Cl^-})$

Sample treatment

At least 50 µl of sweat were collected for each sample. 10 µl of this was extracted and diluted up to 1000 µl (1ml) (100 fold dilution) for chloride analysis by micro-titration against 0.005M Silver Nitrate.

50 µl was extracted from each of these titration samples and diluted up to 5000 µl with Ultrapure deionised water for sodium analysis by flame emission AAS (a further 100 fold dilution). Total dilution factor is a 1 in 10000, and the same was carried out on the standards to bring AAS samples and standards within the appropriate AAS linear range (0.002 to 1.0 ppm).

Worked example: Taking a 50µl normal sweat sample at a presumed sodium and chloride concentration of 40 mM. 10 µl are extracted and diluted to 1 ml. 950 µl is set aside for titration, while 50 µl are diluted to 5 ml for AAS analysis.

Titration

(0.04M)/(100) = 0.0004M titration sample

(0.95).(0.0004) = (V_{AgNO3}).(0.005)

76 µl $AgNO_3$ are required to neutralise the chloride concentration in the sample.

AAS

The remaining 50 µl diluted to 5000µl for AAS

(0.04M)/(10000) = 0.000004M

(0.000004).(58.5) = 0.000234 g/L

= 0.234 mg/L (ppm)

Titration was carried out using a 1ml micro-burette. Flame Emission AAS was carried out under the following recommended conditions:
(Lamp current: 5mA; Fuel: acetylene; Support: air; Flame stoichiometry: oxidising; Wavelength: 589.0nm; Slit width: 0.5 nm; Working range: 0.002 to 1.0 ppm)

3.9 Results and Discussion

A watch device consisting of one sodium PVC membrane electrode and one Ag/AgCl electrode was used for the clinical trial. Its manufacture was described previously in detail from Figure 3.18 to Figure 3.23. The silver wires from both electrodes were connected to high quality shielded cable via a 2-way HE14 socket, to transfer signals to a PC via a shielded box with an impedance correction circuit, enabling continuous

monitoring of the sensor signals during standard and sample analysis. The software allows the monitoring of four channels at once, but in this case only one indicator electrode channel was employed. The sodium electrode was connected to this channel and the chloride pseudo-reference electrode was connected to the reference channel. The flow channels in the array were hooked up to capillary tubing and a peristaltic pump so that samples and standards could be passed through the device.

The device was first allowed to condition overnight, from dry. The signals from the electrodes were monitored and recorded continuously to monitor the hydration of the sodium electrode. The trace obtained is shown in Figure 3.48.

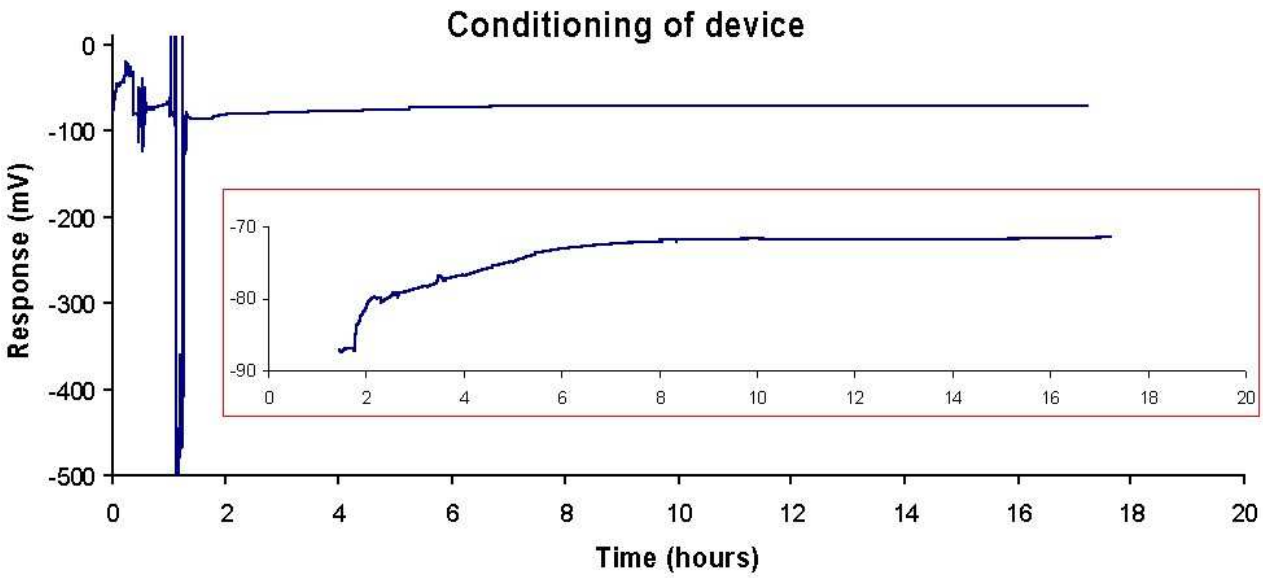

Figure 3.48 Response trace from device left to condition from dry overnight.

The overnight conditioning solution used was the lowest concentration (20 mM) NaCl standard. As can be seen, after approximately 8 hours the device reaches a steady-state voltage at equilibrium. The main graph is the conditioning of the device from dry. The smaller inset graph with the red border is a more detailed look at the

conditioning trace with a smaller x-axis scale, after the initial spikes and noise. It shows the signal increasing as the sub-membrane hydrogel hydrates until an equilibrium steady-state signal is obtained.

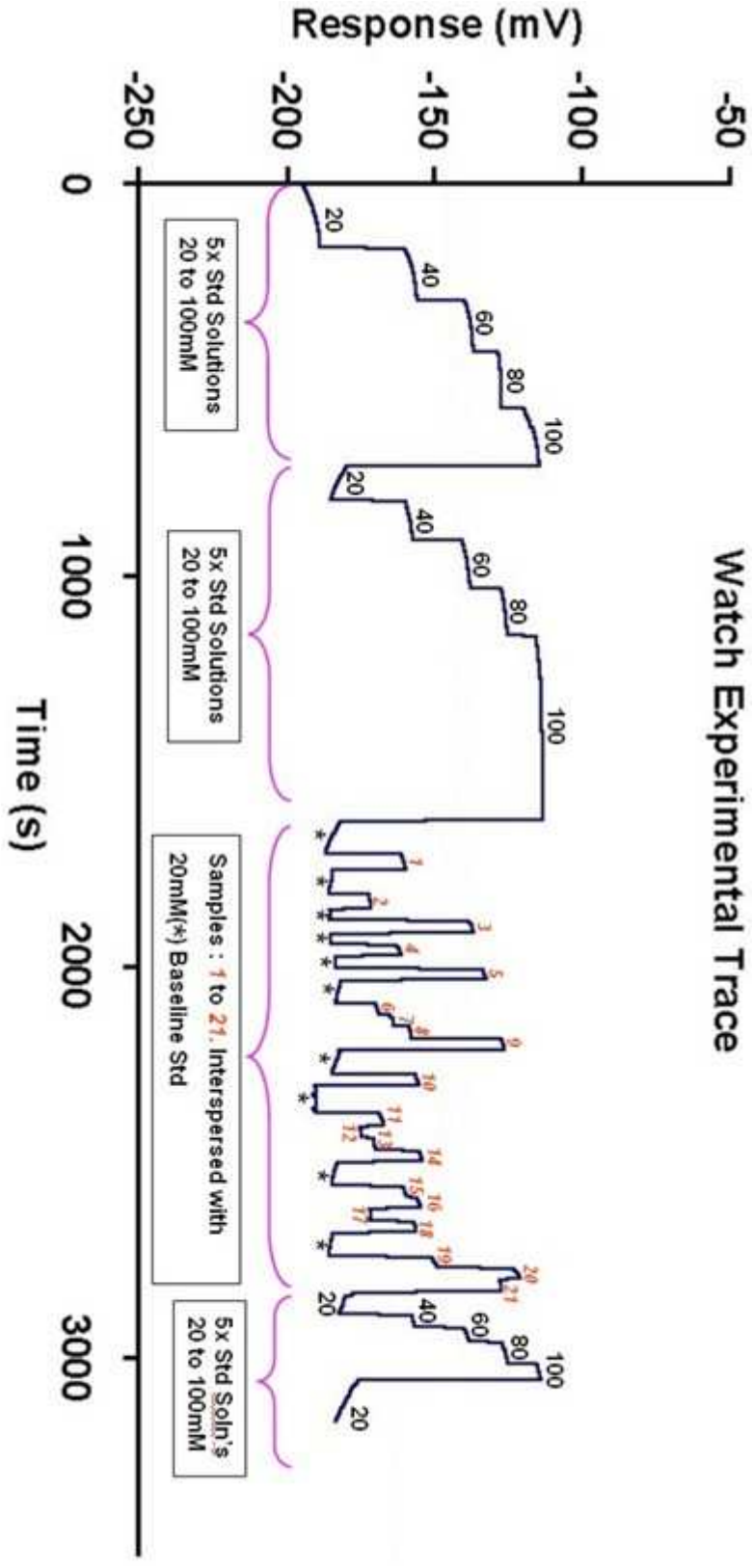

Figure 3.49 Response trace from LabVIEW imported into Microsoft Excel.

The experimental response trace in Figure 3.49 follows the format of the many other similar traces throughout this document, for the previous CF trial, the simulated CF trial, and indeed the calibration traces in this chapter in Figure 3.45, Figure 3.46 and Figure 3.47. The trace can be followed from left to right, and each horizontal portion of the graph represents the response of the device to a particular solution. The first solution is the 20 mM standard, followed by the 40 mM standard, then the 60, 80 and 100 mM standard solutions. This 5-point calibration from 20 to 100 mM NaCl is repeated. The 20 mM standard was then re-analysed, followed by the analysis of each of the sweat samples. The 20 mM baseline standard (denoted by the "*" asterisk symbol) was re-analysed again periodically between sample analyses to establish a continuous base line. Finally, the 5 standard solutions were again passed through the array in a third and final 5-point calibration.

The data from the three calibrations was tabulated (Table 3.5) and the average responses were calculated and used to construct the calibration curve in Figure 3.50.

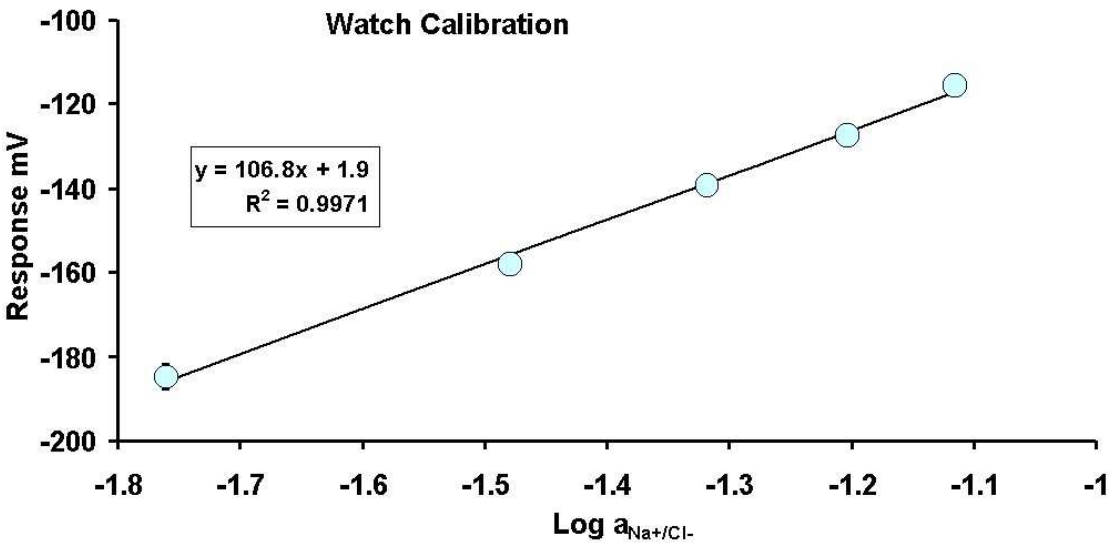

Figure 3.50 Standard Calibration Curve (20 to 100 mM) generated from the triplicate trial calibration data.

Figure 3.49 shows the response of the device to the standards and samples in sequence. All solutions were pumped through the device using a peristaltic pump connected to the capillary tubing in the device flow channels (see Figure 3.13). The device was flushed with each standard solution for approximately 20 seconds using the peristaltic pump's high speed flush mode, and the data acquisition paused during this solution changeover. It was not possible to flush the sample chamber with each sweat sample so liberally and for such a length of time because of sample volume constraints, though with a sample chamber volume of approximately 7.2 µl, and 40 µl of sample to work with, there was adequate margin to ensure complete filling of the chamber for each sample. The calibration curve in Figure 3.50 shows excellent linearity and repeatability, with the slope as expected. Error bars are included and are hidden by the sample points. The standard deviations [see Table 3.5] are also very encouraging at generally less than 1mV. The notable exception to that is the 20 mM standard. As can be seen from the trace, the 20 mM standard was used to set the base

line and was analysed continuously between samples and at the beginning and end of each calibration. Considerably more time could have been expended in allowing the 20 mM standard solution signal to equilibrate each time it was analysed as it does exhibit a good deal of variation across the bottom of the trace and this is reflected in the standard deviation value. The standard deviation value calculated in Table 3.5 however was only calculated from three of the values obtained for the 20 mM standard, namely the values from the three calibrations. If the standard deviation for the 20 mM standard is calculated for the entire base line, a lower value of 3.05 mV is obtained. Again if the signal had been allowed to equilibrate longer each time it was analysed, this would be further improved. Another reason perhaps for the higher standard deviation of the 20mM standard is the frequency with which it was analysed, making it more susceptible to error due to contamination during solution changeover.

Standard			**Calibration**			**St. Dev.**	
(mM)	**a_i**	**log a_i**	**#1**	**#2**	**#3**	**Average**	**(n=3)**
20	0.017	-1.761	-191.1	-182.9	-180.7	-184.8	5.50
40	0.033	-1.480	-157.8	-158.8	-157.6	-158.1	0.66
60	0.048	-1.320	-138.4	-139.6	-139.7	-139.2	0.72
80	0.063	-1.204	-128.3	-126.7	-126.7	-127.2	0.90
100	0.077	-1.115	-116.9	-114.4	-115.3	-115.5	1.30

Table 3.5 Data used to generate the standard curve in Figure 3.50

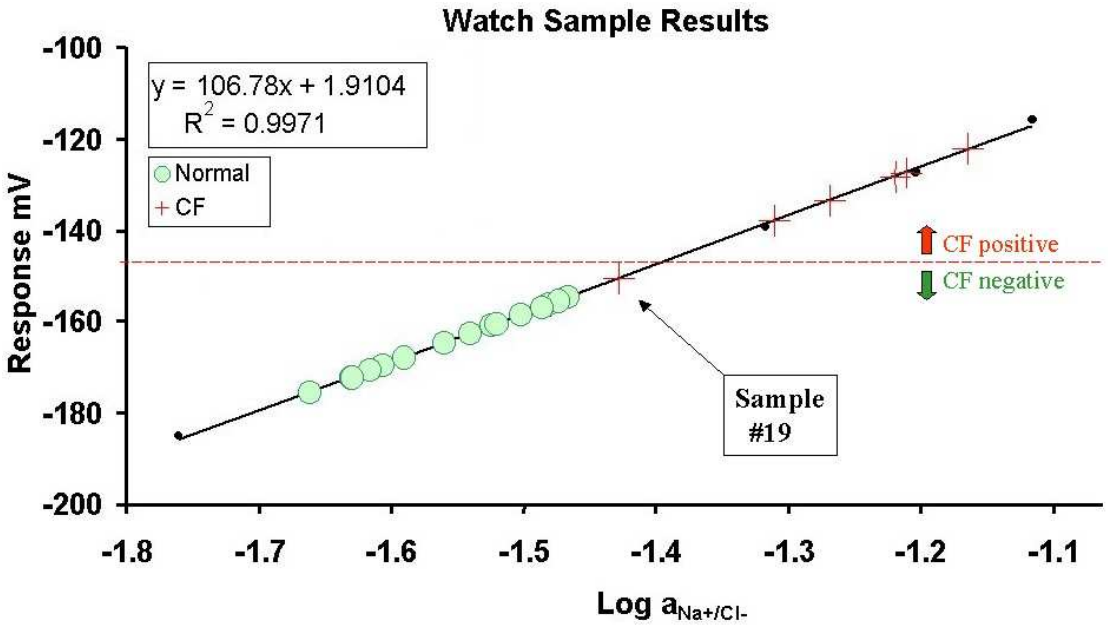

Figure 3.51 Sample activities calculated from the calibration curve and projected onto the curve to illustrate the separation of the CF samples from the normal sweat samples.

Figure 3.51 shows the sample diagnoses on the basis of the watch results. The dotted red line indicates the expected mV response for a 50 mM Na^+ and Cl^- solution, and therefore equates to an approximate diagnostic cut-off. Normal samples are expected to fall below this line and CF positives above it. The graph shows the CF normal samples represented by the green circles to be well clustered together and well below the diagnostic cut-off point. Similarly, with one exception (#19) the positive samples represented by the red crosses are also clustered together and they are above the red line, indicating that they are correctly diagnosed as CF positive samples. In general therefore clear separation of the normal and positive samples was achieved, and all of the samples, except one, were assigned a diagnosis consistent with their source population, i.e. all samples taken from a normal population were diagnosed as normal, and all samples taken from a CF positive population were diagnosed as positive with the exception of samples #19. Sample #19 is marked with a red cross because it was

known to have been sampled from a CF positive population, but on the basis of the watch results it has been diagnosed as borderline normal.

All of the samples are correctly diagnosed therefore bar one, sample #19, which as indicated on the graph falls just below the diagnostic cut-off point indicated by the dotted red line. This does not automatically infer analytical error or failure on the part of the watch device. False positives and false negatives are not unheard of and may be attributed to a procedural error at any point from sampling to analysis, or the patient may in fact have borderline sweat electrolyte levels with or without CF. In borderline cases re-tests are generally carried out and indeed in any sweat-test based diagnosis, at least two sweat tests must be carried out and be in agreement with each other.

In this case sample #19 was taken from a CF positive population and is expected therefore to have sodium and chloride activities consistent with a CF positive diagnosis. This does not seem to be the case, based on the sweat watch results (Figure 3.51). However, this apparent misdiagnosis is mirrored by the flame emission results in Figure 3.52, which show a borderline sodium ion concentration for sample #19. Also in the titration results (Figure 3.53) the chloride ion concentration of sample #19 is at the lower end of the cluster of CF positive samples. These relatively low concentrations of sodium and chloride as indicated by the watch device and sample #19 is therefore a genuine borderline result.

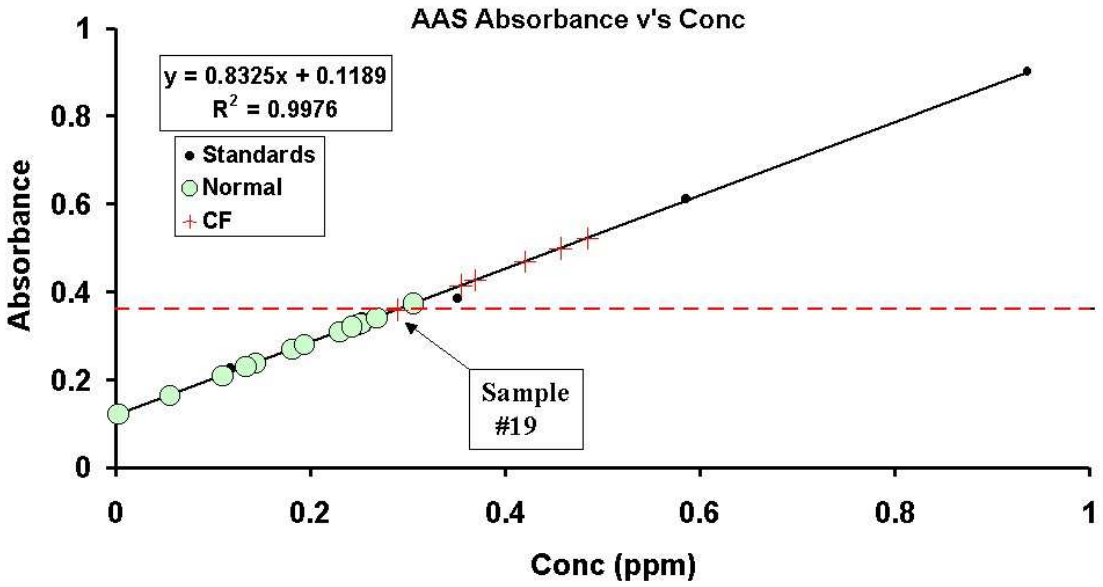

Figure 3.52 Sodium AAS reference method data

The AAS data for sodium, seen in Figure 3.52, shows a degree of overlap between the CF and the normal samples. Sodium is not as discriminatory as chloride in CF diagnosis. As before, the red crosses represent the CF positive samples while the green circles represent the normal sweat samples. The small black circles represent the 5 standard solutions used for calibration. Again, generally speaking, the normal samples are clustered together in the lower portion of the graph and below the 50mM cut off, which is as expected. The CF positive samples are higher up in the concentration range and generally fall between the black circles representing the 60 and 80 mM standards, which is the expected concentration range for CF positive sweat samples. Interestingly, the sample that was diagnosed as borderline by the sweat watch results is also borderline for these AAS results, namely sample #19.

Standard	Abs. mean	RSD (%)	Conc. (ppm)	Conc. (mM)
0	0.011	2.1	0.000	0
1	0.170	7.6	0.059	20
2	0.229	0.5	0.117	40
3	0.386	0.1	0.351	60
4	0.612	1.6	0.585	80
5	0.902	0.1	0.936	100

Sample	Abs. mean	RSD (%)	Conc. (ppm)	Conc. (mM)
1	0.238	2	0.143	24.46
2	0.165	1.3	0.055	9.47
3	0.522	0.3	0.484	82.77
4	0.121	0.1	0.003	0.43
5	0.469	2.4	0.421	71.89
6	0.270	2.7	0.182	31.03
7	0.280	0.2	0.194	33.08
8	0.310	0.7	0.230	39.24
9	0.414	2.7	0.354	60.59
10	0.329	0.1	0.252	43.14
11	0.325	0.3	0.248	42.32
12	0.342	0.2	0.268	45.81
13	0.328	2.7	0.251	42.94
14	0.373	0.7	0.305	52.18
15	0.230	1.2	0.133	22.81
16	0.210	10.2	0.109	18.71
17	0.342	5.3	0.268	45.81
18	0.321	7.1	0.243	41.50
19	0.359	4.1	0.288	49.30
20	0.426	0.4	0.369	63.06
21	0.499	2.8	0.457	78.05

Table 3.6 AAS data for standards and samples. Sodium mM concentrations are calculated. The values obtained are generally consistent with expected sweat sodium levels (>50mM for CF and <50mM for normal).

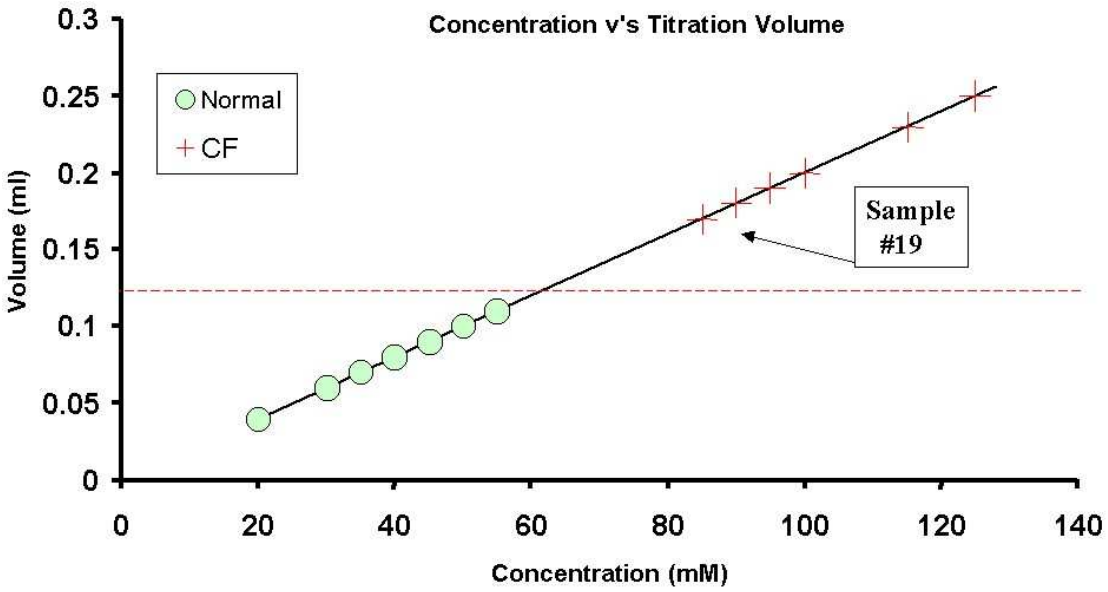

Figure 3.53 Mohr titration chloride-ion concentration data showing good separation of positive and negative sweat samples.

Sample	Vol $AgNO_3$	Conc. (mM)
1	0.11	55
2	0.08	40
3	0.23	115
4	0.06	30
5	0.19	95
6	0.09	45
7	0.07	35
8	0.10	50
9	0.17	85
10	0.07	35
11	0.07	35
12	0.11	55
13	0.09	45
14	0.06	30
15	0.09	45
16	0.04	20
17	0.08	40
18	0.07	35
19	0.18	90
20	0.20	100
21	0.25	125

Table 3.7 Chloride data from Mohr titration. Sample chloride concentrations were calculated from the titration data.

The mM values for chloride ion in Table 3.7, and the graphical separation of the two sample populations in Figure 3.53, illustrate well the innate superiority of the chloride ion in discriminating between positive and negative CF sweat samples. Normal sweat samples all show chloride levels below 60 mM and the CF positive are all above 80 mM with half of them over 100 mM. This amounts to a clear separation of the two sample groups. The lowest positive sample was the same sample (#19) that was diagnosed as borderline negative using the other two methods.

Sample	Population	Na^+ (AAS) (mM)	Cl^- (Mohr) (mM)	CF Watch Result
1	normal	24.5	55	normal
2	normal	9.5	40	normal
3	CF	82.8	115	CF
4	normal	0.4	30	normal
5	CF	71.9	95	CF
6	normal	31.0	45	normal
7	normal	33.1	35	normal
8	normal	39.2	50	normal
9	CF	60.6	85	CF
10	normal	43.1	35	normal
11	normal	42.3	35	normal
12	normal	45.8	55	normal
13	normal	42.9	45	normal
14	normal	**52.2**	30	normal
15	normal	22.8	45	normal
16	normal	18.7	20	normal
17	normal	45.8	40	normal
18	normal	41.5	30	normal
19	CF	**49.3**	90	**normal**
20	CF	63.1	100	CF
21	CF	78.0	125	CF

Table 3.8 Summary of diagnostic results obtained from the CF watch and the two reference methods. Anomalies are highlighted in bold. In all cases, but one, the watch results correctly match sample with population. Sample #19 was taken from a CF population but was diagnosed normal by the CF watch device. The AAS results show that the sodium ion concentration in sample #19 is indeed just below the 50mM cut off point and this must be responsible for the watch misdiagnosis. Sample #14 on the other hand is a normal sweat sample but has a sodium concentration just above the cut-off point and suggestive of CF. The chloride concentration of the same sample at 30 mM is well in the normal region however and the overall watch diagnosis is therefore normal.

Table 3.8 summarises the results obtained for all 21 sweat samples for the three methods used, namely flame emission AAS for sodium, Mohr titrimetric analysis for chloride, and the CF watch which monitored both ions. As stated previously, the generally accepted cut-off levels for a CF sweat test (50mM sodium and 60mM chloride, above which is considered positively diagnostic of CF[12]) are a matter of continuous debate, much of which is prompted by the continued increase in the number of mutations for the CF gene which are being discovered all the time (currently in excess of 1600[13]). These mutations are increasingly rare and are often associated with milder forms of the disease, or are only associated with specific symptoms and not necessarily with the usual clinical presentation of the disease. For a general screening program it is not possible to select a general cut-off value that will account for more unusual cases such as individuals from a normal population with elevated sodium or chloride and individuals with CF symptoms but normal sweat sodium or chloride. For the purposes of the discussion of these results it is sensible therefore to take the generally accepted view that a positive sweat test for CF exhibits sweat sodium and chloride levels equal to or greater than 50mM and 60 mM respectively[12].

A further caveat is that none of the above results represent a true CF diagnosis or non-diagnosis. No CF diagnosis should ever be based on a single sweat test without reference to clinical presentation, family history, genetic mutation analysis, and at least two further confirmatory QPIT sweat tests. What value these results then? Well, the one true diagnosis in Table 3.8 is the population from whence the samples came. The success rate of the analytical methods used in matching samples to population (i.e. diagnostic accuracy) is perhaps the best test of those methods. A

correctly performed sweat test has 98% accuracy[14] in this respect, therefore in the case of the sweat watch, 1 misdiagnosis out of 21 (95% accuracy) may be considered acceptable.

Also, it is part of the design brief of this CF Watch to compete with methods such as: AAS, which requires large expensive bench-top laboratory equipment, dedicated laboratory space, fuel and air lines etc; and with such wet chemistry techniques as titrimetric analysis, which is time-consuming and labour intensive. Therefore a comparison of the methods in terms of their respective abilities to predict a known outcome is also worthwhile.

Based on the generally accepted diagnostic cut off values the CF watch correctly diagnosed all but one sample. Sample 19 is classified as normal, though it came from a CF positive population. The AAS result for sample 19 however is in agreement with this diagnosis with a sodium ion concentration just below the 50 mM cut-off. Generally speaking a lot of the normal population AAS results are quite close to the 50 mM cut-off point and could be classed as borderline. In a complete clinical situation all of these tests of course would be repeated at least twice more along with a full complement of physiological CF tests, which is beyond the scope of this study. But these high normal sodium levels may also be explained by the fact that they were taken from an adult population and it is generally accepted now that due to the increased sweating rates in adulthood, the threshold values used for children, are less applicable for adults[15], and many advocate the use of higher cut-off points for adult sweat tests. Raising the cut-off levels would remove most of the “normals” in this study from the borderline region.

The general diagnostic prediction success rate of the CF Watch based on these results is >95%, which compares well to the standard QPIT accuracy rate of 98% [9] (if performed correctly by a qualified, experienced tester, operating in a dedicated CF laboratory where the QPIT is regularly carried out). It also fares equally well against established reference methods with the advantage of speed, simplicity and significantly lower cost, as well as the monitoring of both marker ions at once.

One important point which sample #19 highlights is the lack of a traditional reference electrode in the watch device. The exclusion of this reference electrode has its advantages in that it aids manufacture by simplifying construction of the device, less materials are required to construct the sensors, fewer sensors facilitate minimisation of the physical size of the device itself, and also there is one less sensor present to fail and cause problems. The disadvantage of this set-up is that the individual sensor responses are inaccessible. The response obtained contains information about the activities of both marker ions, but the individual chloride and sodium activities are not provided. While this may not present a problem in most cases, and in this study it did not present a problem for >95% of the samples, it does present a problem for borderline cases. The watch device diagnoses sample #19 as normal. Had this researcher not been aware that sample #19 had actually originated from a CF positive population it is likely that no questions would have been raised about the validity of this result. Contrast this with the reference method mM values for each ion. Sample #19 has a sodium ion concentration of 49.3 mM and a chloride ion concentration of 90 mM. Based on these individual ion concentrations – a high normal and very borderline sodium level, and a clearly positive chloride level - sample #19 would

likely be correctly diagnosed CF positive, or at the very least investigated further with additional confirmatory sweat tests. Therefore, inclusion of a reference electrode may be a consideration for the future. Alternatively, considering the superior discrimination of chloride ion in separating the two populations, it might be more worthwhile to only monitor chloride. The 2-sensor set-up could be maintained by replacing the sodium electrode with a solid-state reference-type electrode. These and other theories are discussed in more detail in the following section.

3.10 Future Work

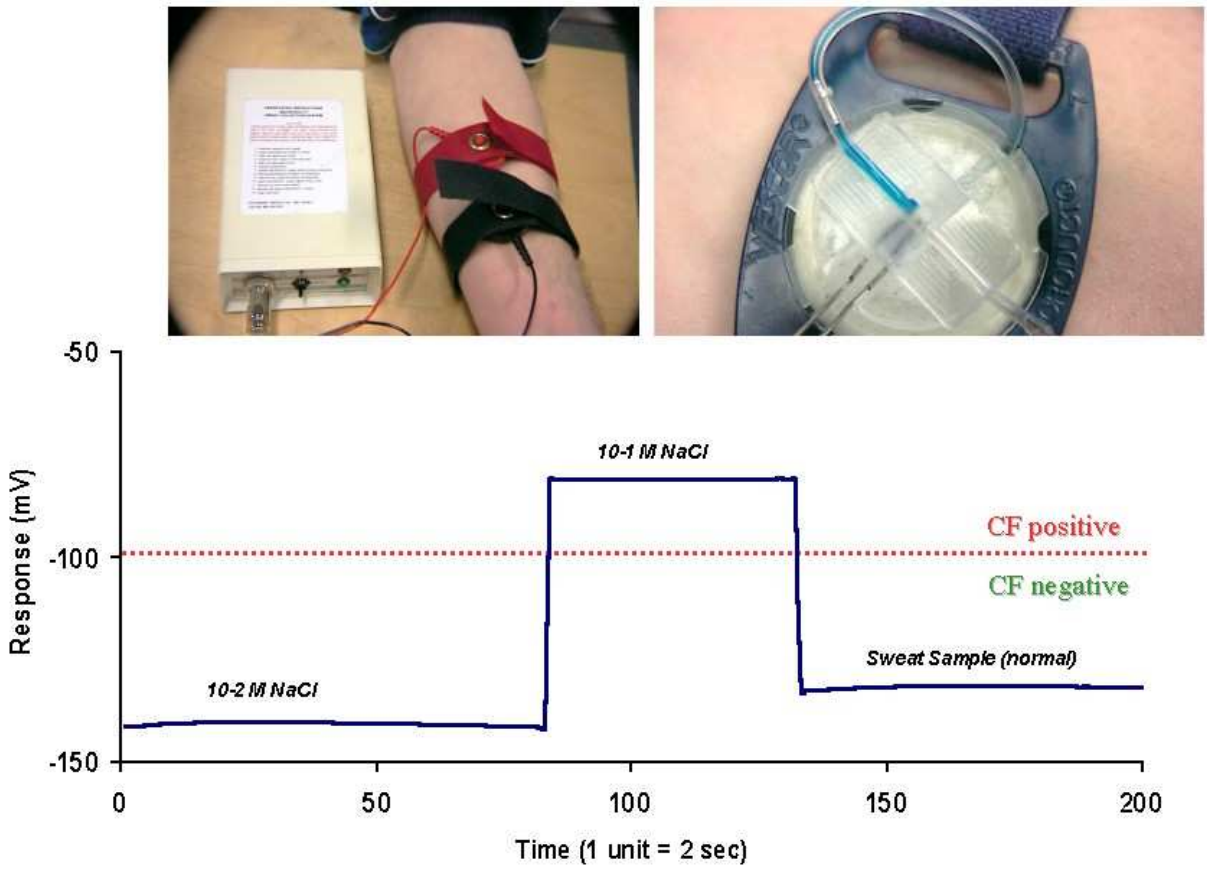

Figure 3.54 Response trace from the device in the analysis of a normal sweat sample.

Figure 3.54 is a simple experiment to show how the finished device might *ideally* be used in the future as a simple screening device, though there are a number of issues that need to be addressed before the device could be used in this manner in the real world. To create the result in Figure 3.54, two calibration solutions were passed through the analytical device using a peristaltic pump and the combined signal was monitored, in the same manner as in the clinical trial. The trace (as before) shows the device response to first a 10 mM NaCl standard and then a 100 mM NaCl standard. While this two-point calibration was being carried out, a non-CF volunteer was subjected to pilocarpine iontophoresis to generate a normal sweat sample. On completion of iontophoresis, the analytical device was fitted to the adapted Wescor Macroduct (as described earlier in Figure 3.10 to Figure 3.13) and strapped to the patient's arm at the site of iontophoresis to collect the stimulated sweat and deliver it to the analytical device as also described earlier in Figure 3.14. Once the sweat had reached and filled the analytical chamber, the data monitoring software was reactivated to measure the response of the device to the sweat sample (again as usual the trace is not in real-time trace, monitoring of the signal was paused during solution changeover and restarted once a stable signal had been obtained). In this case, the normal sweat sample is identified as normal relative to the two standard solutions. This is the device at its simplest with two calibration solutions and an immediate result. To make such a device usable in the field one could pre-package the device pre-conditioned in one calibrant solution, along with a second calibration solution, and a syringe provided, to inject the solution into the device before sample analysis.

Data monitoring issues could also be addressed. Data from the sensors could be stored locally on an SD card for analysis later, or a miniature circuit could be incorporated into the device which would measure the change in mV response and translate it into a simple “positive”, “negative”, or “borderline” result by lighting a red, green or orange Light Emitting Diode (LED) . Alternatively the data could be transmitted wirelessly to a portable receiver/laptop computer. Modern WPAN (wireless personal area network) communication protocols such as ZigBee® and Bluetooth® can easily replace physically bulky and restrictive serial cables, offering low-cost, low-power, monitoring and control of applications over a local wireless network. This marriage of wearable sensors with wireless monitoring is being pioneered by research initiatives such as BIOTEX (Bio-sensing textiles for personalised health management, see www.biotex-eu.com), an EU funded project aiming to develop dedicated biochemical-sensing techniques to monitor body fluids, such as sweat, via sensors distributed on a textile substrate, and WEALTHY (wearable health care systems). Textile based fluid handling systems for the real-time monitoring of sweat pH[16], sweat sodium[17], and sweat conductivity are being investigated and developed[18,19], using a combination of moisture wicking fabrics and superabsorbent materials, which facilitate a capillary-action, passive pumping mechanism to collect the sweat as it is produced and channel it through a sensing area for analysis. Applications are currently aimed primarily at the monitoring of athletes’ sweat electrolytes during exercise, but there are also many useful parallels for the Cystic Fibrosis community, for whom strenuous physical exercise may not be appropriate[20]. Recent breakthroughs in the treatment and management of the Cystic Fibrosis condition have made pertinent for the Cystic Fibrosis community, the issue of the continuous monitoring of sweat electrolytes. The QPIT sweat test is a

diagnosis. Once CF was diagnosed there was neither need for, nor point to, further sweat testing of CF sufferers. However modern drug and genetic therapies are being developed[21,22] which can counter or mitigate the *muco-viscidosis* effects of Cystic Fibrosis by correcting the underlying cause: chloride channel deficiencies which lead to mis-regulation of sodium and chloride ions, resulting in the characteristic sticky mucus in the lungs and thickened secretions from the pancreas and liver. These novel approaches are at varying clinical trial stages in a development pipeline, but progress is being made with such CFTR modulation drugs as PTC124 (Ataluren)[23], VX-770[24,25], and VX-809[26]. These drugs target the underlying genetic cause of the disease, for which elevated sweat sodium and chloride are a diagnostic manifestation and indication that the patient's gastrointestinal system, respiratory system and hepatic system may also be malfunctioning, and threatening the health of the patient in a manner consistent with the characteristics of the Cystic Fibrosis condition. Therefore the ability to continuously monitor sweat electrolytes of patients undergoing these treatments, using a convenient and unobtrusive wearable device could be an invaluable tool for gauging the success of the treatment, and safe-guarding the health of the patient.

The direction of future development of this device depends largely on its precise intended use. On the one hand there is a need for a simple and reliable CF screening device. There are commercially available devices already being marketed as CF screening devices. Wescor Inc. themselves market a conductivity based analyser complementary to the Wescor Macroduct, and now have a "Nanoduct" device which is claimed to be suitable for screening neonates. Similar to the device in this study,

the sweat, as it is being collected, is directed straight into an analytical chamber, in this case a microconductivity cell, where the sweat is analysed and an immediate response is obtained. Sweating rate is displayed automatically, only 3 micro litres of sweat are required and sweat stimulation time is shortened. Some direct comparisons in the literature between the two Wescor products, the Macroduct v's the Nanoduct, have found that the Nanoduct is at least as good as the larger Macroduct [27]. However, borderline results are generally seen more frequently using conductivity-based measurements[28], and the American National Committee for Clinical Laboratory Standards, for example, does not accept conductivity as a definitive diagnostic tool[29]. With a false positive rate of 4.3% and 9.3% overall failure rate, there are few studies confirming the Nanoduct's use other than as a simple bedside test requiring confirmation by more traditional methods. One improvement of the Nanoduct is a significantly reduced failure rate caused by insufficient sweating. Reliable results can be obtained from such lower sample volumes of sweat (~3µl), improving the insufficient sweat failure rate in one study[30] to 2.7% (3 of 111) from the macro-collection system's 15.3%. Similar improvements to our ISE based CF watch could be predicted by similarly reducing its dead volume, and therefore the sample volume required for analysis.

It has also been shown that parents of children undergoing CF screening are subject to much anxiety, distress and upset, emotions which are exacerbated by longer waiting times for results and repeat tests[31]. In the aforementioned Nanoduct study[30], the quick receipt of the results and minimized waiting time for the parents and patients, was an important consideration for nearly all participants and parents. The development and

use of reliable devices such as the nanoduct and our CF watch, which provide rapid in-situ results, is desirable from a patient & parent point of view therefore.

On the other hand, there is also a need for an alternative to the Gibson and Cooke QPIT (quantitative pilocarpine iontophoresis sweat test). This is the original gold standard test[1], it's laborious, it's cumbersome, it's time-consuming, but in the right hands it has proven reliability and accuracy and provides concentration data for both marker ions. As a result it is a test that the CF community is very reluctant to discard, and indeed no CF diagnosis is considered complete, regardless of what simple screening test or sophisticated genetic test is performed, unless it is accompanied by 2 confirmatory standard QPIT sweat tests[32]. In this respect the sweat watch as it is presented here has an avenue of development not open to conductivity based analysers. That is the individual and independent monitoring of sodium and chloride levels simultaneously and almost immediately. Development of the watch in this direction might see the device pose a realistic alternative rather than merely a precursor to the standard QPIT. The results of this chapter, and the previous chapters on the SendX® array, demonstrate that miniature ISE's perform as well as or better than multiple large and expensive laboratory bench-top instruments and techniques in the analysis of sweat samples. Analysis is faster, both ions can be monitored together, and they are suited to miniaturisation to enable samples to be analysed undiluted and without pre-treatment, and to enable direct integration with a modern sample collection technique such as the Macroduct.

3.11 References

[1] L.E. Gibson, R.E. Cooke; Pediatrics, 1959, 23, 545-549.

[2] C.R. Denning, N.N. Huang, L.R. Cuasay, H. Shwachman, P. Tocci, W.J. Warwick, L.E. Gibson; Pediatrics, 1980, 66, 752-757

[3] B.R. Eggins; Analyst, 1993, 118, 439-442

[4] D. Diamond, S. Walsh, J. McLaughlin, E. McAdams, D. Woolfson, D. Jones, M. Bonner; Electroanalysis, 1997, 9, 1318-1324

[5] M.O. Iwunze, R. McCain; Journal of Photochemistry and Photobiology A: Chemistry, 1998, 112, 251 - 253

[6] M. Constantinescu, B.C. Hilman; Laboratory Medicine, 1996, 27, 472-477

[7] K.B. Hammond, N.L. Turcios, L.E. Gibson; Journal of Pediatrics, 1994, 124, 255-260

[8] A. Lynch, D. Diamond, P. Lemoine, J. McLaughlin, M. Leader; Electroanalysis, 1998, 10, 1096-1100

[9] H. J. Veeze; Netherlands Journal of Medicine, 1995, 46, 271-274

[10] E. Karadag, D. Saraydin; Turkish Journal of Chemistry, 2002, 26, 863-875

[11] E. Karadag, Güven; Turkish Journal of Chemistry, 1997, 21, 151

[12] L.E. Gibson, R.E. Cooke; Pediatrics, 1959, 23, 545-549.

[13] Cystic Fibrosis Mutation Database www.genet.sickkids.on.ca

[14] V.A. LeGrys, R.W. Burnett; Archives of Pathology and Laboratory Medicine, 1994, 118, 865-867

[15] B.J. Rosenstein; Clinics in Chest Medicine, 1998, 19, 423-441

[16] D. Morris, S. Coyle, Y. Wu, K.T. Lau, G. Wallace, D. Diamond; Sensors and Actuators B, 2009, 139 231–236.

[17] S. Coyle, K.T. Lau, N. Moyna, D. O'Gorman, D. Diamond, F. Di Francesco, D. Costanzo, P. Salvo, M.G. Trivella, D. E. De Rossi, N. Taccini, R. Paradiso, J.A. Porchet, A. Ridolfi, J. Luprano, C. Chuzel, T. Lanier, F.R. Cavalier, S. Schoumacker, V. Mourier, I. Chartier, R. Convert, H, De-Moncuit, C. Bini; IEEE Transactions on Information Technology in Biomedicine, 2010, 14, 364-370

[18] F. Benito-Lopez, S. Coyle, R. Byrne, A.F. Smeaton, N.E. O'Connor, D. Diamond; Eurosensors, Lausanne, Switzerland, 2009, 06-09.

[19] F. Benito-Lopez, S. Coyle, R. Byrne, A. Smeaton, N.E. O'Connor, D. Diamond; Procedia Chemistry, 2009, 1, 1103–1106.

[20] B. Schazmann, D. Morris, C. Slater, S Beirne, C. Fay, R. Reuveny, N. Moynac, D. Diamond; Analytical Methods, 2010, 2, 342-348.

[21] J.L. Kreindler; Pharmacology & Therapeutics, 2010, 125, 219-229.

[22] M.T. Clunes, R.C. Boucher; Current Opinion in Pharmacology, 2008, 8, 292-299.

[23] E. Kerem, S. Hirawat, S. Armoni, Y. Yaakov, D. Shoseyov, M. Cohen; Lancet, 2008, 372, 719-727.

[24] F.J. Accurso, S.M. Rowe, P.R. Durie, M.W. Konstan, J. Dunitz, D.B. Hornick, S.D. Sagel, M.P. Boyle, A.Z. Uluer, R.B. Moss, B.W. Ramsey, S.D. Freedman, Q. Dong, J. Zha, A.J. Stone, E.R. Olson, C.L. Ordonez, J.P. Clancy, P.W. Campbell, M.A. Ashlock; Journal of Cystic Fibrosis, 2008, 8, S25-S25

[25] F.Van Goor, S Hadida, P. Grootenhuis, B. Burton, D. Cao, T. Neuberger, A. Turnbull, A. Singh, J. Joubran, A. Hazlewood, J Zhou, J. McCartney, V. Arumugam, C. Decker, J. Yang, C. Young, E. Olson, J. Wine, R. Frizzell, M. Ashlock, P. Negulescu; Proceedings of the National Academy of the Sciences USA, 2009, 106, 18825-18830

[26] M.P. Limberis; Drug Discovery Today: Therapeutic Stratagies, 2008, 5, 243-248

[27] J.E. Dankert-Roelse, I. Bon; Journal of Cystic Fibrosis, 2005, 4, S126-S135

[28] M.C. Desax, R.A. Ammann, J. Hammer, M.H. Schoeni, J. Barben; European Journal of Pediatrics; 2008, 167, 299–304.

[29] V.A. LeGrys, M.F. Burritt, L.E. Gibson, K.B. Hammond, K. Kraft, B.J. Rosenstein; 1994. National Committee for Clinical Laboratory Standards. Pub No C34-A2. Villanova, PA.

[30] J. Barben, R.A. Ammann, A. Metlagel, M.H. Schoeni; Journal of Pediatrics, 2005, 146, 183-188

[31] J. Moran, K. Quirk, A.J.A. Duff, K.G. Brownlee; Journal of Cystic Fibrosis, 2007, 6, 250-254.

[32] C.R. Denning, N.N. Huang, L.R. Cuasay, H. Shwachman, P. Tocci, W.J. Warwick, L.E. Gibson; Pediatrics, 1980, 66, 752-757